Technische Universität Braunschweig

Master thesis Nr. 6

Stress Ratio Effects on the fatigue Properties of Biaxially Loaded Tubular FRP-Specimens – Experimental Study

by

Jorge Marques

Matriculation number: 4345066

Supervised by:

Dipl.-Ing. Robert Greif

This thesis encompasses:

65 pages with
5 tables and
15 figures

Institute for Aircraft Design and lightweight Structure
TU Braunschweig

September 2013

WRITTEN DECLARATION

I hereby declare that the present Master thesis was conducted autonomously and without illegitimate help or counsel from third party using only the stated scientific resources and referenced literature.

Braunschweig, 27th September 2013

ÜBERSICHT

In dieser Arbeit werden röhrenförmige faserverstärkte Proben auf ihre Lebensdauer getestet. Die Proben werden biaxial mit Zug- und Schubspannungen belastet, mit einer Winkellast von 30° und 60° und einer Belastung im Verhältnis von R = 0,1. Es gibt viele Faktoren, die die Lebensdauer eines faserverstärkten Materials bestimmen aber das Hauptziel dieser Arbeit ist es, die Auswirkungen der Belastung im Verhältnis R durch den Erwerb von S-N Kurven zu studieren und sie mit früheren Arbeiten zu vergleichen (1). Alle anderen Parameter, wie z. B. Beschaffenheit der Proben, Frequenz und Temperatur, werden die Gleichen wie bei den vorherigen Tests sein (1). Für jeden Test sind die Daten der Steifigkeit, Temperatur der Probe während der Prüfung, Risszählung und des endgültigen Bruchs gespeichert worden.

Vor den Tests wurde die Literatur über die Auswirkungen auf das Last-Verhältnis und der Lebensdauer der Verbundwerkstoffe studiert. Mit dieser Überprüfung schätzt man ab, welche anfängliche Spannung in den Tests angewendet werden sollte. In vorherigen Arbeiten mit ähnlich Proben wurde nur eine Last im Verhältnis von R = -1 getestet und daher ist das Verhalten der röhrenförmigen Proben für ein anderes Last-Verhältnis unbekannt. Alle gewonnenen Daten werden analysiert und im Vergleich zu den früheren Arbeiten auf ihre Unterschiede getestet. Später wird versucht diese Unterschiede zu erklären.

Die Software zum Zählen der Risse, wurde am Institut entwickelt und hat sich früher schon als nüzlich erwiesen. Jedoch führen verschiedene Anpassungen der Software-Parameter zu unterschiedlichen Zählergebnissen für das gleiche Bild. Es wird eine bessere Mehtodik zur Anpassung der Software vorgeschlagen und erklärt.

Nach einem aufgetretenem Fehler, werden alle Daten gesammelt und gespeichert und das Faservolumengehalt für jede Probe wird ebenfalls bestimmt. Die Anzahl der Tests, um die S-N Kurven zu erhalten, entsprechend den bestehenden Normen.

Zusätzlich werden auch einige Verbesserungen für die Einstellung der Prüfmaschine und das Verfahren für zukünftige Tests vorgeschlagen.

ABSTRACT

In this work tubular fiber reinforced specimens are tested for fatigue life. The specimens are biaxially loaded with tension and shear stresses, with a load angle β of 30° and 60° and a load ratio of R=0,1. There are many factors that affect fatigue life of a fiber reinforced material and the main goal of this work is to study the effects of load ratio R by obtaining S-N curves and compare them to the previous works (1). All the other parameters, such as specimen production, fatigue loading frequency and temperature, will be the same as for the previous tests. For every specimen, stiffness, temperature of the specimen during testing, crack counting and final fracture mode are obtained.

Prior to testing, a study if the literature regarding the load ratio effects on composites fatigue life and with that review estimate the initial stresses to be applied in testing. In previous works (1) similar specimens have only been tested for a load ratio of R=-1 and therefore the behaviour of this tubular specimens for a different load ratio is unknown. All the data acquired will be analysed and compared to the previous works, emphasizing the differences found and discussing the possible explanations for those differences.

The crack counting software, developed at the institute, has shown useful before, however different adjustments to the software parameters lead to different cracks numbers for the same picture, and therefore a better methodology will be discussed to improve the crack counting results.

After the specimen's failure, all the data will be collected and stored and fibre volume content for every specimen is also determinate. The number of tests required to make the S-N curves are obtained according to the existent standards.

Additionally are also identified some improvements to the testing machine setup and to the procedures for future testing.

ACKNOWLEDGEMENTS

First of all I have to express my deep gratitude to Dipl.-Ing. Robert Greif, not just for all the patient guidance, sympathy and support during the realization of this work, but also for making possible for me to come to the institute in the first place.

I would also like to extend my thanks to the staff at the institute that I contacted directly, for their sympathy and for their help, which was always promptly offered when I needed.

Additionally I have to thank Professor Dr. Luís Durão at ISEP, who encouraged me to apply for a Master Thesis abroad and even offered his support, despite my previous commitment.

Finally, I have to thank my girlfriend Marta who has always been my biggest support.

CONTENTS

SYMBOLS AND CONSTANTS

Symbol	Unity	Definition
β	Degrees (°)	Biaxially Load Ratio Angle
σ	MPa	Normal Stress
τ	MPa	Shear Stress
M	N.m	Moment
Mt	N.m	Torque
r	mm	Middle radius
R	MPa	Strength
R_t	MPa	Tensile Strength
R_c	Mpa	Compressive Strength
R_s	MPa	Shear Strength
ϕ	%	Fiber Volume Content
S	MPa	Stress
N	-	Total number of cycles (to failure)
n	-	Number of cycles
N_f	-	Number of cycles to failure
K	kelvin	Temperature
C	degrees (º)	Temperature
J	Joule	Energy
s	second	Time
λ	μm	Wave length
t	mm	Thickness
t_m	mm	Medium thickness
a	m^2	Area
F	N	Force

ABBREVIATIONS

Abreviation	Description
FRP	Fiber Reinforced Plastics
GFRP	Glass Fiber Reinforced Plastics
CFRP	Carbon Fiber Reinforced Plastic
FPS	Frames per Second
MTS	Testing Machine
rpm	Rotation per Minute
RTM	Resin Transfer Molding
STD	Standard Deviation

1 Introduction

Composite materials have had a huge grown in usage in recent years since they have very good stiffness and strength and at the same time have very low weight. This makes them in many situations more advantageous than conventional materials and more suitable for lightweight structures. Over the last years composite materials have grown in use, and nowadays they are not restricted to the aeronautical field and can be found in other industries like automotive, railway, marine and others.

This wide use of composites, and specially the structural applications, demands a very good knowledge of the materials behaviour, either for purely static loads or for fatigue loads. There are already models to predict the behaviour of a composite material for purely static loads, and the classical laminate theory is the most well-known. However when it comes to fatigue behaviour, there isn't currently any model that can be widely used.

The Institute of aircraft Design and Lightweight Structures (IFL) has developed investigation on tubular specimens to study fatigue behavior and its effects on global properties of tubular specimens. The use of tubular specimens relates to the fact that they allow the study of multiaxial loads (tension and torsion), which are very relevant for structural applications. During the current projects at the institute, several tests have been conducted with a load ratio of R = -1 (positive and negative loads). For that reason, the motivation for this work is to analyze the behavior of these specimens for a load ratio with only positive loads ($0<R<1$), and to compare these results with the ones previously acquired, so that a better understanding of this material fatigue behavior is achieved.

In order to study this specimen's behavior several tasks have to be performed, with the first being the study of the literature for similar studies where the load ratio R influence had been studied. This study, together with the standards for fatigue testing, provides a better perspective of how the tests should be conducted and what could be expected. The number of cycles that each specimen lasted and the loads that it was submitted to are used to construct S-N curves that characterize the material for this load ratio R. In order to improve the results accuracy and validate them, experimental determination of the fibre volume content is performed for all the specimens. This allows a more accurate calculation of the real stresses applied during testing, and therefore, more accurate results for S-N curves.

Acquisition of stiffness degradation, temperature and crack density is also important to understand how a material degrades until final failure. The temperature is obtained during testing but for crack counting several pauses has to be done and the specimen taken out. Therefore the tests are divided in sets of cycles, the first sets are shorter (less cycles)

because at the beginning of a fatigue test the cracks accumulation is bigger. As the fatigue cycles increases the cracks growth stabilize, meaning that it's not necessary to interrupt the testing so frequently. Stiffness characterization also means that the fatigue testing has to be interrupted, but the characterization is measured by the MTS machine, meaning that the specimen does not need to be taken out.

The results will contribute to a better understanding of this material's behavior and also S-N curves that can be used for fatigue life prediction in further tests with the same load ratio R.

2 Theory

In this chapter the main theoretical knowledge necessary previously to fatigue testing are presented. A special focus will be given to the load ratio R effects on fatigue, as its study is the main goal of this work. A brief review of the non-destructive evaluation methods and their applicability in composite testing are also presented.

2.1 Introduction to fiber reinforced plastics

A composite material is a combination of two or more different materials, with the objective of combine their strengths and obtain a new improved material. Composites have been used for a long time by mankind species, but in rudimentary ways, like straw mixed with mud to fabricate bricks (referred on the bible, Exodus 5.15-18). Composite materials can also be found in nature: wood, flower stems and bones are typical natural composite structural elements. Today a composite material is usually referred as a combination of two materials, a soft material to give shape and a strong material for reinforcement. When the soft material is a polymer and the reinforcement is fiber we are in the presence of a fiber-reinforced polymer - FRP (2).

In the beginning of the 20th century, fiber-reinforced polymers started to grow in use, both for more simple and everyday articles and also in structural components in aeronautics and aerospace engineering. Today they are one of the principal materials in aerospace and aeronautics engineering and continue gaining more applications in other areas, mainly because they have two very important advantages over the traditional materials, very high strength and stiffness and low specific weight. Fiber-reinforced polymers are nowadays the most important composites in terms of performance and in range of applications, due to the two advantages mentioned before and also for the ease of processing compared to the metallic, ceramic or cementitious matrix composites (2) (3).

Fibre-reinforced polymers, as already mentioned, are made from the mixture of fibre and a polymer, and these two materials have very different roles in the final composite material. The fibers are very thin yet very resistant, considerable more resistant than the same material in a solid massive form. For example, glass, in a solid massive form, has a maximum tensile strength of around 170 MPa and glass fibres of around 20μm diameter can reach 3500 MPa of maximum tensile strength (4). Therefore, the fibres can handle very high tensile strengths and are used as reinforcement, but they cannot be used in most engineering applications because they cannot acquire a form by them self. For this reason they are mixed with the polymer, also denominated matrix, that has the function of giving a

stable form to the final material, to distribute the forces by the fibres and also protect them against the environment (3).

Inside the groups of fiber-reinforced polymers, there are many different matrices and can be divided in two big groups: thermosets and thermoplastics. In this work is used epoxy resin, which is a thermoset matrix commonly used for high performance applications due to its excellent properties when compared to other resins: high strength resistance, good abrasion resistance, chemical stability, good adhesion to the fibers, low contraction when cured (2% to 3%), low water absorption, operating temperatures up to 220 °C, and relative ease to process. The main disadvantage of epoxy resin is its price, which can be up to 4 times the price of vinylester resins, for example (3).

In the field of the fibers, carbon fiber and glass fiber are most common. Due to its high price, carbon fiber is mostly used when high stiffness is required and is more commonly seen as a premium product. On the other hand, glass fiber is less expensive, and despite not having the stiffness of the carbon fiber, it has very good mechanical properties that make it suitable for many engineering applications. Fibers can have various forms like roving, mat, woven fabrics, etc, and also different fibers can be mixed to obtain different properties (3).

There are many ways to process fiber-reinforced polymers into their final form, and the process depends on many factors, but the type of the matrix used, the form of the fibers (long fibers or short fibers), the mechanical properties required, the dimensions, the number of parts to be produced and the complexity of the shape are the most important. All the different processes can be generally classified in two types: open mold and closed mold. In open mold only one side of final part has a surface with good form and appearance, but can produce very large components and with very complex geometry. The closed mold processes have a good surface form and appearance finish on both sides, and have very good reproducibility, but the shape of the material is more limited. For this thesis the specimens will be produced using Resin Transfer Molding (RTM), which is a closed mold process, where the mold is closed after the fibers being placed inside and then the pressurized resin is injected in to the mold (3) (5).

In this work it will be used a glass fiber reinforced polymer, also abbreviated as GFRP, with E-glass and a resin/hardener combination of RIM135/RIMH137.

2.2 Engineering Applications of FRP

The aeronautical industry is primarily responsible to the use of composites, starting in the 60’s, and is still increasing their use to the current days. Aeronautical industry is a highly

competitive market, and the use of composites contributes to the reduction of the weight, allowing an increase of the passenger's capacity and therefore a better profitability. The high costs associated with composites manufacture are compensated with by the lower costs of operation, specially the fuel costs which are directly related to the aircraft weight (3).

The excellent composites properties allowed engineers and designers to look to old problems in a different way and find new applications to these materials. Nowadays, with the composites prices lowering, they are not restricted to aeronautical engineering anymore and can be found in many everyday products, such as cars, sport articles, electronic components and even in building construction.

Civil engineering has experienced a growth of this kind of materials, especially fiber reinforced plastics for structural applications, due to their specific stiffness and specific strength, low weight, corrosion resistance, durability and low thermal conductivity to act as an insulator (6). A good example of a civil engineering structure is the Pontresina footbridge in Switzerland (Figure 2.1). Because this bridge is built with glass fiber reinforced plastic, it's weather resistant, maintenance free and lightweight, which allows it to be assembled in autumn and disassembled in the spring every year (2).

Figure 2.1 - Pontresina footbridge in Stwizerland

The wind industry has also grown rapidly in the last years, due to the demand of cleaner energy sources for the future. The use of composites in wind turbine rotor blades has allowed them to grow in size and improve his efficiency, reaching in some cases more than 120 meters long (2).

All this new applications of composite materials demand a good knowledge of this material's behavior, specially concerning to fatigue, and despite all the work that has been done in the past years, there is still a long path to go to reach a maturity of knowledge similar to the one with conventional materials such as metals.

2.3 Importance of fatigue

It's known for engineers that fatigue causes the majorities of failures for conventional materials and it has been studied for more than a century. The study of fatigue is of utmost importance for the design of parts subject to cyclic loads for the reason that the materials lose their properties and initial characteristics and fail to loads that are below their initial static strength. FRP have been replacing conventional materials, like steel and aluminum, and therefore is becoming increasingly important to study their fatigue properties (3).

It was believed for many years that FRP, especially for carbon fibre composites, didn't suffer from fatigue. Nowadays this idea is eradicated and fatigue is also seen as a very important factor to FRP, especially for the reason fibre reinforced composites are very lightweight compared to conventional materials, and live loads (the ones that are applied to the material) are usually much bigger than dead loads (weight of the material itself and permanent loads).

But FRP handle damage very differently from a conventional material. In the first cycles, the damage in a FRP is distributed through the stressed zone rather than accumulated in specific areas. Also, in metallic material it is assumed that compressive stresses were not very significant because they only close the cracks, as on the other hand in FRP the compression strength can be often lower than tensile stresses and causes more damage. Additionally, the great number of different FRP possibilities, that result from the wide variety of fibers, resins and manufacturing processes make it even more difficult to have a widely accepted method to determine fatigue endurance, as exists for conventional materials. This makes the study of fatigue of FRP very important, especially when they are used in critical structure components.

The understanding of the FRP fatigue behavior also allows reduction of costs when designing new components, by making possible to simulate the performance of the new piece without the need of physical prototypes. The durability of the component, which is also of great importance, could also be taken into account in the development process, making the final component better suited for its purpose.

2.4 Fundaments of fatigue testing

2.4.1 Fatigue Damage Mechanisms

Fiber reinforced plastics have good resistance to fatigue if are unidirectional and the load is oriented at 0 degrees to the fibers. However, fiber reinforced plastics with multiple layers oriented in different directions have less resistance to unidirectional loads. Therefore the

damage mechanisms are different: for unidirectional composites with lower loads the damage starts with cracks in resin that spread and start to create delaminations and for higher loads usually starts with some fibers rupture that produce zones with higher stress concentrations, making the fibers in the proximities starting to fail too (3). For composites with multidirectional layers the damage evolution is usually divided in three stages (Figure 2.2).

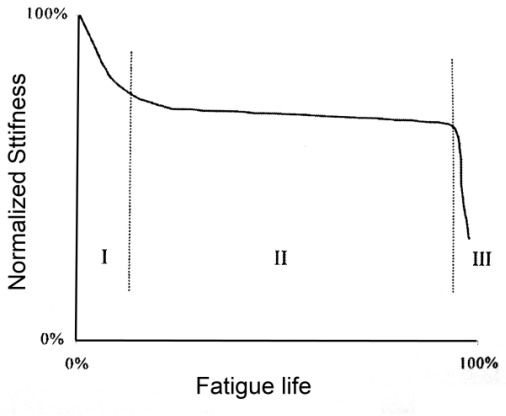

Figure 2.2 - Typical evolution of the normalized stiffness for a fiber reinforced material (3)

First stage: there is a large decrease in stiffness, usually due to cracks initiation in the layers with the bigger orientation difference to the applied load. What usually happens in this layers is a debond between the resin and the fibers due to their difference in stiffness but other factors, such as voids, zones with big resin accumulation, fiber's misalignments and other production defects that may cause stress concentration also promote the crack growth. After the crack initiation, it spreads in the direction of the fiber. Despite the loss of stiffness in an early stage, it happens very often that in the first fatigue cycles the strength of the material is kept almost intact (Figure 2.3).

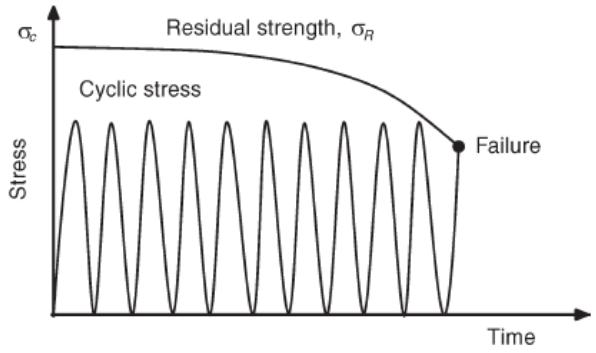

Figure 2.3 - Strength degradation of a fiber reinforced composite in a fatigue testing (7)

Second stage: the density of the cracks grows with the number of the cycles (until they reach a saturation point), and this causes a light reduction in stiffness. The initial cracks are

already formed and crack grow stabilizes, which makes this stage the longer (3). In this stage the strength starts to decrease, and this decrease is getting bigger at each cycle.

Third stage: usually begins when these cracks spread to the interface between different oriented layers, causing delaminations that grow fast and promote the separation of layers an leading to final failure (3). The fatigue theories based on residual strength degradation say that the strength of the material has a fast decrease at this stage and the final failure happens when it goes below the fatigue stress applied (Figure 2.3).

The stiffness degradation is relatively small in the glass-fibers and usually is matrix-driven. Consequently, stiffness degradation is more prominent in laminates that are off-axis (8).

2.4.2 Factors affecting fatigue life

There are many factors that affect fatigue life, but as it was said before, the main focus of this work is the load ratio, and consequently it will be discussed in more detail in the next section. Still, here is a brief review of some of the other most important factors and their influence:

- Fiber type: the fibers are the responsible for the material resistance and, in a general way, fibers with higher tensile modulus have higher resistance to fatigue. This is because they avoid deformation of the material, which avoid the deformation of the matrix and the propagation of cracks (3) (6);
- Orientation and the number of layers: this also has a great impact in fatigue life as the fiber lay-up schemes also influence the fatigue resistance, because different lay-up can create different tensions, between layers and inside the layers, which may be more likely to initiate cracks (3);
- Fiber volume ratio is also important, and the bigger this ratio the better the fatigue resistance due to the increase in the static resistance (3);
- Resin: the most important is the deformation at fracture and the tenacity of the resin, and usually the bigger these parameters are, the better for fatigue resistance. But the adhesion of the resin to the fibers, the shrinkage during the curing process and mechanical resistance are also very important (3);
- Loading frequency: this affects the internal heating of the composite because it has low thermal conductivity which produces temperature gradients. However, loading frequency does not seem to have a big impact in fatigue life, as long the temperature is kept within the material limits (3);

- Manufacturing process: the manufacturing process can affect the number of voids than are found in the material, and typically more voids lead to a worse fatigue performance (1).

2.5 Influence of Load Ratio R

This chapter is aimed to explain the differences that can be expected in a specimen tested for fatigue when different load ratios are used. Therefore, it will first be explained what is the load ratio R and how it affects the single layers and specimen as a whole. Because many fatigue tests made until now used flat specimens, it will be made a small revision of what differences between flat specimens and tubular specimens can be expected. Finally, some fatigue test results from literature will be presented and discussed.

2.5.1 Differences between Load Ratios

As it was said before, fatigue tests consist in load cycles applied to a specimen, below its failure limit, and can be displacement controlled or force controlled and applied at a constant or alternated frequency. Nevertheless, most fatigue tests are frequency constant and controlled by maximum and minimum load, which are kept constant through the test. The load Ratio R in a fatigue test also known as Stress/Load Ratio R or simply R-Ratio) is the relation between minimum and maximum stresses applied:

$$R = \frac{Load_{min}}{Load_{max}} \qquad \textbf{Equation 2.1}$$

The Load Ratio R can be divided in three big different groups:

- R>1 which means there will be merely negative loads;
- 0≤R<1 for positive loads only;
- R<0 for alternate positive and negative loads.

This last group can also be divided into two groups:

- -1<R<0 for positive load stronger than the negative load;
- R<-1 for negative loads stronger than the positive load

When R=-1 means alternating cycles with both Loads (positive and negative) with the same strength. This is shown on a more practical sense in Figure 2.4:

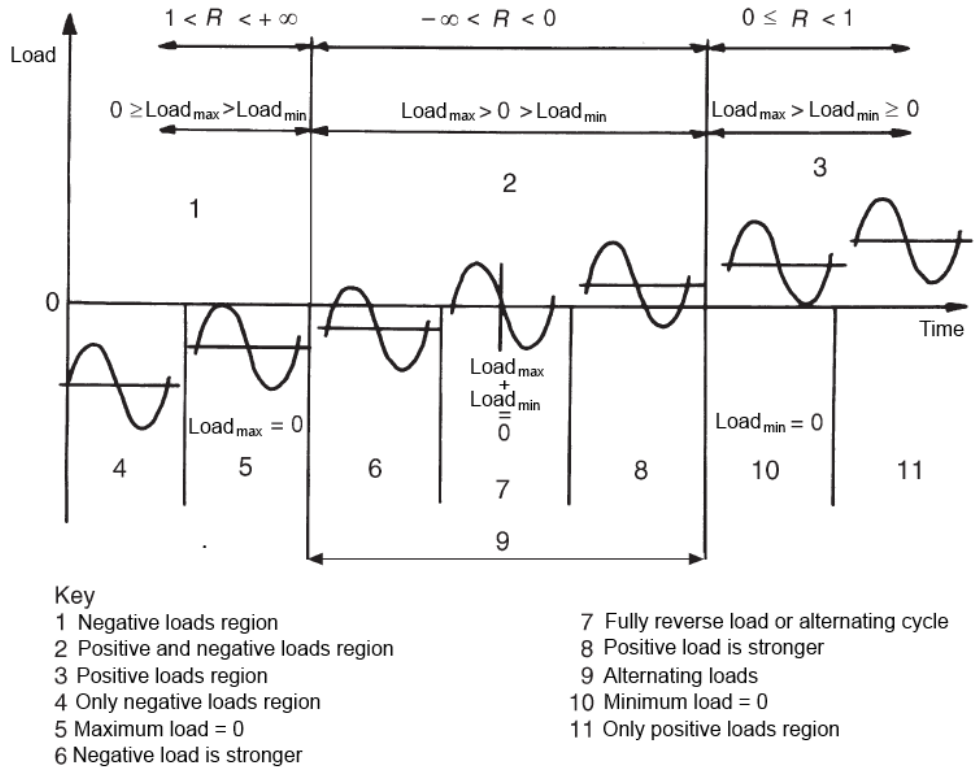

Figure 2.4 - Load ratio R differences - adapted from reference (7)

2.5.2 Basic solicitations and layer resistance

Fibre Reinforced Composites are anisotropic, so different loads applied will have great differences on this materials behaviour. To better understand how a different load affects the whole material we should start to see the basic solicitations for a single layer and its resistance. In Figure 2.5 it is represented the basic solicitation types to a single composite layer.

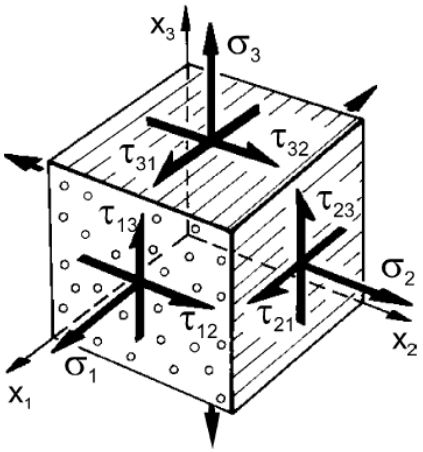

Figure 2.5 - Basic solicitation modes to a single composite layer (9)

Fibres failure take place when the stress applied exceeds their strength

$$\frac{\sigma}{R} \geq 1 \qquad \textbf{Equation 2.2}$$

And in Table 2.1 we can see some typical rupture values for static load testing in unidirectional composites to those solicitations.

Composite	**φ** (%)	$\mathbf{R_{t1}}$ (MPa)	$\mathbf{R_{t2}}$ (MPa)	$\mathbf{R_{c2}}$ (MPa)	$\mathbf{R_{c2}}$ (MPa)	$\mathbf{R_{s12}}$ (MPa)
C(AS4)/Epoxy(3900-2)	0.63	2280	1440	57	228	71
C(IM7)/Epoxy(977-2)	0.65	2818	1612	75	161	109
E-G/Epoxy	0.55	1080	620	39	128	69
K49/Epoxy	0.60	1280	335	30	158	49

Table 2.1 - Rupture strength for some unidirectional composites (3)

In Table 2.1 we can easily see that all the composites represented are more resistant to tensile than to compressive stresses, when the solicitation is aligned with the fibres orientation. When the solicitation is made at 90° to the fibres direction, compressive resistance is bigger than tensile resistance, but still considerable lower than the tensile resistance when the solicitation is at 0° to the fibres direction. This is what should be expected from a fibre reinforced composite since the fibres are responsible for the resistance and the resin, although also has its share in the final resistance of the composite, is mostly responsible for the shape. Not every fibre reinforced composite is exactly like this four examples in Table 2.1, but it is unquestionable that different solicitations to a fibre reinforced composite will have different resistance. Therefore, the load ratio R, which changes the type of loads that the material will be subjected, is one of the most important factors when testing a composite material for fatigue.

2.5.3 Load ratio influence on damage mechanisms

Usually, when a material is tested, it has more than one layer, with different fibres orientations, which makes the problem much more complex, and also adding the interaction between layers that can has influence on the damage mechanisms of the material and can consequently change the number of cycles to final rupture (7). In a material that has multiple layers oriented in different directions, when the load direction changes, there will be one or more layers with a better fibre orientation to resist that load and avoid failure, and this is the biggest advantage of having multiple layers in a single material. But the downside is that there may also be layers that, due to their different orientation, don't have a good resistance

to the applied load, and can start to accumulate cracks, which may spread to other layers, cause delaminations and even leave to final failure (3).

Looking at Figure 2.5 and Table 2.1 it would be relatively easy to say which layer of a fibre reinforced material would have more resistance or fail sooner due to a specific load direction. However, fatigue tests are performed with loads that are below the static failure limit of the material, which means that the static resistance, although very important, can only be used as a guide to fatigue testing, and there are other factors that must be taken into account. What usually happens in a fatigue test is that the accumulation of cracks leads to delaminations that grow every cycle till final failure, and therefore it is significant to see how a different load can affect this cracks initiation and propagation.

Figure 2.6 - Drawing of interface crack opening and contact zone for a transversely loaded fiber under tension and compression in a composite material (7)

There are two main ways for a fibre reinforced material to start accumulating cracks: interlaminar fracture and intralaminar fracture. The first case is when the failure develops inside one matrix layer and can be caused by fibres rupture, matrix rupture or interface deboning between the fibres and the matrix. The second case is when 2 layers, with the same load, start to debond from one another due to their different fibre orientation (3).

Unfortunately there seems to be little information in literature about how different fatigue loadings affect each one of these damage mechanisms, possibly because even for static testing it can be difficult to quantify them. However, for long fibre composites with low fatigue loads (fatigue load that is far from the static failure load), the majority of the damage is related to interface deboning between matrix and fibre (3).

Gamstedt and Sjögren (1999) studied the effects of a tension-tension load and a tension-compression load on cross-ply glass/epoxy and single fibre model composite, with the fibre oriented perpendicularly to the loading direction. With their study they concluded that fibre reinforced composites with transverse layers degrade more rapidly in tension-compression when compared to tension-tension fatigue loading, which can be seen in Figure 2.7. The

reason for this was attributed to a more rapid debond with tension-compression loading, due to a more effective crack tip opening under compression (7).

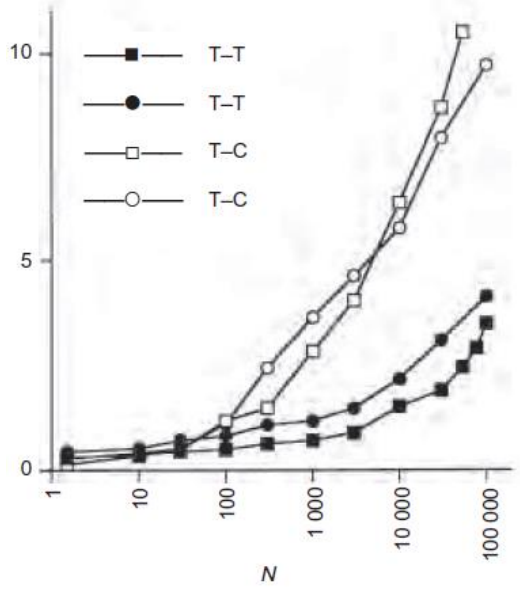

Figure 2.7 - Evolution of transverse crack length in a fatigue life test with tension-tension (T-T) and tension-compression (T-C) loadings (7)

The mechanism of crack opening under tension and compression can be seen in Figure 2.6. This debonds lead to an earlier initiation of cracks in tension-compression loads, that then propagate parallel to the fibre (7) (3).

Ramani and Williams also tested carbon/epoxy laminates in various loads combinations and concluded that the higher the compressive stress the more adverse were the effects to fatigue life (7). This means that load ratios that include compression will likely cause more damage in an early stage then load ratios with just tension loads.

As a final note, it is important to mention that the fact that different load ratio makes a big difference in the damage suffered by a fibre reinforced material, the same does not work for the maximal applied stress, since it has yet not been found a clear relation between the maximal applied stress and crack growth (10) (7).

2.5.4 Damage failure modes

As mentioned before, there are two ways for a fibre reinforced material to start accumulating cracks: interlaminate fracture (between layers) and intralaminate fracture (inside the layer).

For interlaminate fracture there are three modes. These three modes can be easily seen in Figure 2.8. Of these three modes, Mode I is usually the most critical because its initiation value is lower than the Mode II and Mode III.

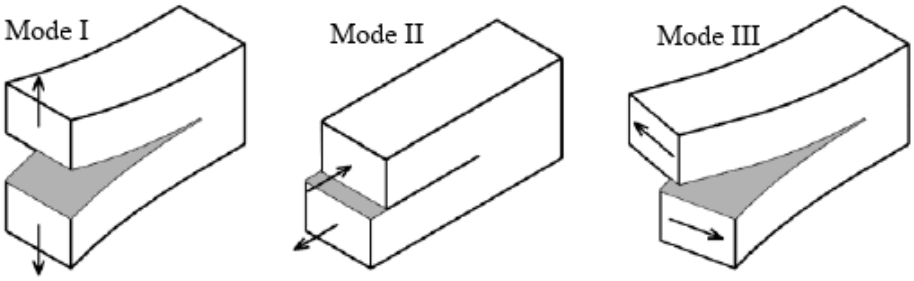

Figure 2.8 - Interlaminate solicitation modes (3)

For intralaminate fracture (or inter fiber fracture), Puck described three different modes: Mode A. Mode B and Mode C (Figure 2.9).

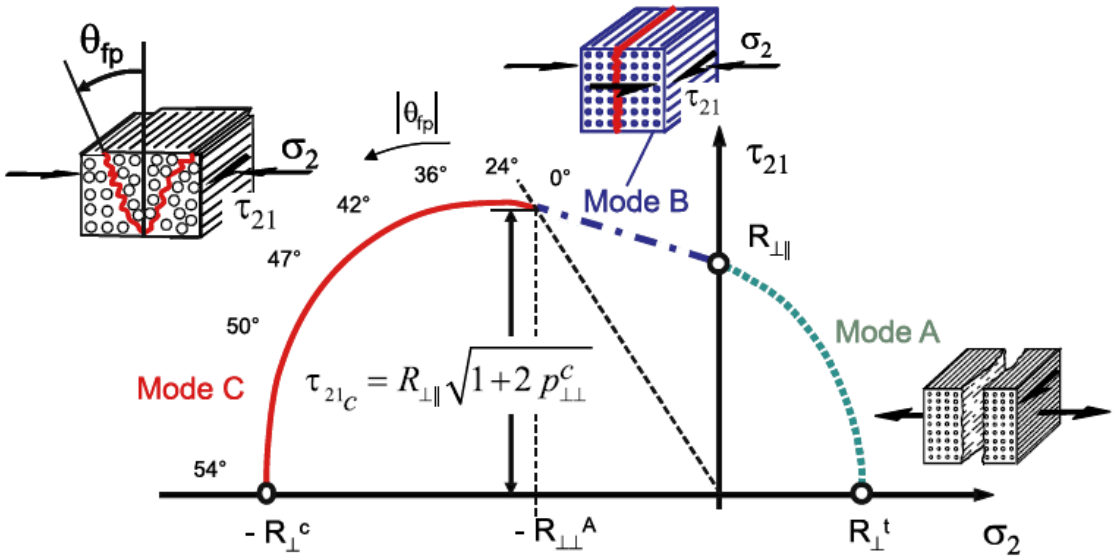

Figure 2.9 – Puck's different intralaminar fracture modes and fracture curve (9)

Mode A: Transverse tensile stressing or longitudinal shear stressing cause fracture, alone or in combination. The fracture surfaces are separated due to tensile stressing, which leads to a degradation of Young's and shear modulus.

Mode B: Longitudinal stressing causes fracture, but he crack does not open because the transversal normal stressing is compressive. The degradation of stiffness is much less significant than for mode A.

Mode C: occurs when the ratio between compressive normal stressing at fracture and transverse compressive strength exceeds 0,4. Fracture occurs on an inclined plane.

2.5.5 Specimen's geometry

It is important to say though that most fatigue studies performed on FRP done until now, that also focused on different load ratio R behaviour, were performed with pure tension or compression loads. Only some studies used biaxially loaded specimens, and usually the specimens are flat and not tubular as the ones that will be used in this work. Therefore the applicability of these conclusions to the tests that will be executed further ahead is limited and should be taken with caution. Nevertheless, the basic damage mechanisms for a fibre reinforced material, with similar fibre and resin should be comparable, despite its final geometry, although the geometry is responsible for the way stresses are distributed across the material. For tubular specimens, as the one that will be used in this work, have stress gradients across the thickness of the tubular wall, and this causes them to be more unpredictable when compared to flat specimens (11). Norman *et al.* compared carbon/epoxy cylinders with plane specimens and concluded that cylinders had a fatigue life almost order of magnitude higher when compared to the plane specimens, but if the maximum applied stress was a percentage of static failure load of the specimen, the fatigue life for cylinders and plane specimens were identical (7), which supports the idea that the damage mechanisms must be similar, and therefore the load ratio should have comparable effects.

2.5.6 Review of experimental results in literature

As expected, many studies have shown that composites materials behaviour and life time period can be distinguished between the R-Ratio groups showed in the beginning ($R>1$ for negative loads only, $0 \leq R<1$ for positive loads only and $R<0$ for alternate loads).

Anastasios P. Vassilopoulos and Thomas Keller (2) did some extensive research on glass fibre reinforced plane specimens obtained from plates with 4 layers, 2 unidirectional and 2 with fibres oriented with +45° and -45° each, and cut in different orientations relatively to the unidirectional layers. Four different load ratios were used, R=10 for compression-compression, R=-1 for tension-compression loading, and for tension-tension loading was used R=0.1 and R=0.5. An antibuckling device was used to prevent buckling from compressive loads and the load frequency was 10 Hz. The S-N curve results for the specimens with the unidirectional layers on-axis with the load, in Figure 2.10, showed that with a load ratio of R=0.1 had higher maximum tensile stresses for the same number of cycles, when compared to the load ratio of R=10, meaning that in this case compressive loads are more adverse than tension loads.

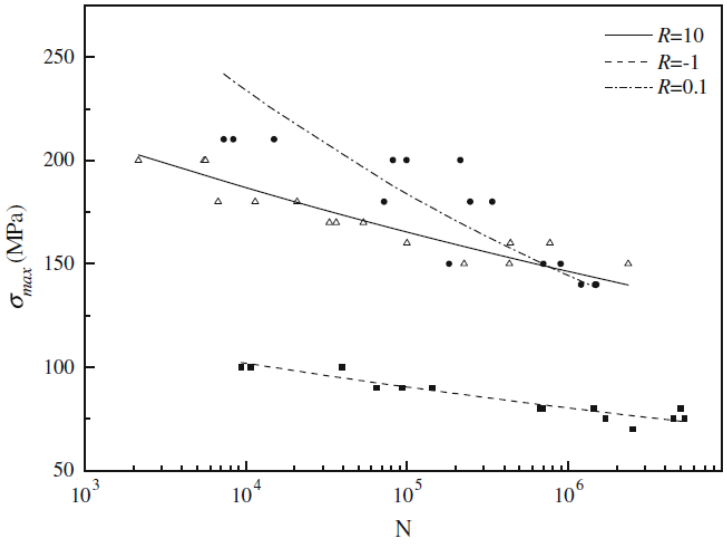

Figure 2.10 – S-N curves results from Anastasios P. Vassilopoulos for specimens tested with unidirectional layers on-axis (2)

This is what could be expected, since as it was said before, compressive loads are more adverse then tensile stresses. What is more interesting is that the S-N curve for R=0.1 is steeper than the one for R=-1, meaning that for stresses lower than 150 MPa, a load ratio of R=0.1 can be more harmful that a load ratio of R=10, although that for such low loads the number of cycles would be in both cases above 10^6cycles. Also interesting is the fact that the S-N curve for a load ratio of R=-1 has a much lower maximum stress compared to R=10 and R=0.1, which indicates that tensile and compressive loads are more critical than tensile or compressive stresses alone (2). It is however curious to notice that for the load ratio of R=-1, the S-N curve is the one with the less slope of the three, and the results appear to have less scatter also.

The S-N curves for the specimens cut at 90° showed rather different results Figure 2.11. Tension-tension loads have a more critical effect in fatigue life than compression-compression loads, and even tension-compression alternate loads seem to be a little more degenerative than compression-compression loads.

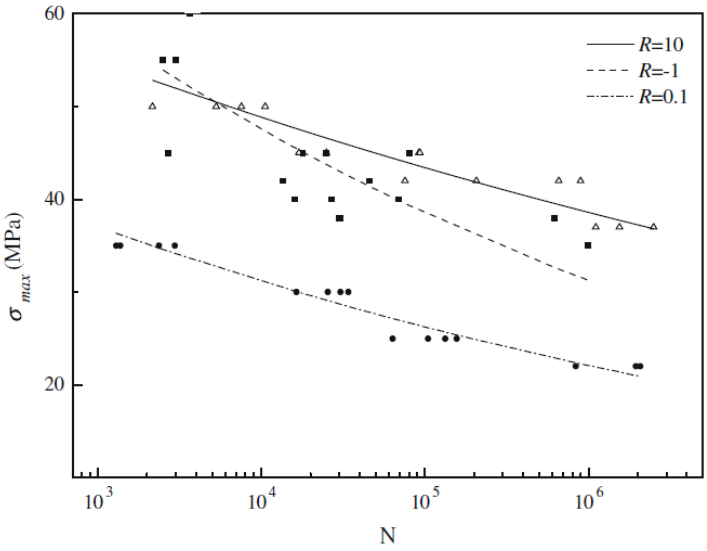

Figure 2.11 - S-N curves results from by Anastasios P. Vassilopoulos for specimens tested with unidirectional layers oriented at 90° from load direction (2)

This can be explained by the absence of fiber in the load direction, but when compared to the specimens on axis on Figure 2.10, the maximum stress are much lower for any given load ratio, and it should also be taken into account that the antibuckling device helps to prevent buckling damage that otherwise could have a big influence in this results.

M.J. Owen and J. R. Griffiths (12) also performed extensive research in fatigue life tests in tubular specimens made with E-glass and polyester resin and with load ratios of R=0, R=1, R=-1, R=0,5 and R=-0,5, which results can be seen in Figure 2.12. Focusing only on the results which were performed without internal pressure (α=0°) it's possible to conclude that a load ratio of R=-1 is the most harmful for the specimens fatigue life. This is in accordance to could be expected, since of all the load ratios this is the one with the highest compressive load. The load ratio of R=0 is the one that shows a better fatigue performance in the first cycles, since this load means that here is no compressive stresses. However, its curve is steeper, meaning that, for cycles longer than 10^4, this load ratio can be more critical than a load ratio of R=0,5. The load ratio of R=-0,5 is less degenerative for the specimen fatigue life when compared to the load ratio of R=-1, which is also what could expected since for R=-0.5 the compressive load is not as strong as it is for R=-1.

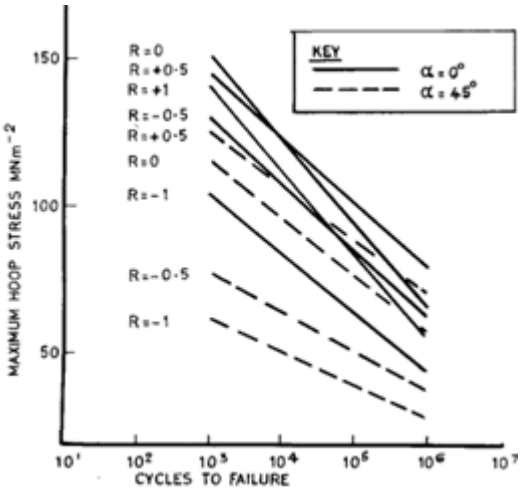

Figure 2.12 - M.J. Owen and J. R. Griffiths results for fatigue life testing with tubular specimens for different load ratios and with internal pressure (α=45°) and without internal pressure (α=0°) (2)

L. Ferry *et al.* (13) executed fatigue tests for bending and torsion in flat glass fiber/epoxy specimens, and, in relation to the load ratio influence, the results were conclusive (Figure 2.13).

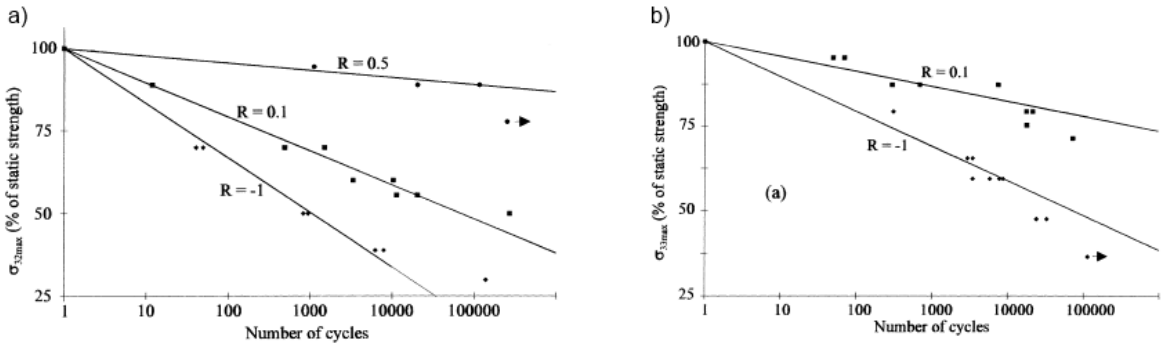

Figure 2.13 - L. Ferry et al. results for bending tests (a) and bending and torsion combined tests (b) in glass fiber/epoxy flat specimens, under different load ratios (13)

None of the tests were performed with a compression-compression load ratio, but the load ratio of R=0,1 for tension-tension and R=-1 for alternated tension-compression show that the stress ratio with compressive loads is more degenerative for the specimens fatigue life, whether it is in bending testing or bending and torsion combined testing. For the bending test only, a load ratio of R=0,5 was also used and is even less degenerative than the other two load ratios. This indicates that for a tension-tension load ratio, a lower amplitude between max and minimum stress may lead to a longer fatigue life.

Regarding load ratio effects on stiffness degradation, there are also differences found in literature. In Figure 2.14 are some results, from De Smet and Bach, for various laminates, including one hybrid glass/carbon fiber, that show that 10% Stiffness degradation is reached

sooner for a load ratio R=-1 than for R=0,1. This mean that the initial stiffness degradation is larger for a load ratio R=-1, and Bach attributed this phenomenon to microbuckling in the regions where voids are present (8). It is also worth noting that for a load ratio R=-1, off-axis laminates seems to have a direct relation between normalized maximum stress and stiffness degradation, but for the load ratio of R=0.1 there seems to be no such relation.

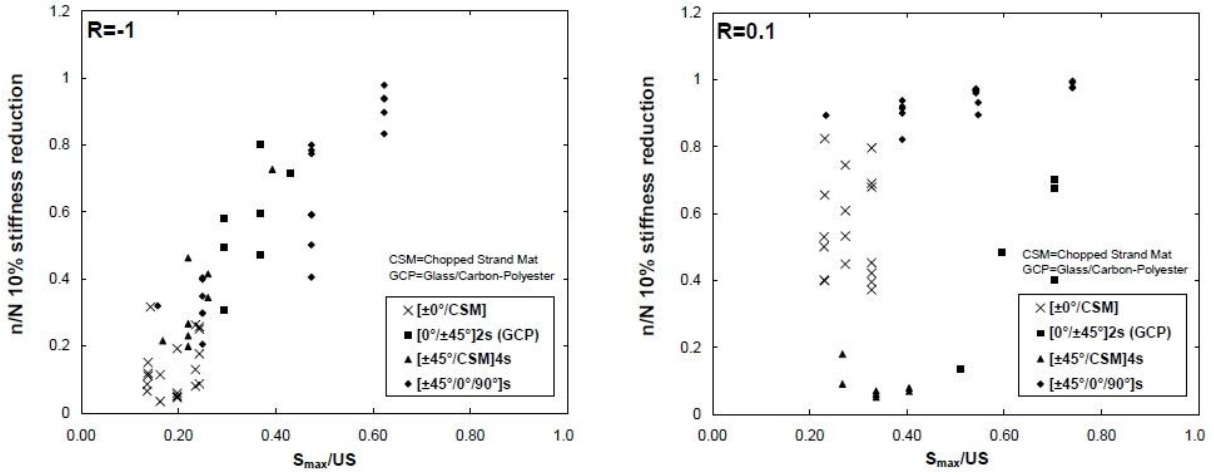

Figure 2.14 - 10% stiffness degradation at normalized life and stress for various glass laminates for a load ratio R=-1 and R=0.1 (8)

2.5.7 Conclusions

After a literature review It is possible to conclude that, generally, for FRP, compressive loads have a much more degenerative influence than tension loads. Therefore, load ratios with $0 \leq R < 1$ It can be expected a longer fatigue life ten other load ratios. Also, positive and negative stresses applied simultaneously are usually more critical then when only one type is applied. The higher the compressive load on the load ratio the shorter is the fatigue life, and therefore specimens tested under a load ratio R of -1 usually exhibit shorter lives when compared to other load ratios (2). This are some general conclusions that can be taken from the fatigue results present in literature, however their applicability to new tests should always be taken with caution, especially when a different specimen shape, resin, fiber and/or fiber-layup is used.

Concerning the specimens that are used in this thesis, since the 0º layers have a mass fraction of 49% (chapter 3.1), and this layer have very good resistance to traction loads, it can be expected that for a load ratio R=0.1 the specimens should perform generally better. The layers at 90º should not perform very well and may start initiating cracks very early, but since they represent only 5% of the specimen's mass fraction, this should not be critical. The 90º layers should also help to delay stiffness loss when compared to a load ratio that contains negative loads. For these reasons, it is decided to increase the load percentage

over static failure for the first specimens, for something between 50% and 60%, and from that first results build a testing plan.

2.6 Non-destructive evaluation

2.6.1 Thermography

Thermography technics are based in the fact that above 0º K (-275.15 ºC) everything radiates thermic energy. This thermic energy is radiated mainly at the infrared zone, which can be captured and recorded with a specific camera. These cameras can capture infrared radiation, which is below the wave length of the visible light, and produce an image somehow similar to a “standard” camera, but with very different information. Figure 2.15 shows an example of an image obtain from the thermocamera during testing.

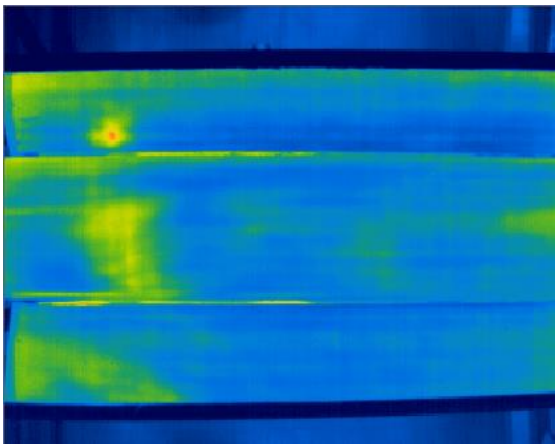

Figure 2.15 – Example of a thermography photo taken during testing, with a visible hotspot in the up reflector

The main advantage of this method for composites testing is that it allows temperature measurement without direct contact with the specimen, which could damage the device when a failure happens. Although the absolute temperature may not be always 100% accurate (depending on the type of camera and the conditions), infrared thermo cameras are very sensitive to temperature differences, which make them perfect for hotspots detection.

To understand the working principle of an infrared camera is necessary to first understand the radiation laws.

Plank law: this law defines the relation between the spectral radiance variation ($W_{\lambda b}$) and the temperature and wave length for a black body (Figure 2.16).

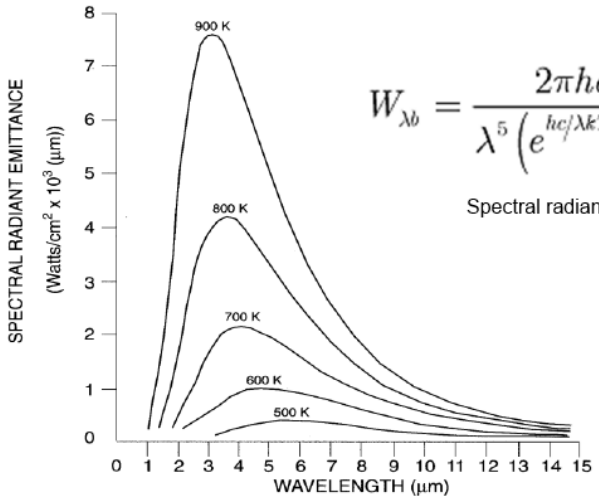

$$W_{\lambda b} = \frac{2\pi hc^2}{\lambda^5\left(e^{hc/\lambda kT} - 1\right)} \times 10^{-6}[Watt/m^2, \mu m]$$

Spectral radiance of a black body with a wavelength of λ.

c	Speed of light = 3 x 10^8 m/s
h	Planck constant = 6,6 x 10-34 J.s
k	Boltzmann constant = 1,4 x 10-23 J/K
T	Absolute temperature (K) of a black body
λ	Wavelength (μm)

Figure 2.16 - Plank law - adaptded from (14)

Wien law: This law relates in an easy way, the body temperature and the wave length, to which the maximum radiance emission is achieved.

$$\lambda_{max} = \frac{2898}{T} \qquad \text{Equation 2.3}$$

The temperature must be given in Kelvin and the result is given in μm.

As the temperature increases, the maximum radiance is obtained for lower values of wave length, and this is the reason why it's used infrared cameras.

Stefan-Boltzmann law: integrating the Plank law for all the wave lengths we obtain the total radiation emitted as a function of temperature of the body:

$$W = \sigma.\varepsilon.T^4 \qquad \text{Equation 2.4}$$

W	Total emitted radiation (W/m^2)
σ	Boltzmann constant (5,8 x 10-^{8} W/m^2.K^{-4})
ε	Emissivity
T	Temperature (K)

The total emitted radiation can be limited or even canceled depending on the capability of emission of radiation from the body. This capability is called emissivity ε and it's a physical property of a body, which can range from 0 to 1.

Real body's radiation: on a real body there are three radiation coefficients, absorption coefficient (α), reflection coefficient (ρ) and transmission coefficient (τ). The sum of these three is the total of the radiation energy.

$$\alpha + \rho + \tau = 1$$ Equation 2.5

Kirchhoff law this law states that emission coefficient (ε) and absorption coefficient (α) are equal to one another, so the expression can be written as:

$$\varepsilon + \rho + \tau = 1$$ Equation 2.6

This allows the application of the Stefan-Boltzmann law to real bodies. In an extreme case, a black body has $\varepsilon = 1$, and ρ and τ are zero. The perfect mirror has $\rho = 1$, and ε and τ are zero. A transparent body has $\tau = 1$, and ε and ρ are zero. But because thermography usually does not apply to transparent bodies, we can write Equation 2.6 as:

$$\varepsilon + \rho = 1$$ Equation 2.7

This means that if we know the emissivity (ε) it's possible to obtain the reflection coefficient (ρ), and therefore determine the temperature of the body. The Table 2.2 shows typical emissivity ε values for some materials.

Material	Emissivity ε
Oxidized aluminum	0.85
Polished aluminum	0.1
Concrete	0.95
White plastic	0.84
Black plastic	0.95

Table 2.2 - Typical emissivity ε values for some materials

Besides the emissivity ε adjustment factor, there are two main constrains when using a thermo camera, the room temperature and, most importantly, the atmospheric absorption (Figure 2.17). For that reason there are usually two types of thermo cameras, the ones that work with short waves and the ones that work with long waves. As one can see in Figure 2.16, short wave cameras take advantage of the stronger radiation, but they are more vulnerable to atmosphere radiation (Figure 2.17). Long wave cameras are more stable, due to less atmosphere interference, but they may not be as sensitive. The thermo camera used for this work is short wave, which makes sense since the atmosphere at testing is closed and temperature controlled. Therefore, a short wave thermo camera will get better results, due to better sensitivity.

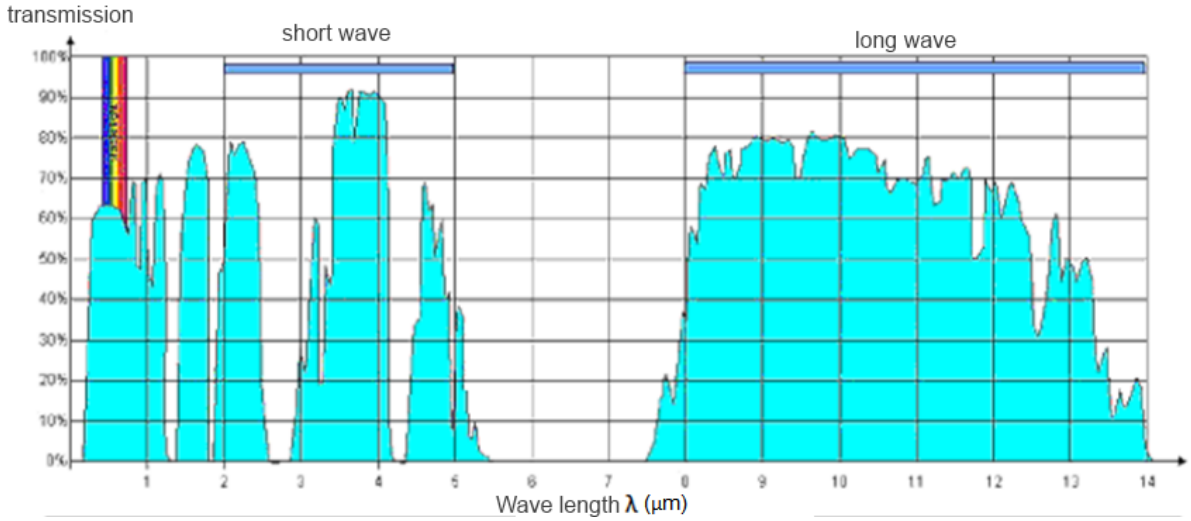

Figure 2.17 - Atmosphere radiation transmission coefficient variation for different wave lengths – adapted from (14)

2.6.2 Crack Counting

Unlike the CFRP, the transparency of GFRP allows the counting of cracks because they become visible as white lines. Although the failure of this material is not only related to the cracks accumulation, they can give information about the state of the material and also the evolution of the crack densities for different load ratios and different stresses applied.

The crack counting is done with pictures taken at 18 different areas on the specimen, taken between fatigue sets, in a microscope outside the testing machine. The number of cracks for every picture is counted with the help of software developed at the institute. This software identifies the orientation of the crack and counts them for the four different orientations: 90º, 45º, -45º and 0º. These orientations are related to the central axis of the tubular specimen (Figure 2.8).

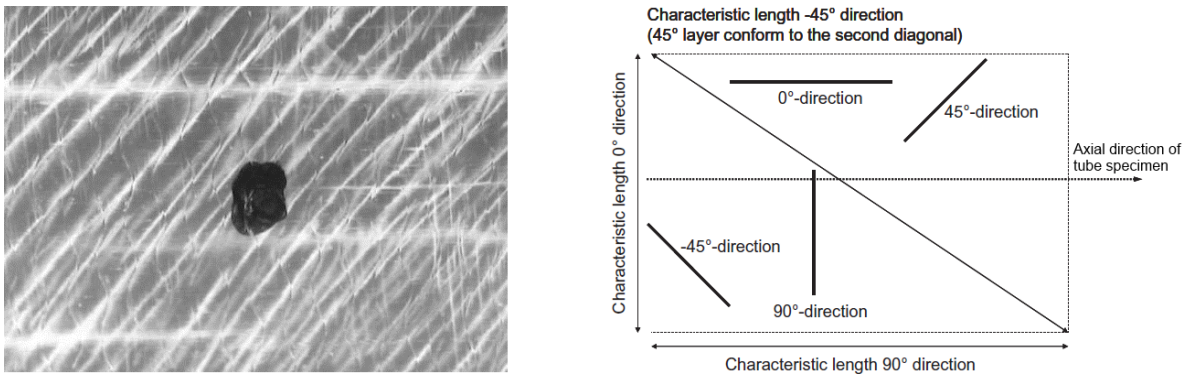

Figure 2.18 - Typical picture for crack counting obtained at microscope (left) and orientation identification (right) – adapted from (1)

The recognition of cracks is made by contrast differences and can be adjusted. The first adjustment is the amount of light when taking the picture. Independently of what is chosen, it should be kept the same for all the following pictures or it may have an unpredictable influence in the results.

The software for crack counting also allows the following adjustments:

- Ranking: is the multiplication between the intensity of the crack and its length;
- Spacing: is the minimum distance between cracks;
- Width: is the minimum width of a crack to be counted.

These adjustments sometimes need to be changed for pictures of different cycles of the same area, to improve cracks counting. Different light with the same adjustment can also lead to different crack counting numbers, so that's the reason why it is better to keep the same light conditions.

For this work all the pictures were taken with two different light intensities. The reason for this is to compare which light intensity is better for crack counting and what adjustments should be made.

3 Specimens Manufacture

In this chapter will be shown the most important information about the manufacturing process of the specimens, such as the properties of the resin and matrix used, the lay-up scheme and the manufacturing process itself.

3.1 Specimen's geometry

The specimens are tubular with 46 mm outer diameter, 328 mm length and approximately 2 mm thickness. At the ends are used 70 mm steel inserts, bonded in the inside, to prevent damage caused by the fixing pressure of the testing machine. There are also non-metallic exterior inserts to fit the grip's dimensions of the machine Figure 3.1.

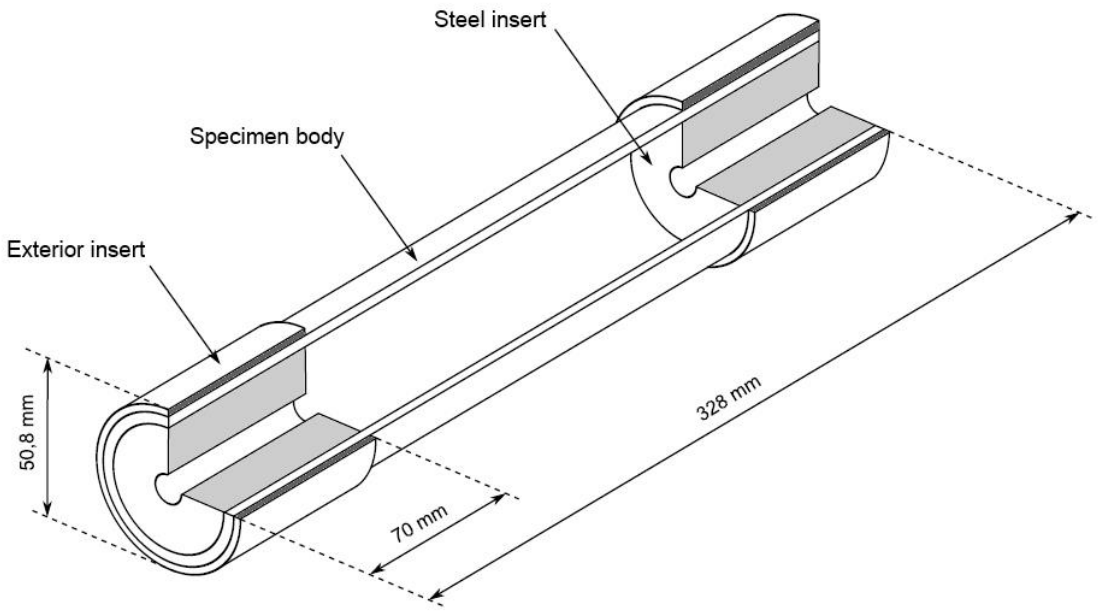

Figure 3.1 - Specimen' dimensitions and insert's position – adapted from (15)

The specimen body are 8 layers with a $[0°/45°/90°/-45°]_s$ lay-up scheme. The 0° layers mean that the fibres are oriented in the axial direction of the tube specimen. The relative mass fractions for each layer can be seen in Table 3.1:

Layer	Orientation (degrees)	Relative mass fraction (%)
1	0	49
2	-45	23
3	90	5
4	45	23
5	45	23
6	90	5
7	-45	23
8	0	49

Table 3.1 - Specimen's lay-up relative mass fractions

3.2 Fibres and Matrix properties

The specimens used are made of E-Glass-fibre roving (Owens Corning OC111A) and a combination of resin/hardener RIM135/RIMH137. The mechanical properties of the matrix and the fibres can be seen in Table 3.2:

Fibre OC111A	
Fibre Young's Modulus (GPa)	80,7
Fibre Tensile Strenght (GPa)	2,56
RIM135/RIMH137	
Modulus of elasticity (kN/mm^2)	2,7 - 3,2
Tensile strength (N/mm^2)	60 - 75
Compressive strength (N/mm^2)	80 - 90
Elongation at rupture (%)	8 - 16
Density (g/cm^3)	1,18 - 1,20

Table 3.2 - Mechanical properties of the resin and the matrix of the tubular specimens (16)

3.3 Manufacturing process

The tubular specimens manufacturing process is Resin Transfer Molding (RTM) and they are produced using a costume made winding machine and molding (Figure 3.2):

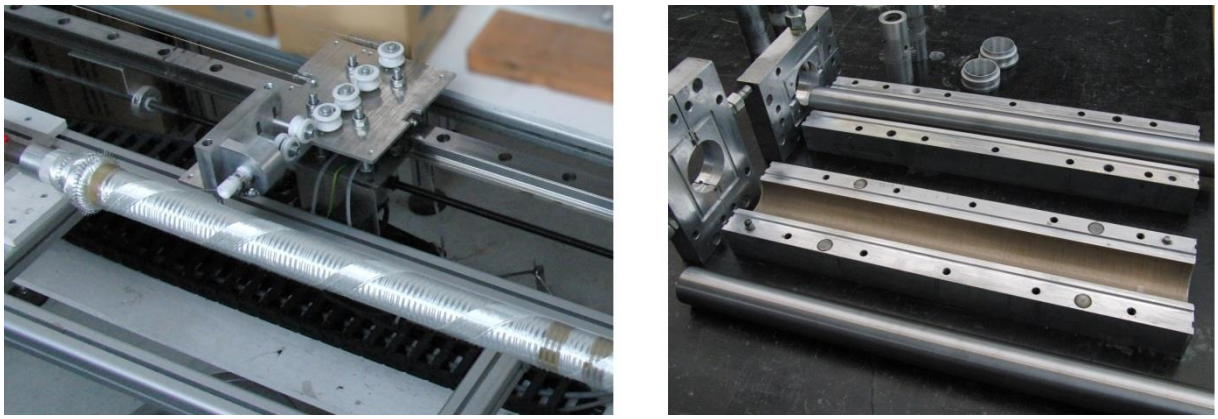

Figure 3.2 - Costum made winding machine (at left) and molds (at right) used for the specimens manufacture - Institut für Flugzeugbau und Leichtbau, TU Braunschweig

This costume made winding machine machine allows the manufacturing of arbitrary lay-ups and the adjustment of the thread tension and ensuring an accurate alignment and tension. After the fibers are being wounded around the cylindrical core they are inserted in the molds for the injection of the resin. The molds and the resin are pre-heated to 40 °C, the cure is made at 60 °C for 2 hours and then the specimen is annealed at 80 °C for about 6 hours.

After this process the thickness of the samples is measured at multiple points and those values are saved. Two rings, one in the upper part and another down are also cut for calcination testing, and the samples are cut to 328 mm. Finally the exterior inserts to fit the testing machine grips are bonded to the specimen.

4 Testing apparatus

In this chapter will be described all the testing setup as well as all the non-destructive evaluation tools used during testing in order to demonstrate their utility but also their weaknesses in fatigue testing control. The specific machines models will be described and their suitability discussed.

4.1 Fatigue testing machine

The fatigue testing was performed with a Servohydraulic Universal-Tension-Torsion Testing Machine MTS 319.25 with circular clamping grips which has an adaptive controller that is able to grant amplitude and phasing in repeating load cycles for both, tension and torsion, even if nonlinear material behaviour is existent (17). The main characteristics of the testing machine are in Table 4.1:

Load	±250 kN
Torsion Moment	±2,2 kNm
Displacement	80 mm
Temperature	Up to 200 °C specimen temperature

Table 4.1 - Servohydraulic Universal-Tension-Torsion Testing Machine 319.5 main characteristics (17)

The loads are applied in the lower grip while the upper grip keeps the specimen in place (Figure 6.8). The fatigue testing area has a surrounding cooling chamber connected to an Air Conditioning to keep the temperature constant. This cooling chamber is opened at the front, where the Thermo camera, the High Speed Microscopy camera and light are placed for the non-destructive evaluation (Figure 4.1).

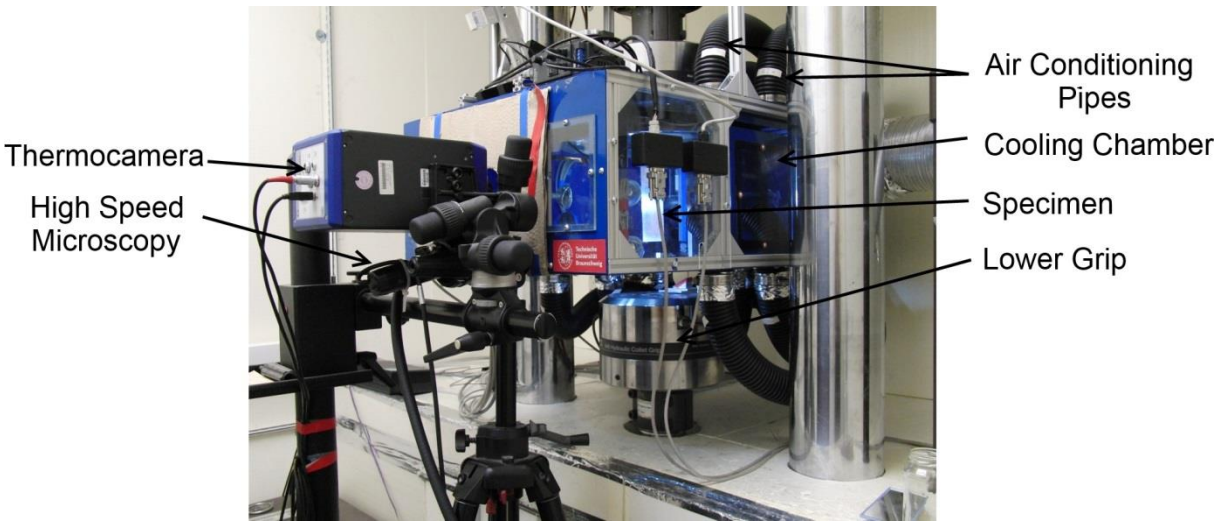

Figure 4.1 – Testing apparatus: MTS 319.25, cooling chamber, Thermo camera and high speed microscopy

Additionally to the machine load and displacement sensors there is also an optical sensor and a reflector, placed at the back of the specimen, which values are also saved during testing for comparison with the values given by the machine.

4.2 Thermography

The temperature is an important factor to fatigue testing because if the temperature is too high can cause thermal damage of the matrix which may influence the final result. Furthermore, it was already said in chapter 2 that using the Thermo camera is possible to locate the area of final failure due to the hot spots on the specimen. To monitor the temperature is used an Infrared Thermo camera “Flir Titanium 520M”, placed in front of the specimen (Figure 4.1). This is a medium wave thermo camera, meaning that the camera is more sensible to temperature variation, but is also more affected by the atmosphere temperature. Since the tests are performed inside a close compartment, with controlled temperature, the medium wave thermo camera is the best solution. On both sides of the specimen are two aluminum reflectors, to visualize the temperature on the back of the specimen, which are also used to the high speed microscopy (Figure 4.2). The main characteristics of the Thermo camera are in Table 4.2:

Cooling type	Integral stirling cooler
Number of Pixels	320 X 256
Spectral Response	3,6 – 5,1 µm
Frame rate resolution	1 Hz step
NETD	<25 mK @ 25 °C (20 mK Typical)

Table 4.2 - Thermo camera main characteristics

4.3 Optical sensor

The Optical sensor is used to compare its values for displacement with the ones from the MTS machine. The sensor model is a “Micro-Epsilon optoNCDT 2200-100” and is placed at the back of the specimen testing area, attached to the upper grip and the reflector is placed on the lower grip, which is the one that moves (Figure 4.2). The reflector is placed at an angle of 30,5° and the measuring point is at a distance of 71,77 mm from the axis of the specimen. Calibrations need to be done regularly since when turning the reflector on its own axis, the trajectory is not completely circular and this error need to be taken in to account when calculating the movement of the lower grip.

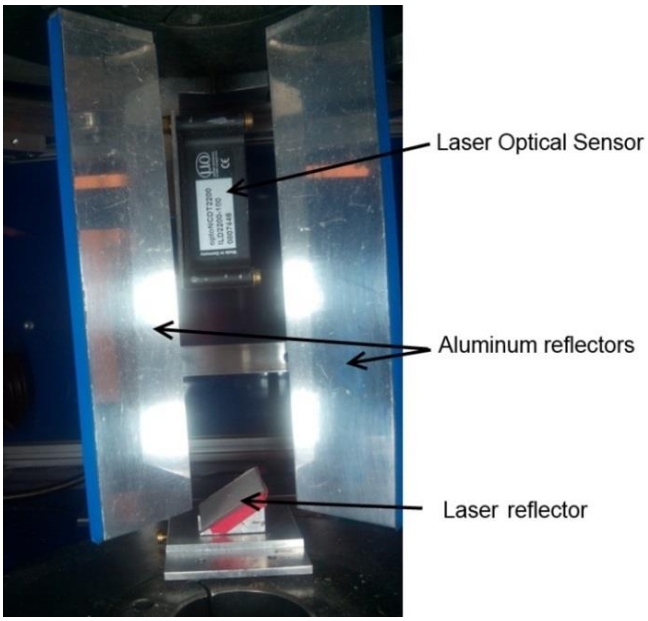

Figure 4.2 - Laser optical sensor and aluminum reflectors positioning inside the cooling chamber

The main characteristics of the Optical Sensor are in Table 4.3:

Measuring Principle	Laser optical triangulation
Measuring range	100 mm
Start of measuring range	70 mm
Midrange	120 mm
End of measuring range	170 mm
Linearity	±30 µm
Resolution	1,5 µm
Light source	670 nm, red (Wave length) 1 mW (Max. power)
Temperature stability	0,01% Full Scale Output

Table 4.3 - Optical sensor Micro-Epsilon optoNCDT 2200-100 main characteristics

4.4 High speed microscopy

The register final failure of the specimen is very important because if the failure occurs on the clamping zone it can mean that the specimen failed not due to fatigue but because of the stress concentration in this area. The High Speed Microscopy controller used is a “Keyence VW-600” and the camera is a “VW-100M” also “Keyence”, and their main characteristics can be found in Figure 4.3. To register the final failure of the specimen is used a looping function of the High Speed camera, which is constantly recording the testing but only saves a few seconds before and after a trigger signal. This trigger signal is only activated when the angle displacement of the machine is higher than the previously entered limit, meaning that the

specimen can't handle the load and failed. This trigger system allows the visualization of the final failure initiation and propagation at a speed of 250 FPS.

Controller recording memory (for high speed)	2 GB
Camera Sensor	Monochrome 1/2" CMOS
Image resolution	640 x 480
Max recording frame rate at 640 x 480	250 FPS
Lamp	80 W metal halide

Figure 4.3 – High Speed Microscopy Keyence VW-6000 Controller and VW-100 Camera and their main characteristics

4.5 Crack counting

Crack counting is performed with a microscope "Zeiss Stemi 200-C", which has a sliding base installed to the specimens (Figure 4.4). This microscope has a camera connected to the computer that allows taking pictures.

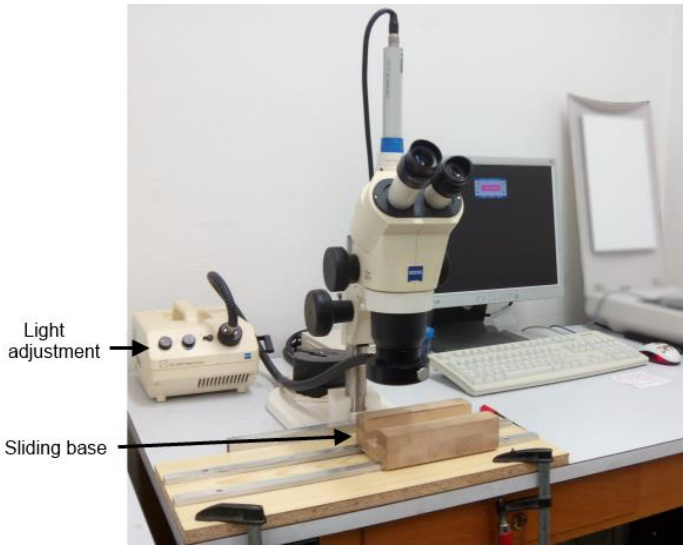

Figure 4.4 - General purpose microscope Zeiss Stemi 200-C

After the pictures are taken is used a software for crack counting, which allows automatic crack counting, but the results are variable and need to be well adjusted.

4.6 Microscopy

Microscopy is used to see cracks and damage of specimen cuts that are considered relevant. With this equipment is possible to see inter fiber fractures to understand with more detail what damage mechanisms happens during fatigue. For sanding and polishing is available a “Struers Labopol” with two speeds : 250 rpm and 500 rpm. To cleaning between polishing steps is used an ultrasonic bath with “Sonorex Digitec DT 52”. The microscope is a “Keyence VHX-600”, which is capable of taken pictures with good resolution and also has lots of different software modes and different lenses to improve pictures quality and contrast. All this machines can be seen in Figure 4.5.

Figure 4.5 – From left to right: ultrasonic bath Digitec DT 52, Sanding machine “Struers Labopol” and microscope “Keyence VHX-600”

4.7 Calcination

Calcination is used to determine fiber content and it’s a relatively simple test. It requires only calcining vessels, a very precise scale and a woven able to reach 600 ºC (Figure 4.6).

Figure 4.6 - Calcination woven (at left) and precision scale with a calcining vessel inside (right)

5 Procedures

In this chapter will be described all the steps taken in the testing procedures and their previous preparation.

5.1 Specimen preparation for testing

After the manufacturing process (chapter 3.3) the specimens need some preparation to be tested. The specimens have their thickness measured in 252 equally distant points that are marked along the central axis with numbers, and along the diameter with letters. After measure, the ends are cut off, leaving the inner part with 328 mm (Figure 3.1), and the exterior inserts at the ends are put in place, which will function as a clamping area for the machine grips (Figure 5.1).

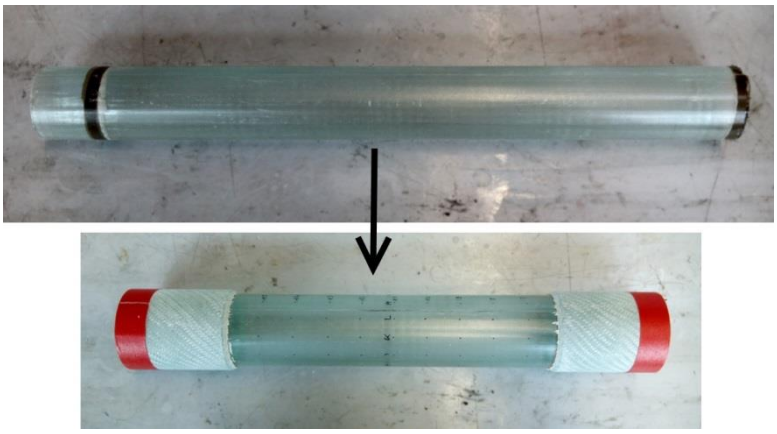

Figure 5.1 - Specimen's after the molding process (up) and after cut with the outer inserts (down)

The ends that are cut off are also marked with the letter and numbers and are kept for calcination testing. For the specimen to be ready for testing also needs the steel inserts (Figure 5.2) in the inside of the clamping zone, to avoid damage by the machine clamping pressure. The steel inserts are drilled to avoid internal pressures when bonding and also allow the placement of black paper inside the specimen.

Figure 5.2 - Steel insert before bonding

In order to reduce the probability of the insert to start to debond from the specimen, the steel inserts are bevelled on the inside (Figure 5.2), and when gluing, some extra adhesive is also used in this edge. This two technics are known to improve adhesives lifespan (3).

The resin/hardener combination used is Araldite AW 106 and HV 953 U with a mix ratio of 100 resin weight parts by 80 hardener weight parts. All the surfaces that are about to be bonded are previously cleaned with acetone and curing is done at room temperature for about 12h.

After gluing the steel inserts a black paper is inserted on the inside of the specimen to avoid reflections when taking photos take at the microscope and also to improve the cracks visibility at the naked eye.

Before the first cycle, the specimen is taken to the microscope to take initial microscopy photos. There are taken pictures of 18 different areas, to try to cover a wide area of the specimen. When choosing the points to microscope photos a red mark is made so that finding these points in the future is easier. Photos all around the specimen with a regular photographic machine are also taken previously testing so that the global initial state of the specimen is recorded.

A new protocol is also created for the specimen, which includes the points where the crack's pictures are taken, the distance between the outside inserts, the medium thickness and radius, the area, the loads applied, the calibration number for the laser, and other annotations.

5.2 Fatigue testing

5.2.1 Testing schedule preparation

Since there were no previous tests conducted in this tubular specimens for a load ratio of R=0.1, the loads for first tests were estimated taken in to account the previous tests with the load ratio R=-1 and also the literature, which showed that for a load ratio of R=0.1, fatigue behavior usually improves when compared to a load ratio of R=-1 (chapter 2.5). The fatigue tests are multiaxial; meaning that there will be shear and tension stresses applied simultaneously. In order to distinguish between different multiaxial load cases a biaxially load ratio β is used as follows:

$$\beta = arctang\left(\frac{\tau}{\sigma}\right) \qquad \textbf{Equation 5.1}$$

For the case of β=0° the loads are pure tension (tension/compression if a different load ratio R is used) and for β=90° the load is pure shear. The biaxially load ratios used in this work are a combination of tension and shear, β=30° for a predominant tension stress, and β=60° for predominant shear.

To fulfil the Standard ASTM E739-10 requirements, a minimum number of 6 specimens for each load angle β must be tested, as this work fits as a "Research and development testing of components and specimens" (18). For this case the standard also requires replication of the load used in different specimens from 33% to 55%. The replication percentage is calculated as follows:

$$\%\, replication = 100\left[1 - \frac{Number\ of\ different\ stresses}{Number\ of\ specimens}\right] \qquad \textbf{Equation 5.2}$$

The factor chosen to claim that a test is a repetition is the load over static failure, so for every percentage two specimens were chosen. However, since the loads applied are normalised for the specimen's fiber content, and every specimen is slightly different, it's difficult to say with certainty whether a test is a repetition, or just very similar. This is even more critical when the calcination tests give different values from the values that were first predicted analytically and used for the loads calculation, meaning that the real percentage over static failure is also different from the one pretended.

As the fatigue testing consists in load cycles applied to a specimen below its failure limit, several tests were conducted previously at the institute with this kind of specimens to determine the static failure load for the different multiaxial cases (Table 5.1). Previous fatigue tests with a load ratio R=-1, done with a 43% load over static failure had a lifespan of around 34.000 cycles, for β=60° (1). For β=30° a load of 41% over static failure lead to a lifespan of just 11000 cycles (1). However, as it was referred in chapter 2.5, a load ratio of R=0,1 is expected to cause less harm, so, for the first tests, the load percentage over static failure is increased to 55% for both loading angle β of 30° and 60°. Then, based on these first results and on the standard, a testing plan is built.

The first specimen for β=60° was the W1RP-367 and had a lifespan of 37686 cycles for a load of 55% over static failure. When this first specimen had more than 25000 cycles a second specimen (W1RP-389) was started with a load of 60% of static failure load. This second specimen last a merely 5991 cycles and therefore no tests with a higher percentage of 60% over static failure were performed. From these two results was decided to do a test with an intermediary load of 58% and one with a lower load of 52%, making a total of 4 different loads. To meet the standards repetitions requirements, all these loads were

repeated with another specimen, making a total of 8 specimens and a replication percentage of 50%. After finishing these first 8 tests, and since the specimen with the bigger lifespan had just 64663 cycles, another test was performed to obtain a lifespan over 100000 cycles. The loads for this test were calculated using the S-N curve build with the first 8 tests. Unfortunately, due to some problems with the machine, this last test was not finished in time for this work. It was tested successfully until 99000 cycles, but since there is no failure, the data collected is not valid for S-N curves purposes.

The first specimen for β=60° was the W1RP-370 and had a lifespan of 9478 cycles. From this point was decided that 55% over static failure was the higher percentage for fatigue testing for β=60° and for the next specimens it will only go lower. The following percentages were used: 55% (first specimen), 52%, 49% and 47%, making a total of 4 different loads. Unfortunately the first result for β=60° (W1RP-370) was misleading and all the specimens tested after had a lifespan shorter than expected (this will be further discussed in chapter 6).

Once again, to comply with the standard all the tests were repeated, making a total of 8 specimens, and the results were fairly constant, although that the specimen with the higher lifespan had a merely 26430 cycles. One attempt was made to have at least one specimen with a lifespan over 100000 cycles, and the loads were estimated using a S-N curve with the previous tests. This last specimen was estimated with a percentage of 43% over static failure load for 120000 cycles but failed soon after 36000 cycles, and caused the S-N curve to become even steeper. Unfortunately, due to the lack of time, this test was not repeated and no further specimens were tested to achieve the 100000 cycles mark.

When choosing the specimens for testing, a visually inspection is performed to guarantee that they have good geometry and, preferably, no visible voids. However, in a RTM manufacturing process, the presence of manufacturing defects, such as voids, is unavoidable. Therefore, the specimens chosen may contain a small number of voids, as long as they are not concentrated in a small area, and small geometry defects, especially in the joint of the moulds. Since this kind of defects are normal for the RTM process, and therefore, as long as the defects are not very extensive, specimens will be tested as they are.

5.2.2 Loads calculation

The fatigue testing is load controlled, so the first step is to calculate the shear and tension stress that will be applied. The loads are calculated based on a percentage of the static failure load of similar specimens previously tested, and the results are in Table 5.1.

B (°)	R_t (MPa)	R_t Standard deviation	R_s (MPa)	R_s Standard Deviation
0	534,7699072	19,98347433	0	0
15	502,5849155	6,994432597	134,8554705	1,992755177
30	330,2445974	9,855996522	190,3820329	5,188930299
60	97,10786766	1,858167499	166,5490186	3,296999103
90	0	0	144,5504103	3,851076774

Table 5.1 - Static failure load limits for the tubular specimens previously tested at the IFL

As mentioned in the Testing schedule preparation, a percentage of the loading over the static failure is used, and with this percentage is obtained the stresses for the testing.

$$\sigma = R \times (\%\ over\ static\ failure) \quad \text{Equation 5.3}$$

This stress obtained must be normalized for a fiber volume content of 0.5, taken into account the fiber volume content ϕ of the specimen, estimated analytically.

$$\sigma_{norm.} = \frac{\phi}{0{,}5} \times \sigma \quad \text{Equation 5.4}$$

The analytical estimation of the fiber volume content is calculated using the thickness average from the 252 measured points.

$$\phi = \frac{132{,}0165054}{\pi . 46 . t_{ave.} - {t_{ave.}}^2} \quad \text{Equation 5.5}$$

Now that $\sigma_{norm.}$ can be calculated, normalized shear stress $\tau_{norm.}$ can also be obtained with Equation 5.1, using the biaxially load ratio angle β of 30º or 60º, depending on the case.

Now that the stresses are calculated, the necessary loads to introduce on the MTS machine can be obtained with Equation 5.6 for normal stress σ and Equation 5.7 for shear stress τ.

$$F = \sigma \times a \quad \text{Equation 5.6}$$

$$Mt = \tau \times 2\pi \times r^2 \times t_{ave} \quad \text{Equation 5.7}$$

Since the load ratio R=0.1, the minimum loads can be easily obtained with Equation 2.1. The frequency is the same used in previous works - 3 Hz (1).

After the calcination tests new values of fiver volume content will be obtained, and therefore the loads that are applied will correspond to different percentages of load over static failure. This will be calculated and discussed in chapter 6.

5.2.3 Testing procedure

The fatigue testing in this work is performed with several steps. As mentioned before, tests need to be stopped to take the specimen out and taking pictures at the microscope. This means that the tests are separated in sets, which are repeated until the specimens fails. The number of sets will therefore correspond to the number of microscope photos available for crack counting. The first sets have a lower number of cycles between them, and this number increases as the number of cycles increases. In Figure 5.3 is represented a scheme of the testing procedure.

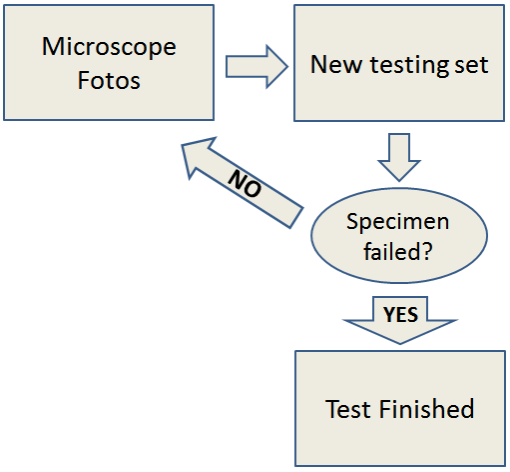

Figure 5.3 - Fatigue testing procedure

Inside every set, the cyclic loading also has several stops for characterization steps. In Figure 5.4 is represented the testing scheme inside every set. This testing scheme is repeated until the set is finished or the specimen fails. The characterization steps also apply loads to the specimen, much lower than the one applied for fatigue damaging, however enough for calculating young's and shear modulus. The loads applied in a characterization step are $\pm 12.5\ \mathrm{kN}$ of force and $\pm 100\ \mathrm{N.m}$ of torque.

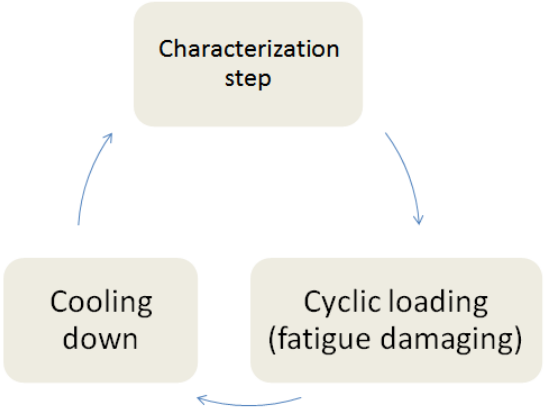

Figure 5.4 – Testing procedure for every set

During the cooling down, the temperature is cooled to 19 ºC. Through the cyclic loading the specimen warms up due to the applied loads, but the air conditioning and the cooling chamber keep the surface temperature of the specimen refrigerated, and never exceeds 30 ºC (except if there is an hotspot). This ensures that there is no damage caused by excessive temperature.

The testing scheme followed is similar scheme to the ones used before at the institute. Some studies in the revised literature (2) revealed that when the fatigue testing isn't continuous, such as the one performed here, the results can be different from of the same fatigue testing performed continuously. This can also mean that different pauses between fatigue testing can have different results. For this reason, the specimens were tested with a set scheme that was the same to all of them, and is showed in Table 5.2. There are, however, some specimens that were exceptions to this scheme, which will be shown in chapter 6.

Set	Characterization steps	Fatigue cycles between characterizations	Cycles per set	Total number of cycles for the specimen
1	5	10	50	50
2	3	50	150	200
3	3	100	300	500
4	5	100	500	1000
5	20	100	2000	3000
6	20	100	2000	5000
7	20	200	4000	9000
8	40	200	8000	17000
9	40	200	8000	25000
10	50	200	10000	35000
11	80	200	16000	51000
12	80	200	16000	67000
13	120	200	24000	91000

Table 5.2 – Used number of cycles and characterization steps per set

The definition of failure in a composite isn't always clear, and depends on the kind of test or usage. However, for this case, failure is defined as the instance when the specimen can no longer bear the intended fatigue load, causing a partial separation of parts of the specimen, until the testing machine reaches one of the its motion limits and shuts down.

As it was said in chapter 4.3, calibrations to the laser need to be done regularly, and if the last calibration as more then 3 or 4 specimens tested, a new one should be performed. This calibration consists in record the reflector deviation from its own axis, by rotating it manually with the machine stopped, and recording the displacement found. When a test is performed,

the deviation on the reflector own axis can be distinguished from the movement of the testing machine while testing.

Before starting the MTS machine, the Thermography and the High Speed Microscopy are prepared and started. A trigger box connected to the computer sends signals to this two cameras, so that they start recording at the right time.

5.3 Crack counting

As it was mentioned in subchapter 5.1, before the first set of fatigue testing are taken 18 microscope photos to different areas, and subsequently at the final of every new set. These 18 points are chosen so that they cover a wide area of the specimen but avoiding the areas with visible defects or cracks. For every one of the 18 areas chosen, two pictures were taken, one with more light and one with less. The aim of having the same photo with different light is to evaluate later, on the software for crack counting, which photos produce better results. The pictures are first run through a *Matlab* script that makes them centered and equal sized. This step is made to eliminate differences between photos that could influence the crack counting results.

Once the pictures are ready for the crack counting software, the first important decision for counting the cracks is to choose whether to use the pictures with more light, less light, or a combination of both. For the first cycles, pictures taken with more light give better contrast for cracks viewing, making it a slightly easier to count them, even without the software. But sometimes, because the cracks are white and reflect the light, pictures taken with more light become too bright. This makes very difficult to count cracks properly, either manually or with the software. So, it is clear that after some cycles, the pictures with less light are preferable to the ones with more light.

However, although less light improves legibility, it does not solves the problem completely, because the problem is not only the amount of light reflected on cracks, but the cracks them self's. As the number of cycles increases, cracks grow in width and length, overlapping them self's, making it difficult to distinguish from one another's. This happens no matter with which amount of light the picture was taken, the crack counting will always be difficult and even a little bit subjective. However, as it was said, darker pictures do improve legibility, and in some cases, when the picture with more light has become too bright, are the only solution to count the cracks that otherwise would be completely obfuscated. This is visible in Figure 5.5 for example. In the picture with more light, some parts of the bottom have become completely white and impossible to see cracks, unlike the picture with less light, which remains visible.

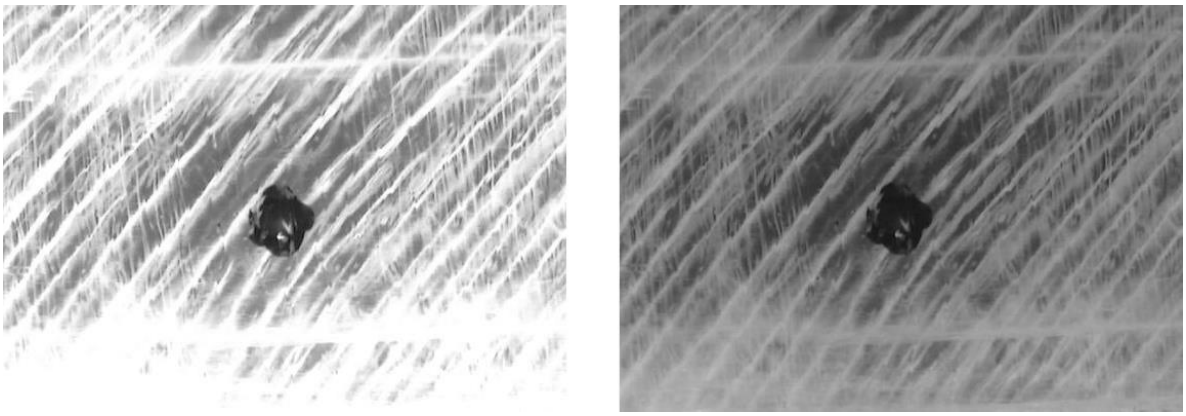

Figure 5.5 - Difference between pictures with more light and less light for crack counting, specimen W1RP-371 with 35000 cycles

So the best solution could be to start taking pictures with more light and after some cycles, change to less light. Yet, the ideal transition point from lighter to darker pictures is not very clear. Indeed, it can happen that for the same specimen and number of cycles, a picture taken with more light in one area can be already too bright, but the picture of a different area still has good contrast. Or even that the pictures with more light have good contrast until the specimen fails, making it unnecessary to have pictures with less light. This being said, it's clear the difficulty of knowing when to use pictures with less light or more light.

The solution found was to always use pictures with less light. After some experimentations, it has been concluded that pictures with less light in the first cycles, with the right adjustments, can produce the similar results for the first cycles that the ones with more light. This is very important because it is in the first cycles that the number of cracks changes more rapidly. And as the cracks accumulate and grow, the pictures with less light only get better for crack counting, since there will be no excessive brightness.

To adjust the crack counting parameters, the principal initial condition established is that all the crack counting must be zero, or very close to it, for all the pictures, before the specimen is loaded with any fatigue cycle. For this reason becomes clear that it's very important, when choosing the area for the picture with low light, that they have no defects.

The second condition is that after the third set, the number of cracks counted by the software should be very close to the number of cracks counted manually. This can be done for pictures with more cycles, but the more the cracks spread, the more difficult it is to see and count the cracks manually. Also, it's usually the first cycles that most of the cracks appear. This second condition is the most important for the reason that is the one that demands more adjustment to the parameters. The orientation of +45º is the one with more cracks and therefore, to match the manual counting, has a lower ranking. The cracks with -45º have the highest ranking because there are very few cracks in this direction. The spacing between

cracks was increased relatively to the ones used before for other experiments, except for 0º, which was already very high. This has improved the cracks counting by avoiding counting the same crack twice when it enlarges. The final parameters used are in Table 5.3:

Direction	Ranking	Spacing
0º	40	20
+45º	20	16
90º	62	15
-45º	70	16

Table 5.3 - Crack counting software parameters

This rankings used in the beginning are kept constant until the final picture, for two reasons: first because it is used the pictures with low light, so there are no reflections in the cracks, and the amount of brightness is kept constant; second is because, to have a crack counting of zero for pictures with less light in the beginning, the ranking is already set relatively high, except for the cracks with +45º.

The crack density is calculated for every crack direction and for every set, so that it is possible to monitor the development. The average number of cracks, for a direction, for all the pictures of the specimen, for each set, and divided by the characteristic length of the crack direction, in mm.

$$CD = \frac{Average\ number\ of\ cracks}{Characteristic\ length} \qquad \text{Equation 5.8}$$

These characteristic lengths (Table 5.4) are simply the size of the picture's area taken for the crack counting (Figure 2.18).

Direction	Length (mm)
0º	5.2
90º	7,05
+45º / -45º	8,76

Table 5.4 - Reference crack lengths

5.4 Calcination

As it was mentioned in chapter 5.1, the rings cut from the ends of the specimen are kept for calcination. In order to achieve good results, the specimens cuts, obtained during the specimen preparation, are dried in the woven for 12h at 85ºC, and then are kept in a sealed container with silica inside, while cool down. The silica helps to keep the rings dry. The calcination procedure takes the following steps:

- The calcining vessel is whipped with paper and weighted;

- The composite ring, previously dried and cooled down, is placed inside the calcining vessel and are weighted;
- Calcining vessel with the ring goes to calcination woven at 600 ºC for around 2h;
- Calcining vessels are placed inside a glass container with silica for cool down, for at least 1h;
- Final weight after calcination is measured and the fibers are thrown away.

All the weightings are performed twice, and the machine must return to zero in between measurements. The weight used for calculations is the average of the two weights. All the weights are registered in a protocol, with the respective time and date of the measurements. Calcination tests are performed according to the European standard (19).

The fiver volume content ϕ is then calculated using Equation 5.9. To have the fiber volume content in percentage, the calculated value should be multiplied by 100.

$$\phi = \frac{1}{1 + \frac{Fiber\ density}{Resin\ density} \times \frac{m_1 - m_2}{m_2 - m_3}} \qquad \text{Equation 5.9}$$

m_1 (g)	Composite ring plus calcining vessel
m_2 (g)	Fibers plus calcining vessels (after calcination)
m_3 (g)	Calcining vessel

5.5 Microscopy

In order to see cracks internally, the tested specimens are cut, with the cut being made on the place that is to be observed, and properly identified. The piece cut is then placed inside a small mould, with the cut side that is to be observed, placed to the bottom. The mould is then filled with resin/hardener combination of Mgs lr285 and Larit 287 blue, with a mix ratio of 100 resin weight parts by 40 hardener weight parts. The cure is performed during night (more than 10 hours) at room temperature. After cure, the specimen is demoulded and begins the polishing of the bottom. Preparation for microscopy is performed in several steps:

- Sanding with sandpaper 220 at 500 rpm;
- Cleaning with water;
- Sanding with sandpaper 500 at 500 rpm;
- Cleaning with water;
- Sanding with sandpaper 800 at 500 rpm;
- Cleaning with water;
- Sanding with sandpaper 2000 at 500 rpm;
- Cleaning with water;

- Polishing with “Largo Plate” and 9 μm Fine grinding liquid;
- Cleaning with the ultrasonic bath;
- Polishing with 3 μm liquid;
- Cleaning with the ultrasonic bath;
- Polishing with 3 μm liquid;

After polishing, the specimen ring is then taken to the microscope to take photos.

5.6 Thermography

The thermo camera is triggered in the beginning of every cyclic loading and stopped at the end. It records 1 frame per second, with the temperature information on the specimen and on the reflectors. As it was mentioned, these pictures are used to check for hotspots that indicate the initiation of the final failure. The data of the temperature obtained for the specimen area only is then compiled to obtain 3 different parameters:

- Initial temperature;
- Final temperature;
- Average temperature.

6 Results and discussion

In this chapter the results will be presented, discussed and compared with previous works. Due to the very high amount of data from testing, in some chapters are only shown one typical result per load angle case, and the remaining results are in the Appendix.

6.1 Specimen's tested

A total of 18 specimens have been tested, 9 for a load angle of β=60º and other 9 for β=30°. Two of these 18 specimens were considered invalid, one due to bad failure and the other is a run out (no failure). The other 16 specimens are resumed in the following Table 6.1:

Specimen	Load Angle β (°)	ϕ	Normal Stress (Mpa)	Shear Stress (Mpa)	Cyclic load over static failure (%)	Lifespan (cycles)
W1RP-411	60	0,504	56,7	98,2	58,4	10606
W1RP-389		0,525	58,0	100,4	59,7	5991
W1RP-334		0,530	56,3	97,6	58,0	38123
W1RP-402		0,507	55,0	95,3	56,7	15901
W1RP-367		0,493	53,8	93,2	55,4	37686
W1RP-400		0,489	53,0	91,8	54,6	23354
W1RP-381		0,523	50,8	88,0	52,3	64663
W1RP-405		0,517	48,4	83,8	49,8	25048
W1RP-370	30	0,530	187,7	108,4	56,8	9478
W1RP-409		0,505	171,5	99,0	51,9	3070
W1RP-407		0,516	168,4	97,2	51,0	6334
W1RP-403		0,517	159,2	92,3	48,2	11481
W1RP-404		0,506	160,3	92,5	48,5	13379
W1RP-406		0,504	150,7	87,0	45,6	26430
W1RP-413		0,503	159,1	91,9	48,2	12939
W1RP-371		0,530	144,6	83,5	43,8	36042

Table 6.1 – Loading programme, fibre-volume and lifespan of all the specimens tested and validated

All the Stresses represented in the table are normalized for a specimen with 50% fiver volume content. These results were calculated using Equation 5.4 with the results from the calcination test (Table 6.4).

6.2 Stiffness degradation

When a new fatigue set is started, the first characterization step gives bigger values for shear and young's modulus, comparatively to the last characterization and also to the following. This happens for both load cases of β=60º and β=30º and a typical result with this phenomenon is shown in Figure 6.1. This phenomenon can be explained by the materials relaxation, which is possible because the fatigue testing is paused. Vassilopoulos and Keller already demonstrated that for fatigue testing in FRP, the lifetime for specimens tested with pauses, can be up to 1.4 times longer than for specimens continuously loaded (2). When a fatigue testing is paused, the material can recover some of their initial properties, which gives it more resistance to the following cycles.

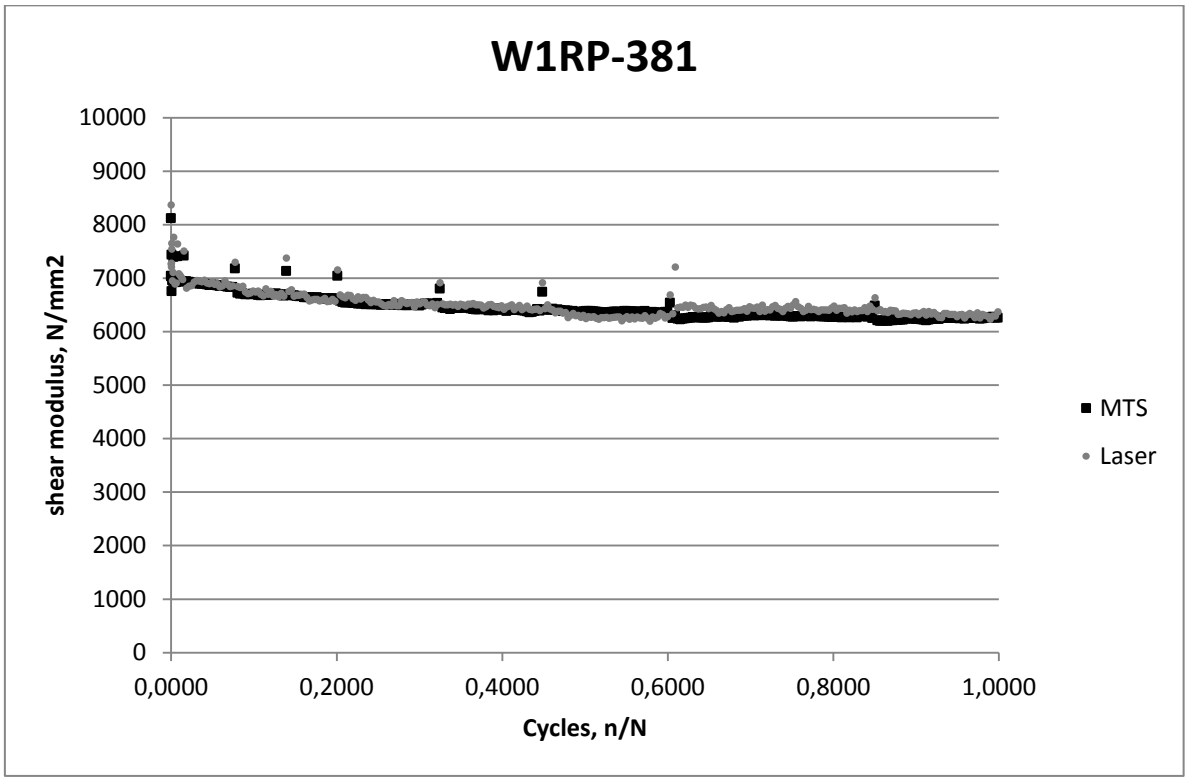

Figure 6.1 - Shear modulus degradation for negative shear stress for specimen W1RP-831

These values for the first characterization steps are therefore eliminated for further evaluation and comparison with previous works.

In Figure 6.1 is also visible some differences between the data given by the MTS machine and the optical sensor laser. The optical sensor as a very good precision (Table 4.3), but probably due the measures necessary (the distance to the center axis of the machine and angle of the reflector) and also the calibrations that needs to be done from time to time, this can increase error in the measurements. Furthermore, the results of the optical sensor sometimes seem to vary randomly for different characterizations, inside the same set, which

may indicate that there are not only systematic errors. Overall, the MTS machine gives more consistent values and is therefore used for all the results shown from this point.

6.2.1 Load angle β=60°

The average initial young's modulus for the specimens tested with a load angle β=60º is 25620 Mpa and the average shear modulus is 7195 Mpa. Both shear and young modulus suffer degradation throughout the test, but is more pronounced for the shear modulus. On average, the young's modulus suffers a decrease of 6,2% with a standard deviation of just 0,4% and the shear modulus 12,9% with a standard deviation of 1,7%. These degradation percentages are therefore very consistent for all the specimens tested.

	Cycles	Young's modulus, N/mm2			Shear modulus, N/mm2		
β=60°	**N**	**Initial**	**Final**	**Decrease (%)**	**Initial**	**Final**	**Decrease (%)**
W1RP-411	10606	25589,7	23890,9	6,6	7278,0	6479,9	11,0
W1RP-389	5991	26183,6	24458,1	6,6	7322,0	6405,4	12,5
W1RP-334	38123	26276,3	24635,4	6,2	7484,4	6497,3	13,2
W1RP-402	12939	25054,4	23570,1	5,9	6909,0	6090,9	11,8
W1RP-367	37686	25256,3	23616,2	6,5	7020,9	5974,7	14,9
W1RP-400	23354	24685,3	23220,6	5,9	6872,3	5955,6	13,3
W1RP-381	64663	26315,3	24940,8	5,2	7386,4	6215,7	15,8
W1RP-405	25048	25599,1	23954,9	6,4	7287,6	6532,6	10,4
	Average	**25620,0**	**24035,9**	**6,2**	**7195,1**	**6269,0**	**12,9**
	STD	**565,6**	**552,5**	**0,4**	**214,5**	**224,8**	**1,7**

Table 6.2 - Stiffness degradation for the load angle β=60º

In comparison with results obtained for a load ratio of R=-1 with the same load angle β, the degradation of the both modulus for R=-1 is more pronounced, with 11,7% with a standard deviation (STD) of 2,2% for young's modulus, and 26.7% with a standard deviation of 4,1% for shear modulus.

In Figure 6.2 is shown typical stiffness degradation for this load case, with specimen W1RP-367, which has a lifespan of 37686 cycles. Both moduli show a rapid decrease within the first 10% of the life span (phase I of fatigue life) and then stabilize to a linear decrease (phase II and III of fatigue life). Shear modulus decrease however has a faster decrease, as one could expect from the 12,9% average decrease.

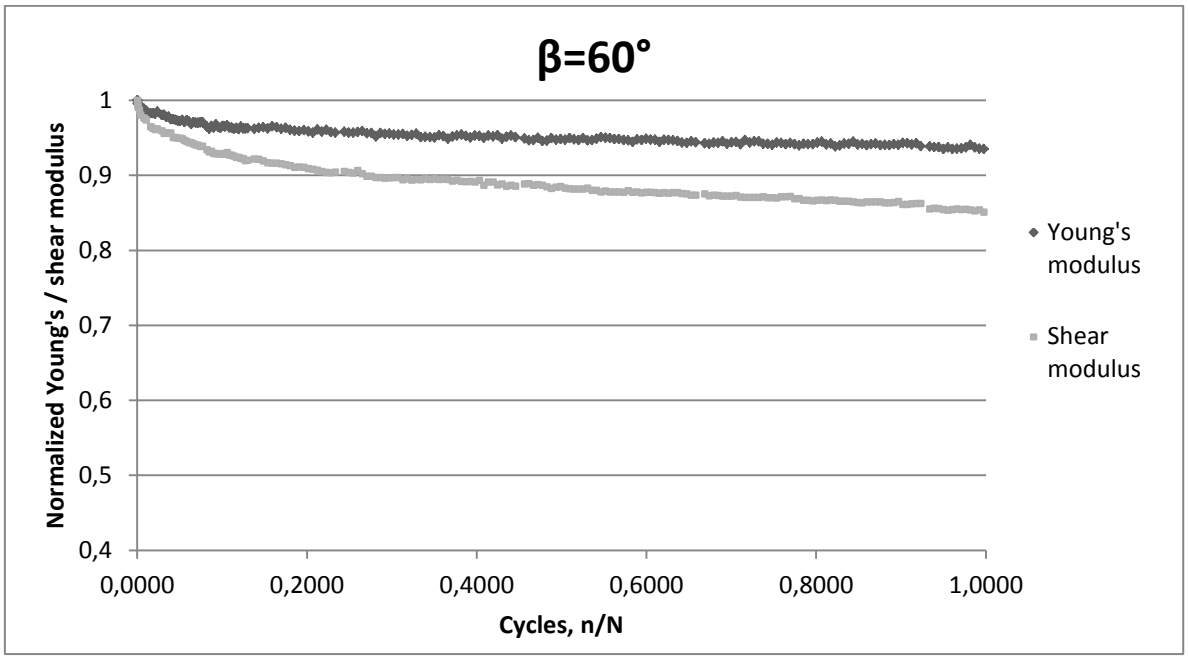

Figure 6.2 – Typical Shear and Young's modulus degradation for β=60º (specimen W1RP-367)

In Figure 6.4 and Figure 6.19 are the comparison between two typical results for a load ratio R=-1 and for the and R=0,1. The specimen for the load ratio R=0,1 is the same as in Figure 6.2, and, as it was said, the life span is 37686 cycles. The specimen for the load ratio R=-1 is the W1RP-137 and has a life span of 33987 cycles, only slightly inferior. In both cases, young and shear modulus, the load ratio R=-1 has a more pronounced decrease. This is the result expected, as many other experiments, reviewed in literature, showed similar behavior.

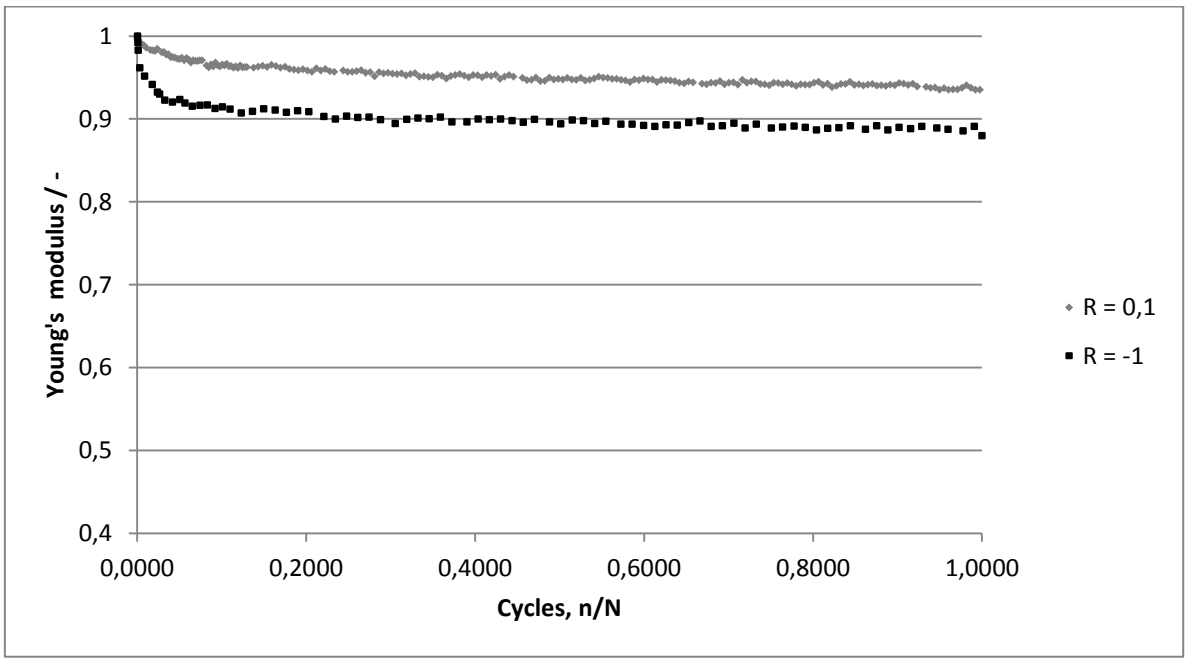

Figure 6.3 – Comparison of the young's modulus degradation between load ratios R=-1 (W1RP-137) and R=0,1 (W1RP-367) for a load angle of β=60º

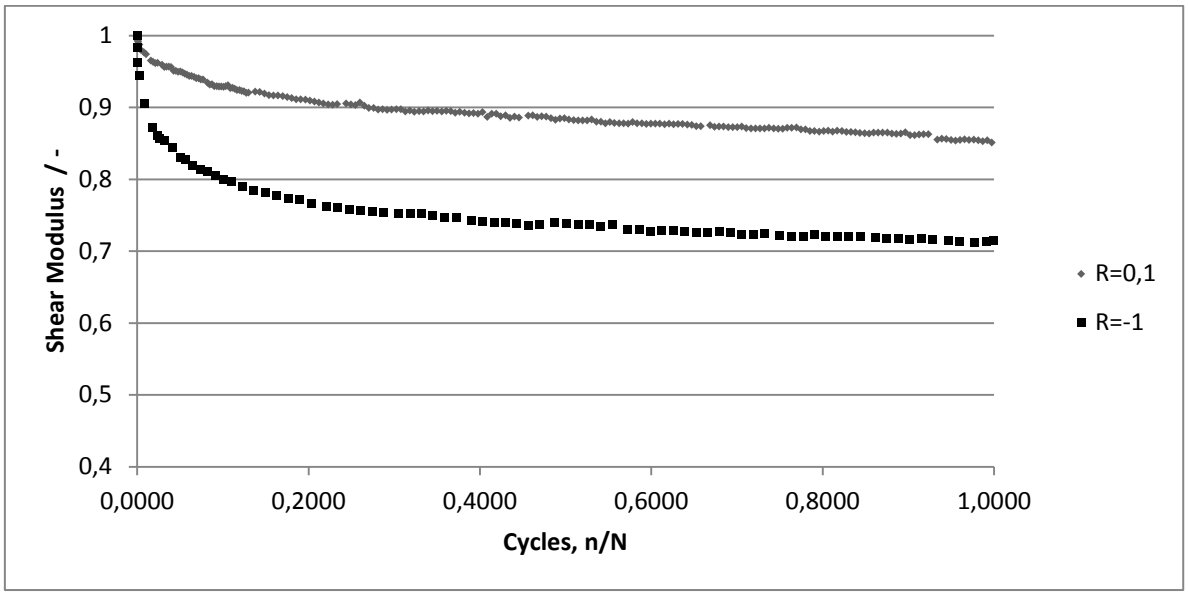

Figure 6.4 - Comparison of the shear modulus degradation between load ratios R=-1 (W1RP-137) and R=0,1 (W1RP-367) for a load angle of β=60º

6.2.2 Load angle β=30°

The average initial young's modulus for the specimens tested with a load angle β=30º is 25957 Mpa and the average shear modulus is 7421 Mpa. Like the load angle β=60º, for the angle β=30º both shear and young modulus suffer degradation throughout the test, and is also more pronounced for the shear modulus, although the difference is lower than for the load angle of β=60º. On average, the young's modulus suffers a decrease of 7% with a standard deviation of 1,2%, and the shear modulus has a decrease of 10,8% with a standard deviation of 2,4%. These degradation percentages are again very consistent for all the specimens tested for the load angle of β=30º (Table 6.3).

	Cycles	Young's modulus, N/mm2			Shear modulus, N/mm2		
β=30°	**N**	**Initial**	**Final**	**Decrease (%)**	**Initial**	**Final**	**Decrease (%)**
W1RP-370	9478	27253,6	25507,7	6,4	7723,6	6794,1	12,0
W1RP-409	3070	25751,6	23601,3	8,4	7393,1	6775,9	8,3
W1RP-407	6334	25467,8	24091,2	5,4	7325,6	6723,2	8,2
W1RP-403	11481	25581,8	23873,6	6,7	7167,8	6479,8	9,6
W1RP-404	13379	25353,1	23869,5	5,9	7274,8	6589,0	9,4
W1RP-406	26430	25128,2	23453,4	6,7	7125,8	6385,6	10,4
W1RP-413	12939	26294,8	23918,5	9,0	7614,4	6661,7	12,5
W1RP-371	36042	26821,5	24821,8	7,5	7739,7	6523,6	15,7
	Average	**25956,6**	**24142,1**	**7,0**	**7420,6**	**6616,6**	**10,8**
	STD	**708,6**	**641,5**	**1,2**	**227,2**	**137,7**	**2,4**

Table 6.3 - Stiffness degradation for the load angle β=30º

The results for the load ratio R=-1 with the same load angle β=30° have shown a higher degradation, with an average decrease of 9,9% for the young's modulus, with an standard deviation of 2%.

In Figure 6.5 is shown typical stiffness degradation for the load angle of β=30º, with specimen W1RP-370, which has a lifespan of 9478 cycles. Once again, both moduli show a rapid decrease within the first 10% of the life span (phase I of fatigue life) and then stabilize to a linear decrease (phase II and III of fatigue life). Shear modulus however has a slightly faster decrease.

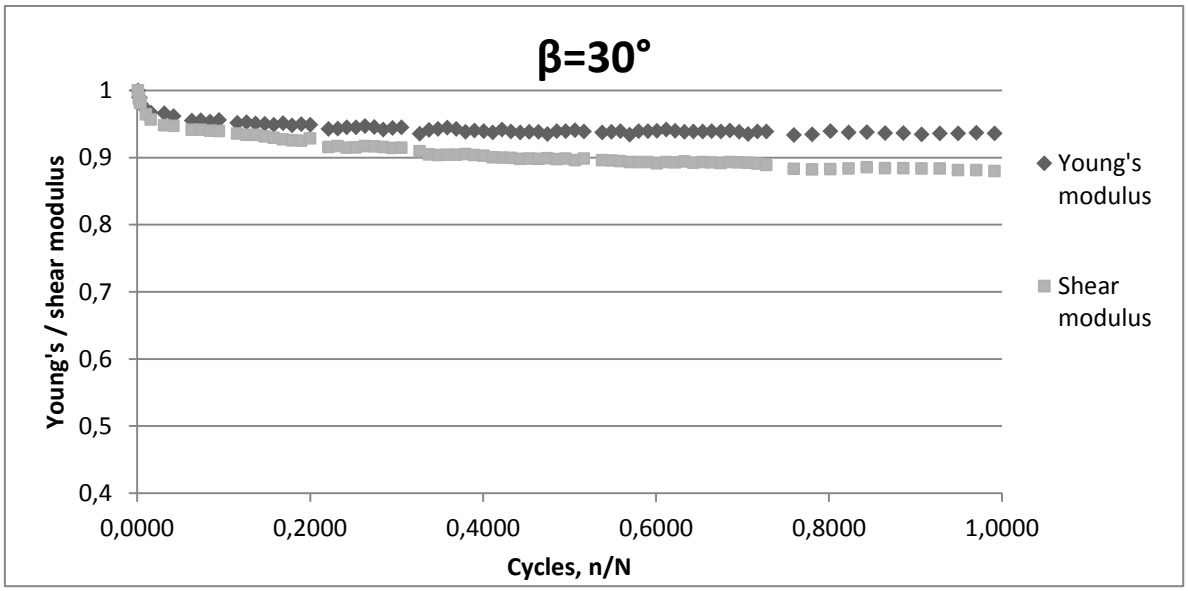

Figure 6.5 - Typical Shear and Young's modulus degradation for β=30º (specimen W1RP-370)

In Figure 6.6 and Figure 6.7 are the comparison between two typical results for a load ratio R=-1 and for the and R=0,1. The specimen for the load ratio R=0,1 is the same as in Figure 6.5, and, as it was mentioned, the life span is 9478 cycles. The specimen for the load ratio R=-1 is the W1RP-132 and has a life span of 10900, only slightly superior. In both cases, young and shear modulus, the load ratio R=-1 has a more pronounced decrease. This is once again, the result expected, however, the difference between R=-1 and R=0,1, for the degradation of young's modulus is very small.

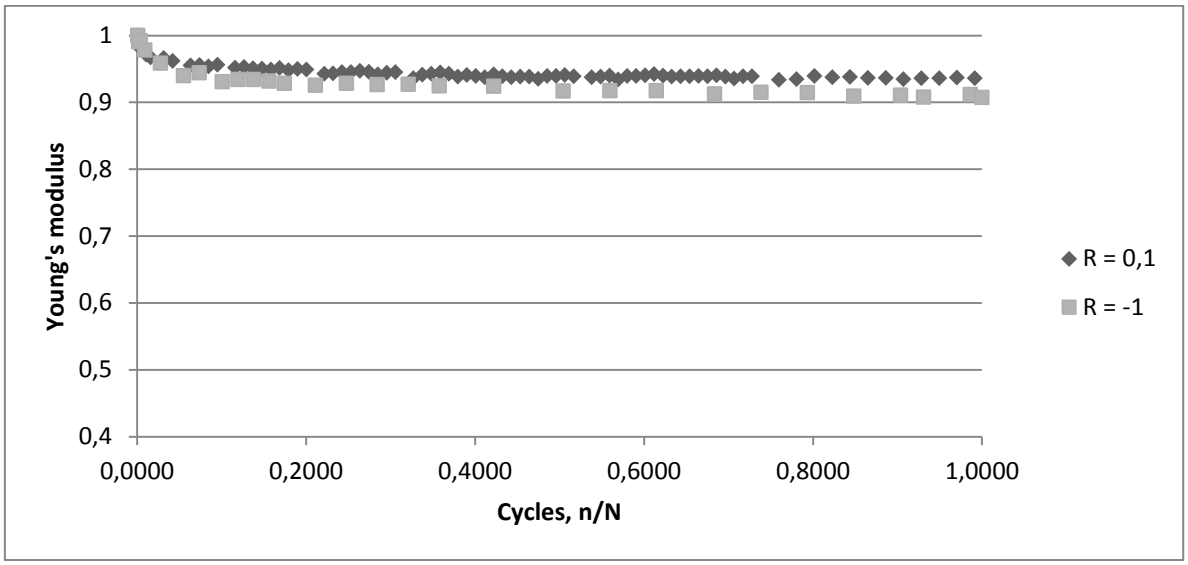

Figure 6.6 - Comparison of the young's modulus degradation between load ratios R=-1 (W1RP-132) and R=0,1 (W1RP-370) for a load angle of β=30º

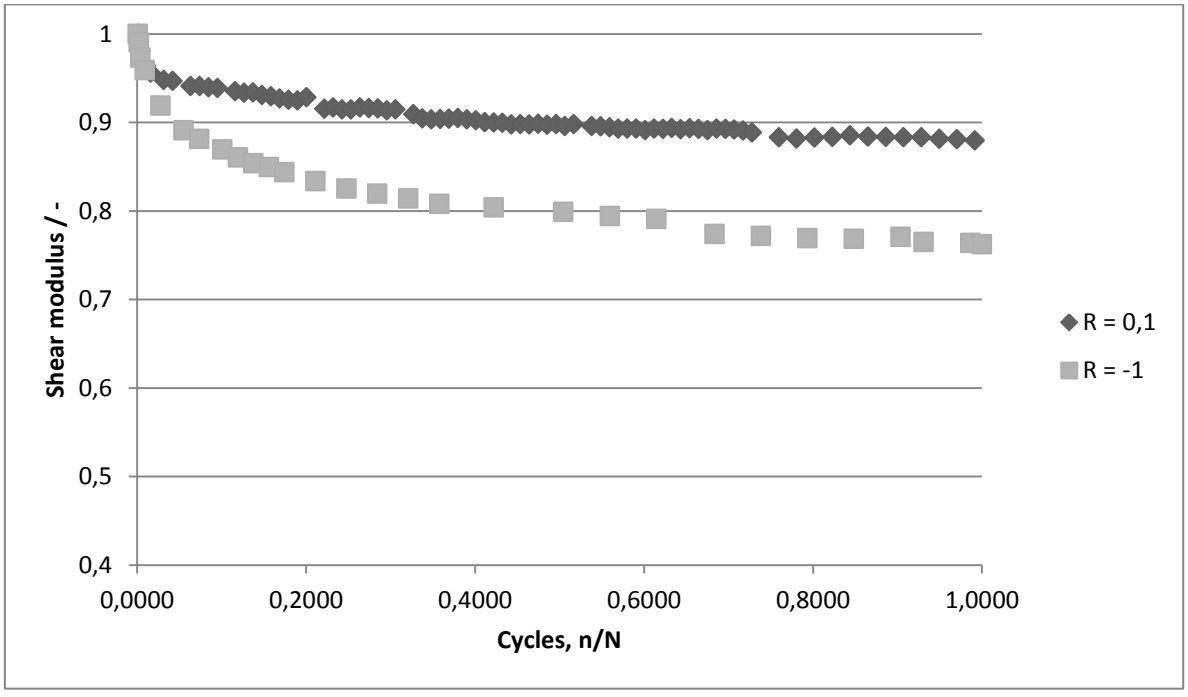

Figure 6.7 - Comparison of the shear modulus degradation between load ratios R=-1 (W1RP-132) and R=0,1 (W1RP-370) for a load angle of β=30º

All the results from the MTS machine and the optical laser are inside the DVD handed together with this thesis, and also in the Hard Drive available at the institute.

6.3 Crack counting

For both cases, β=60º and β=30º, cracks oriented at 45º are, by far, the most prominent. This phenomenon can be explained by the loads applied and the direction of the fibers, relatively to these loads, that are shown in Figure 6.8.

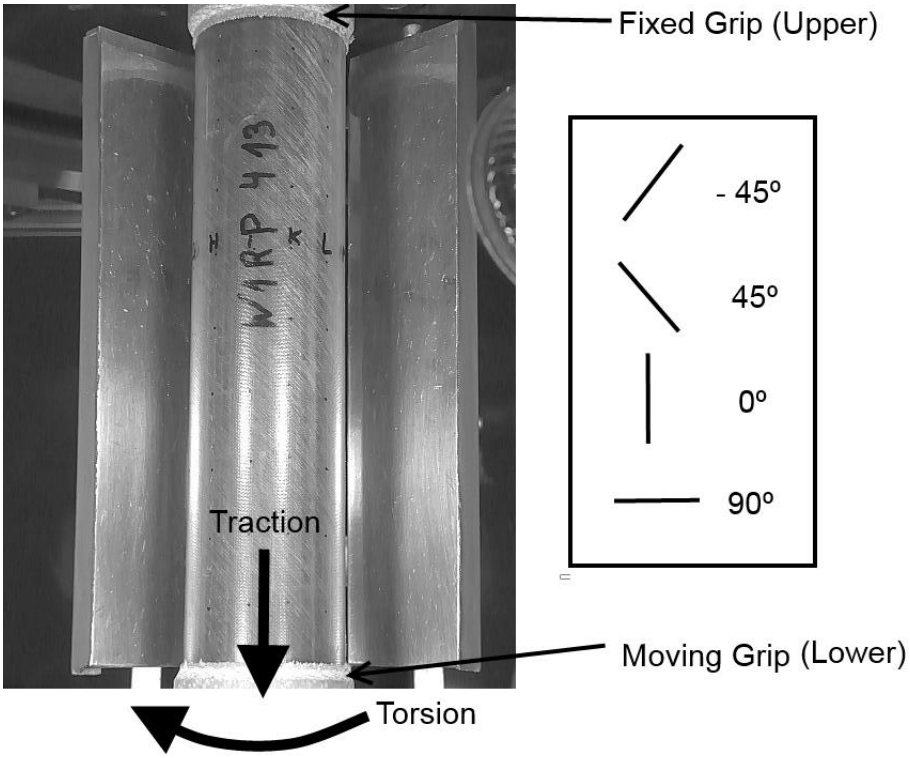

Figure 6.8 – MTS Loads and specimen fibers directions

Since the load applied is a combination of torsion and shear, the layers at 45º are the ones that have the largest offset to the direction of the load. Therefore is no surprise that, for all the pictures, cracks oriented at 45º are the most prominent. The cracks oriented at 0º usually only appear at the last cycles of the specimen life, and in a very small number. Cracks oriented at 90º are usually very thin and difficult to count, either manually or with the software, and this may have influenced the results of the crack counting.

6.3.1 Load angle β=60°

Typical results for the crack counting can be found in Figure 6.9. As one could expect, cracks at +45º are the ones in higher number.

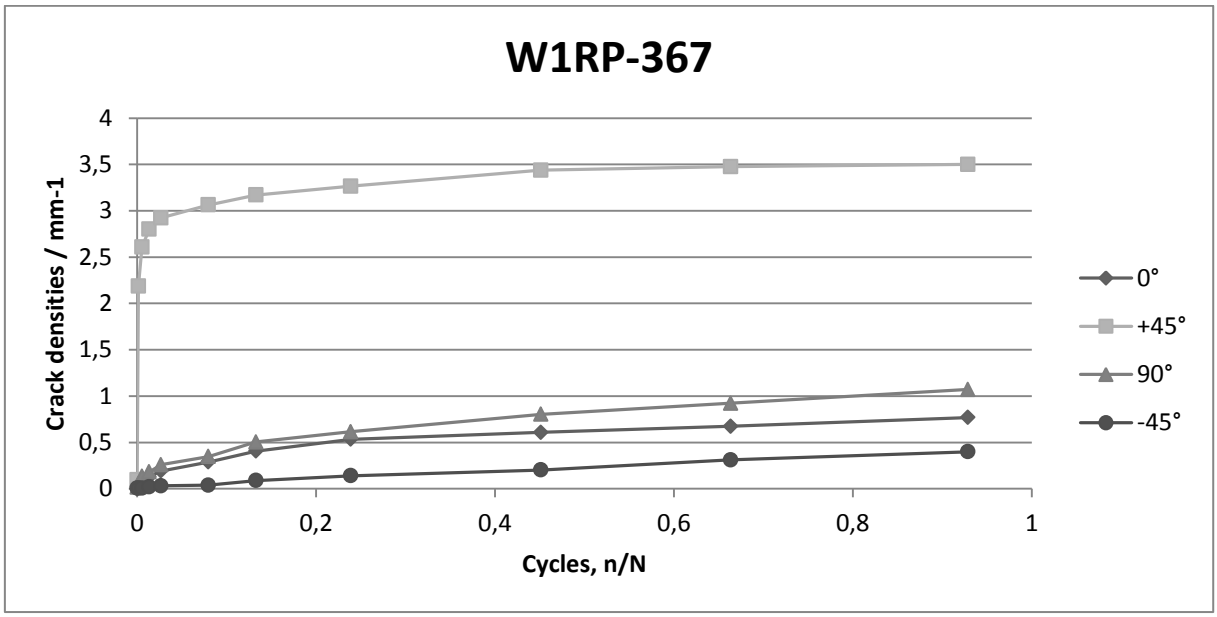

Figure 6.9 – Typical crack counting densities (specimen W1RP-367), β=60º

The amounts of cracks oriented at +45º, increases rapidly in the first 10% of the life span, and then continue growing but much more slowly. Around 20% of the life span cracks oriented at +45º reach saturation, with a density between 3 to 3.5 cracks per millimeter. Cracks with other orientations have a lot less density and there is not a clear trend for all the specimens.

When comparing this result with a typical result for a load ratio R=-1 and also a load angle of β=60º, it's clear that the load ratio R=-1 produces more cracks, either for +45° and -45° (Figure 6.10). For both load ratios the crack saturation is reached around circa 20% of the lifespan. Both specimens have similar lifespan, 37686 cycles for the specimen loaded with the load ratio R=0,1 and 33978 for the specimen loaded with the load ratio R=-1. With a load ratio R=-1 the crack density saturation is reached for 5/mm^{-1}, while for the load ratio R=0,1, the crack density is reached with just 3,5/mm^{-1}. Once again, the Load ratio R=-1 seems to be more harmful by causing a bigger crack density. The load ratio R=-1 also caused a bigger stiffness loss, so it's possible to conclude that there is direct relation between stiffness loss and crack density: the bigger the stiffness loss, the greater is the crack density.

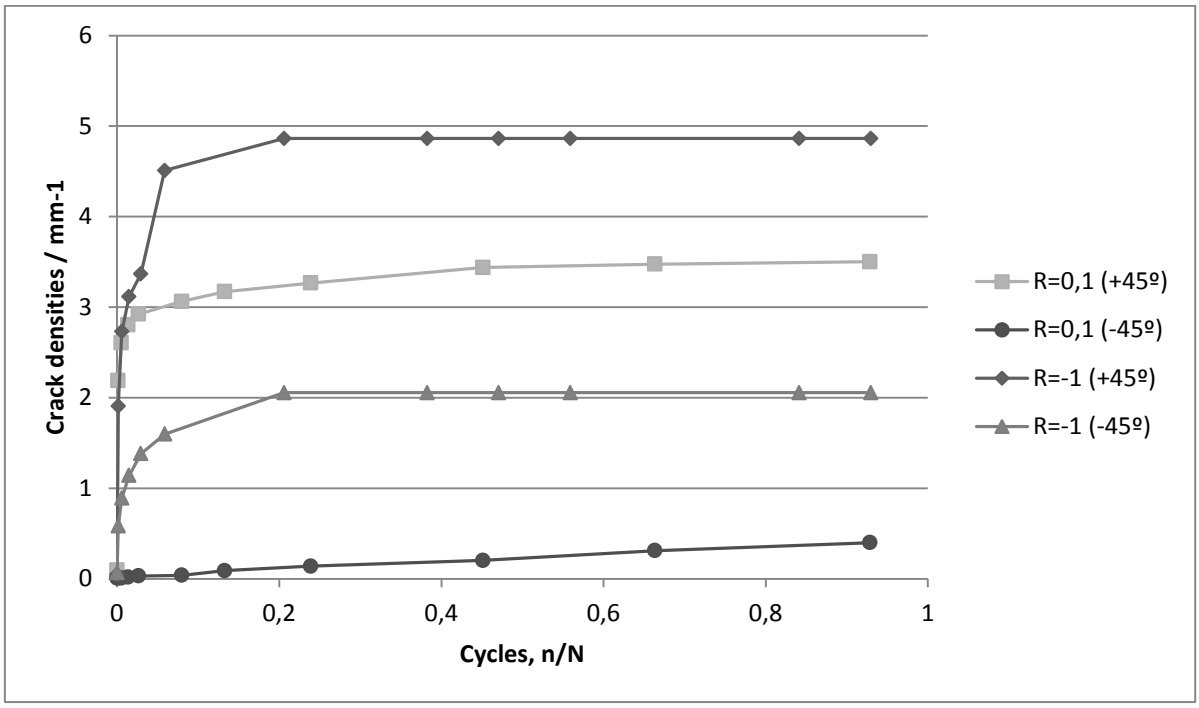

Figure 6.10 - Typical crack densities for load ratio R=-1 (W1RP-137) and for load ratio R=0,1 (W1RP-367), for load angle of β=60°

The results for the other orientations (0° and 90°) are not compared since the density of the cracks is much lower, and there isn't a clear trend for the specimens with load ratio R=0,1 .

6.3.2 Load angle β=30°

The results for the load angle of β=30º are similar to the load angle of β=60º. This means that the cracks at +45º are again in a much higher number (Figure 6.11). However, there seems to be a bigger crack density for cracks oriented at 0° for the specimens with a load angle β=30°, with the crack saturation reached around 1,5/mm^{-1}. The load angle of β=30º has a predominant tension part, and therefore more cracks in the 0º orientation would not be expectable. One possible explanation is the combination of the stresses normal and shear are more harmful with this angle. Taking a look to the stress applied (Table 6.1), the shear stresses are always between 80 to 110 Mpa, for both load angles β but the normal stresses however are much bigger for the load angle β=30°. Therefore it's possible that when the fibers at 0° have a bigger normal stress, they become more sensitive to shear stresses, causing more cracks. The crack density saturation is again usually reached around 20% of the lifespan.

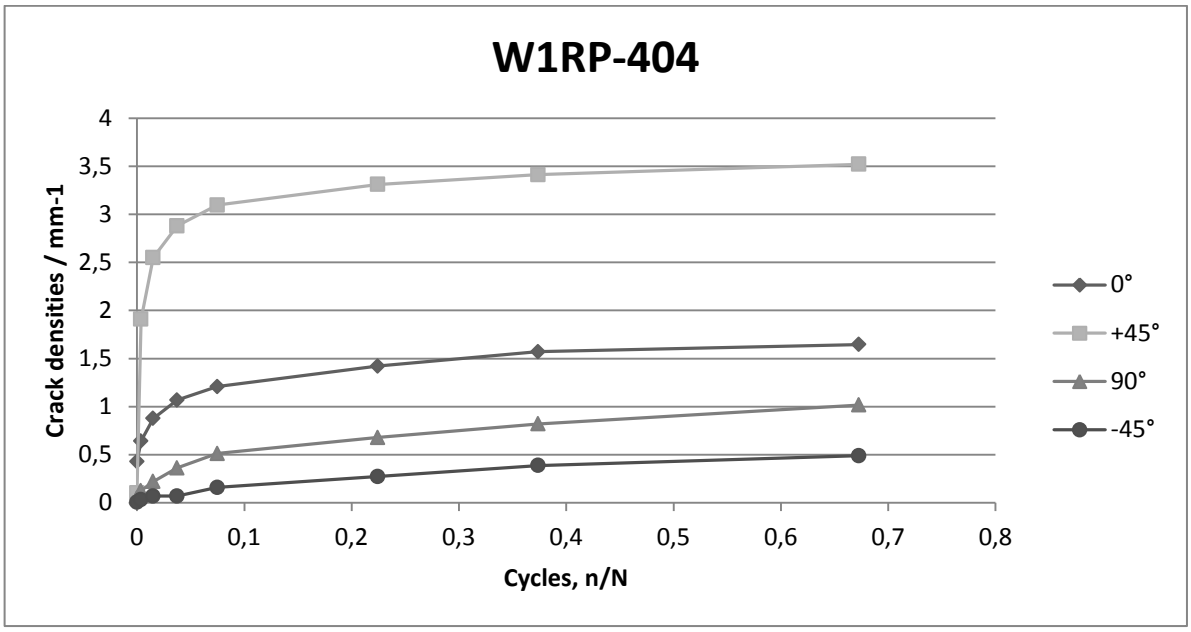

Figure 6.11 – Typical crack counting results (specimen W1RP-404), β=30º

The comparison of these results with the ones obtained with a load ratio R=-1 is similar with the one for the load angle of β=60° for the cracks oriented at +45° and -45°, the load ratio R=-1 is always more harmful (Figure 6.12).

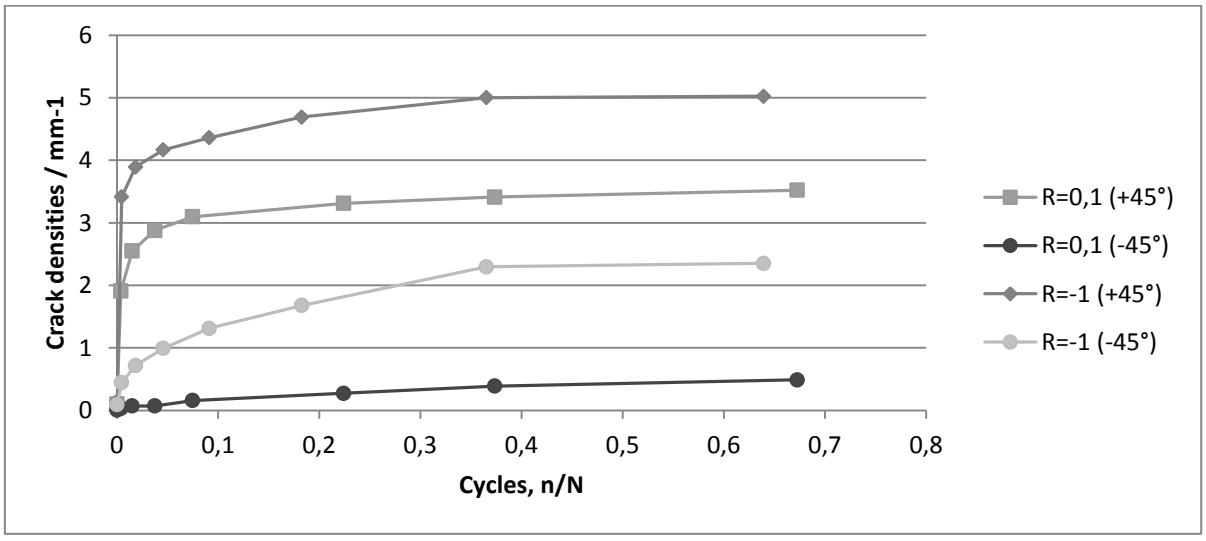

Figure 6.12 - Typical crack densities for load ratio R=-1 (W1RP-132) and for load ratio R=0,1 (W1RP-404), for load angle of β=30°

The load ratio R=-1 also caused a bigger stiffness loss for this load angle β (chapter 6.2.2), so a bigger crack density for load R=-1 is again an expected result.

The pictures obtained for crack counting are saved in the institute's external hard drive. The results from the crack counting software are inside the DVD delivered with this thesis.

6.4 Thermography

6.4.1 Load angle β=60°

For this load angle, the difference between initial temperature and maximum temperature is relatively constant through the test, with just a slight decrease. Only at the last cycles this difference has an increase, usually in the last 10% of the specimen's lifespan. However, this increase never reaches more than 4ºC for the specimen's with this load angle. The average temperature is very constant for the whole test, with an increase of less than 2 ºC from the initial temperature. Typical temperature evolution is shown is Figure 6.13:

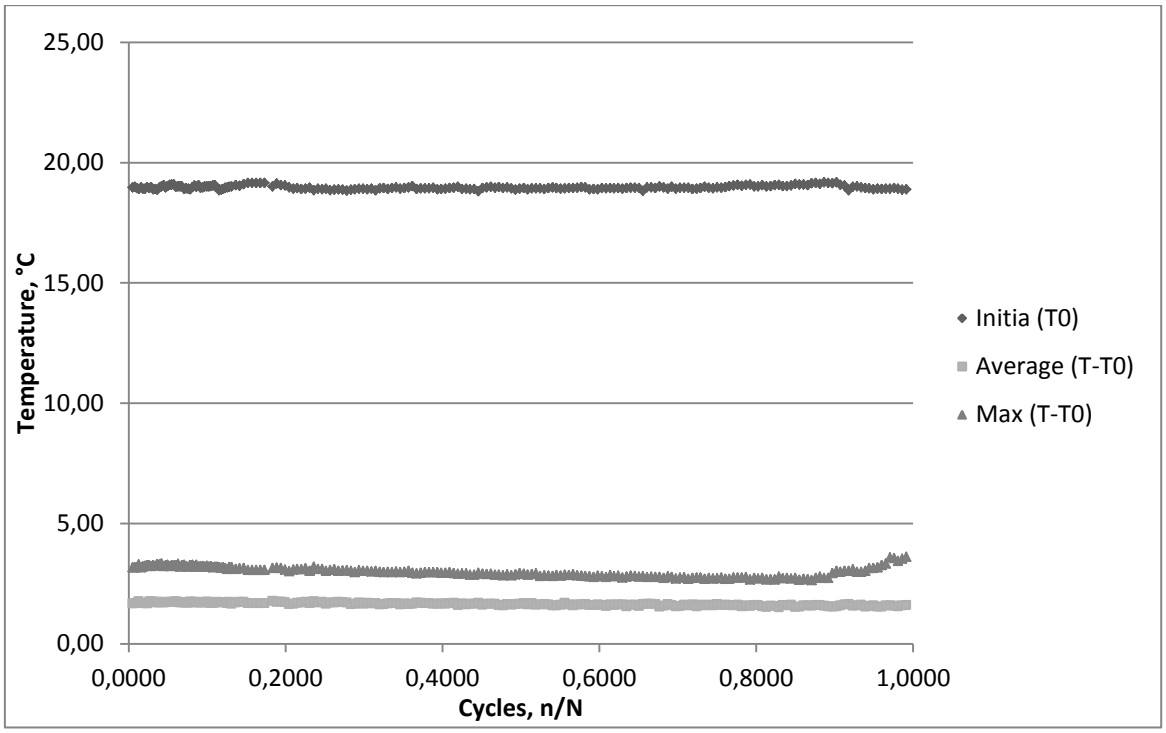

Figure 6.13 – Typical temperature evolution for a specimen with a load angle β=60º and load ratio R=0,1 (specimen W1RP-334)

Comparing the maximum temperature obtained for the load ratio R=0,1 with the load ratio R=-1, it's visible that the load ratio R=-1 reaches a higher maximum temperature for the whole lifespan (Figure 6.14). Also, the maximum temperature for R=-1 has an characteristic curve, with an initial pronounced decrease in the first 10% of the lifespan, where for the load ratio R=0,1 there is no such initial decrease.

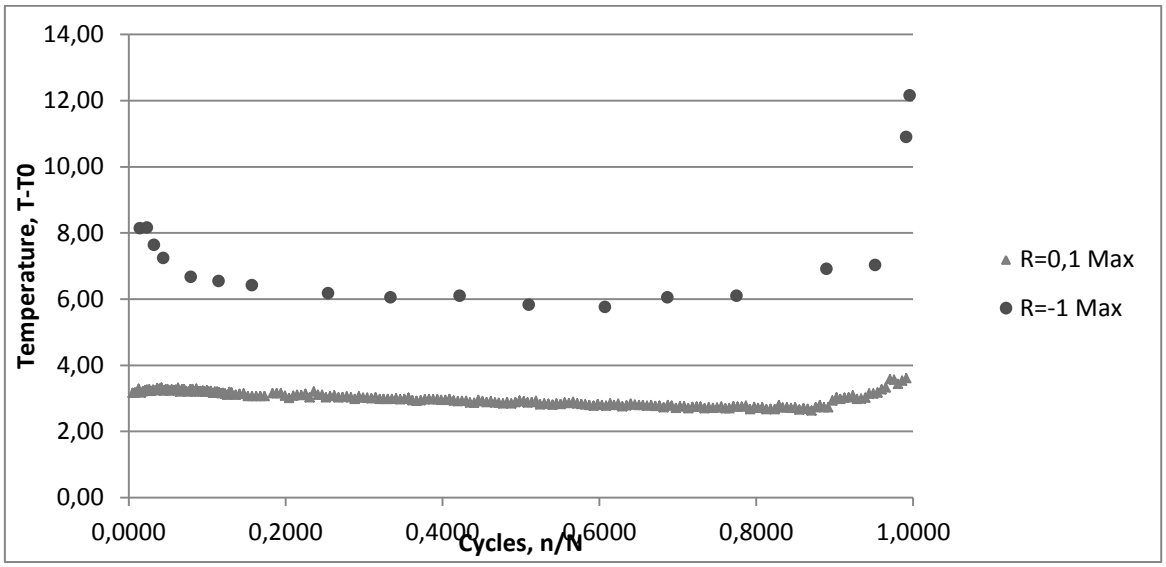

Figure 6.14 - Typical maximum temperature evolution for load ratio R=-1 (W1RP-137) and for load ratio R=0,1 (W1RP-334), for load angle of β=60°

The load ratio R=-1 also reaches a higher maximum temperature for the whole lifespan (Figure 6.15). It also has an initial decrease in the first 20% of the lifespan and then stabilizes, where for the load ratio R=0,1 is almost constant, with a very slight decrease along the lifespan.

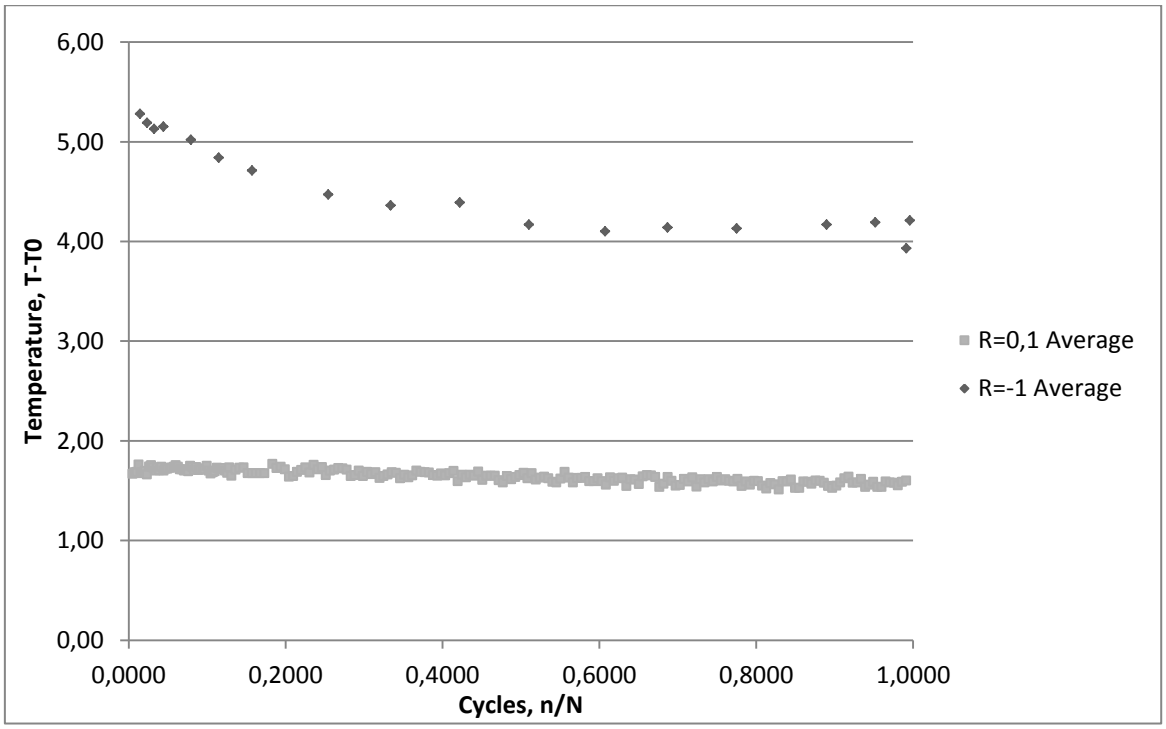

Figure 6.15 - Typical average temperature evolution for load ratio R=-1 (W1RP-137) and for load ratio R=0,1 (W1RP-334), for load angle of β=60°

6.4.2 Load angle β=30°

For the load angle β=30º the difference between initial temperature and maximum temperature is relatively constant through the whole test, and at the last cycles, around 10% of the lifespan, has an increase. The average and maximum temperatures are higher, when compared to load angle β=60º, which may be related to the higher stiffness loss. A typical result can be found in Figure 6.16:

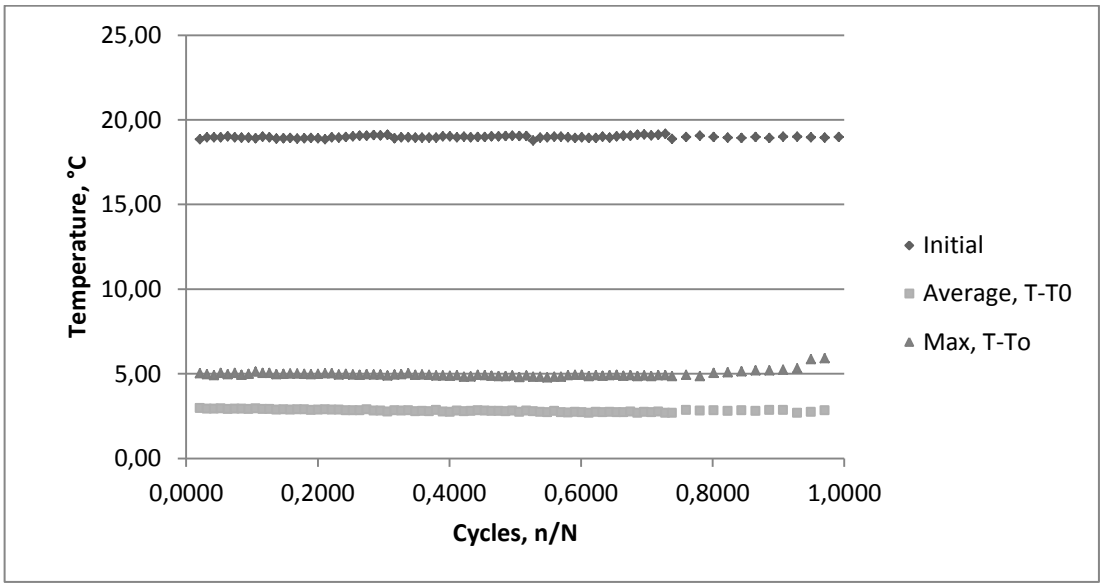

Figure 6.16 - Typical temperature evolution for a specimen with a load angle β=30º and load ratio R=0,1 (specimen W1RP-370)

Again, when comparing the maximum temperature obtained for the load ratio R=0,1 with the load ratio R=-1, it's visible that the load ratio R=-1 reaches a higher maximum temperature for the whole lifespan, although that the difference is not as big as it was for β=60°. Like for the load angle of β=30°, the load ratio R=-1 has an initial pronounced decrease in the first 10% of the lifespan.

For the average temperature, both load ratios have a slight decrease along the lifespan, with the average temperature of the load ratio R=-1 being higher through the whole lifespan of the specimen (Figure 6.18).

The hotspots detected with the thermo camera showed very good relation to the areas of failure initiation seen in the high speed camera, as it is discussed in chapter 6.5

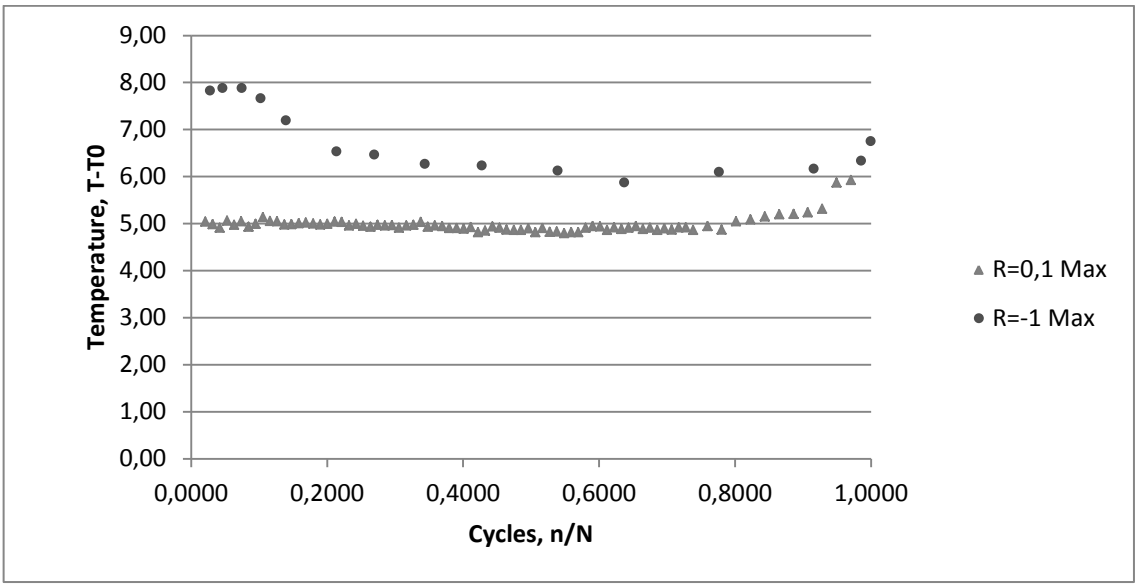

Figure 6.17 - Typical maximum temperature evolution for load ratio R=-1 (W1RP-132) and for load ratio R=0,1 (W1RP-370), for load angle of β=60°

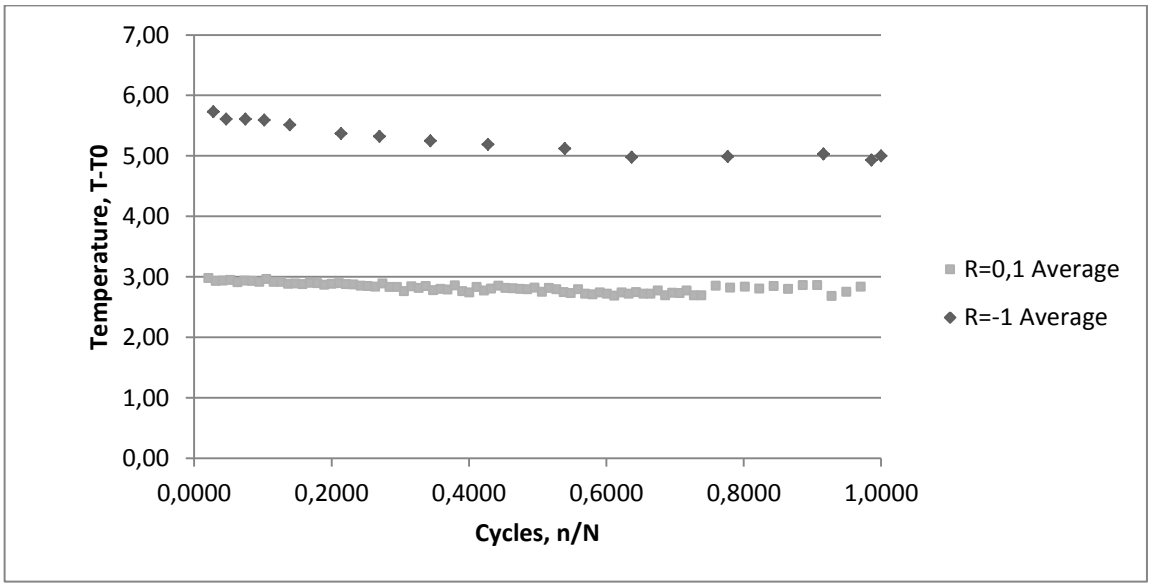

Figure 6.18 - Typical average temperature evolution for load ratio R=-1 (W1RP-132) and for load ratio R=0,1 (W1RP-370), for load angle of β=60°

.

The data obtained from the thermo camera is in the institute's external hard drive. The results from the data evaluation are inside the CD delivered with this thesis.

6.5 High speed microscopy

For all the specimens is obtained a high speed microscopy video that validates or invalidates, the specimen's failure, by making it possible to see how and where the specimen started to fail. Specimens that have the failure initiation in the clamping zone are rejected since the cause for failure may not have been fatigue, but the stress concentration in the clamping zone. As for previous studies, there is good relation between the area of the initial failure visible with high speed microscopy and thermography. A good example of this relation can be found in Figure 6.19:

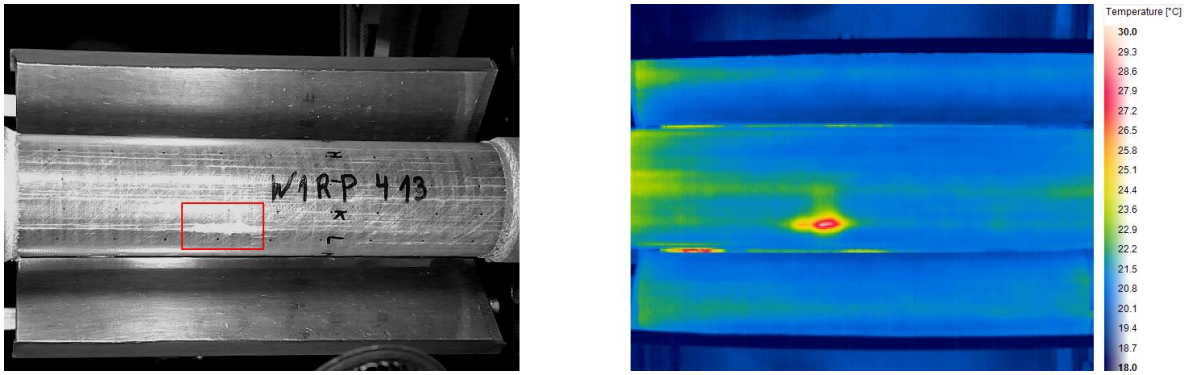

Figure 6.19 - Area of initiation of the failure, marked with a red rectangle in the high speed microscopy (left) and the hotspot (red area) visible with the thermo camera (right), for specimen W1RP-413

The area marked with a red rectangle, on the left picture, shows the delamination area where the failure initiates, the frame before it starts to spread. At the right picture is the hotspot detected with the thermo camera, also right before the specimen fails. Hotspots usually become visible approximately on the last 10% of the life span of the specimen, which is also what was found for the load ratio of R=-1 in previous works (1).

In addition to validating the failure, high speed microscopy also lets evaluate how the failure spreads. The reason for final failure for the load angle β=60° seems to be due to the torsion moment, as it also seen in previous works with a load ratio R=-1. The failure usually starts in one delamination, and spreads around the specimen, usually oriented at -45º, like the one found in Figure 6.22. However, some specimens, especially the ones with the load angle β = 30º, showed that, although the failure also seems to be due to the torsion applied, the failure area first spreads along the axis (0º), and then spreads with the -45º direction. One typical result that show this effect is shown in Figure 6.20.

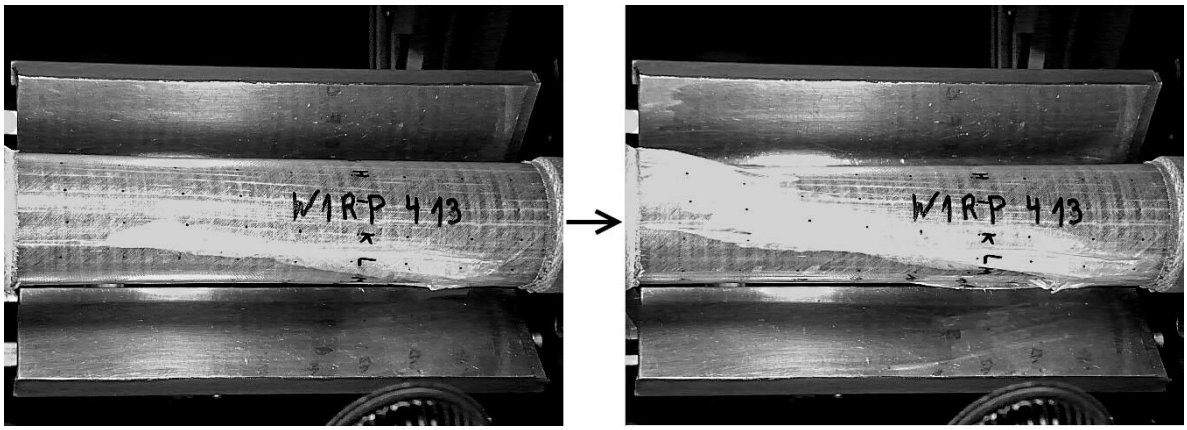

Figure 6.20 - High speed microscopy of the specimen's W1RP-413 failure

This seems to be related with the mold joint, left from the RTM process and will be discussed in chapter 6.4.

The results of specimen W1RP-401 were excluded from this work based on the high speed microscopy and also the thermography results. Although the lifespan of the specimen is in accordance with the other results, the specimen's failure seems to start on the clamping zone, and then spread along the specimen (Figure 6.21).

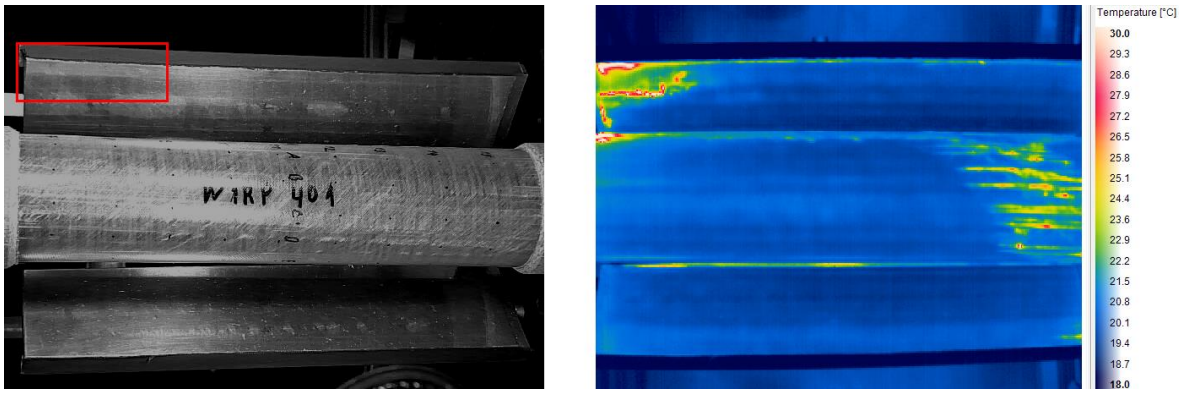

Figure 6.21 - W1RP-401 high speed microscopy (left) and thermography (right) right before failure

The failure initiation is only visible in the reflector (marked with the red rectangle). In the high microscopy video is visible the failure's growth, starting at the clamping zone and then spreading.

High speed microscopy also allowed the detection of local buckling in specimen W1RP-389 (Figure 6.22). This specimen was tested for β=60º and the loads were calculated for 60% over static failure, which was the higher percentage used. These high loads degraded the specimen very early, and started to create large delaminations right after 500 cycles. The total number of cycles before failure is merely 5991.

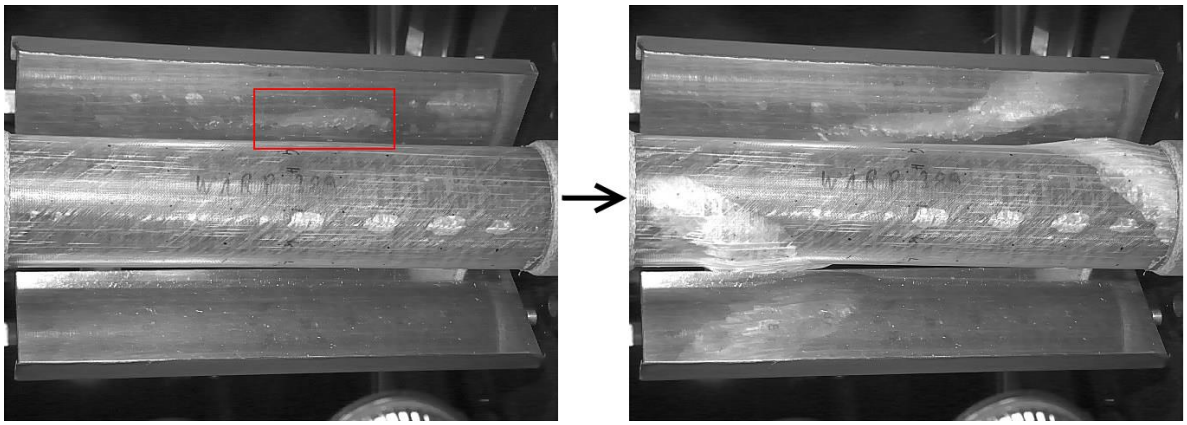

Figure 6.22 - High speed microscopy of specimen W1RP-389, before failure (left) and after failure (right), with the larger delamination marked with a red rectangle

The buckling happened in an area with a large delamination, which leaded the specimen to final failure. This phenomenon was not found in any of the other specimens tested, not even in specimen W1RP-411, which had very similar loads, but did not developed big delaminations like W1RP-389. Therefore, is possible that the buckling was a singular occurrence, which only happened because certain conditions were combined:

- High loads, that not only cause the delaminations in the first place, but also apply a greater effort to the specimen and cause greater deformation;
- A very large delamination area, which reduces drastically the stiffness locally;
- Load angle β = 60°, because the shear stress is dominant shear and more likely to create buckling effect.

The high speed microscopy videos obtained for all the specimens are saved in the Institute's external hard drive.

6.6 Visual inspection

There seems to be a relation between delamination areas and the mold joints. In Figure 6.23 is visible one example of the accumulation of delaminations near the joint left from the RTM process, and then the specimen's failure, which propagated through this area.

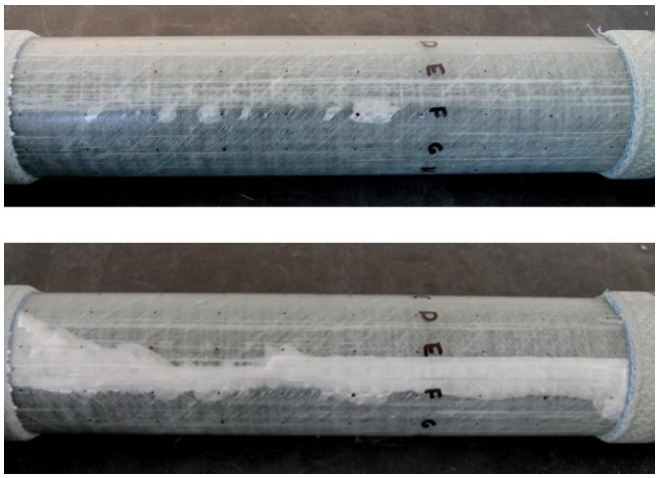

Figure 6.23 - Specimen W1RP-403 after 9000 cycles (up) and after failure (down)

Almost all the specimens with a load angle β=30° showed this similar failure, which can be seen in Figure 6.24.

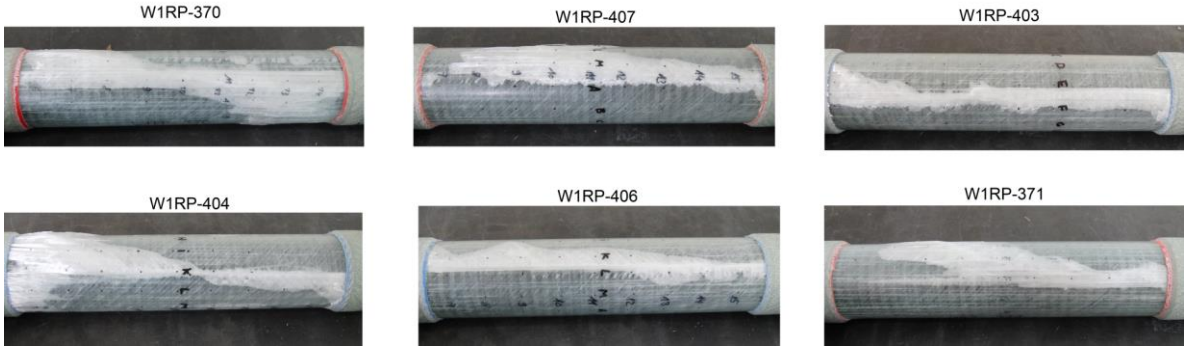

Figure 6.24 – After failure pictures of specimens with load angle β=30º

When comparing the area of the failure and the measured thickness, in many cases they match the lines measured along the axis with lower average thickness.

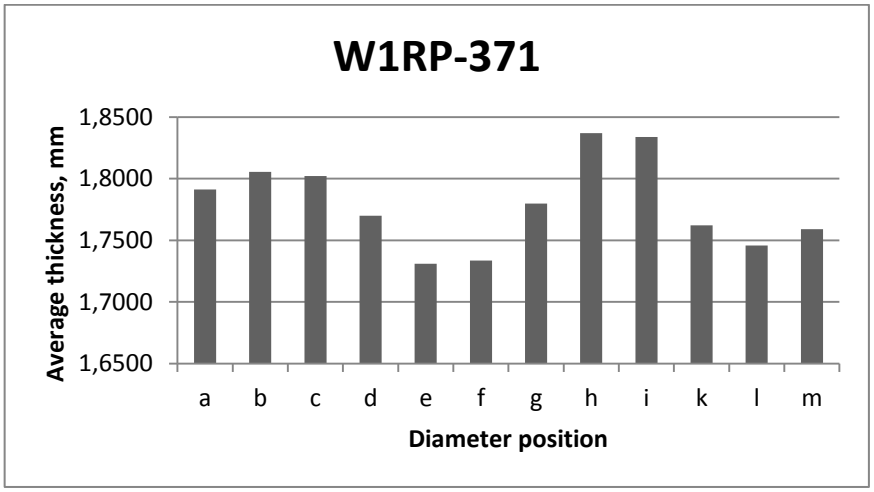

Figure 6.25 – Average thickness measured along the axis for specimen W1RP-371

The mold joints for specimen W1RP-371 are located between letters E and F, which match the measured average lower thickness (Figure 6.25). The same happens in specimen W1RP-407, with the mold joints between letters M and A and the other between letters F and G (Figure 6.26).

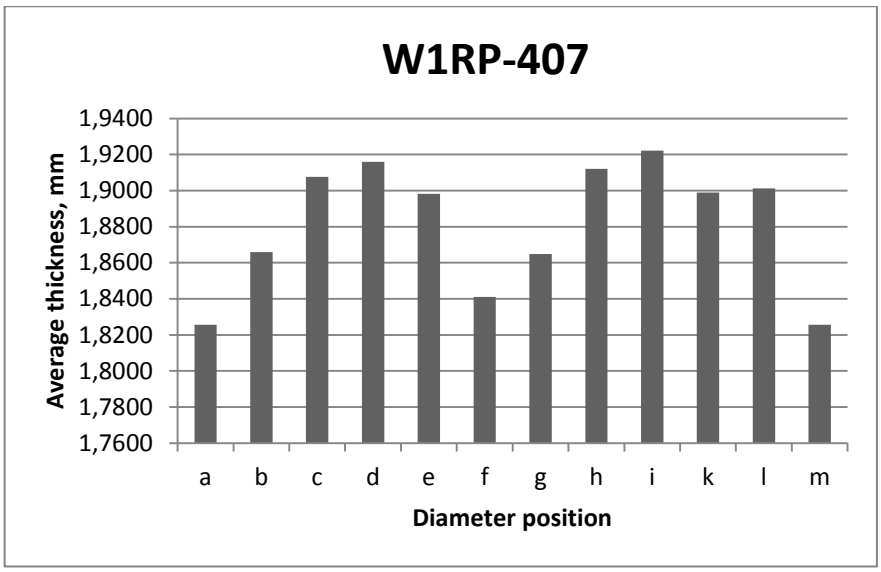

Figure 6.26 - Average thickness measured along the axis for specimen W1RP-371

Only a few specimens with a load angle β=60º also showed this phenomenon, and it was not as pronounced as for the specimens with a load angle β=30º. Specimen W1RP-381 is the only one for the load angle of β=60º where this phenomenon is clearly visible (Figure 6.27).

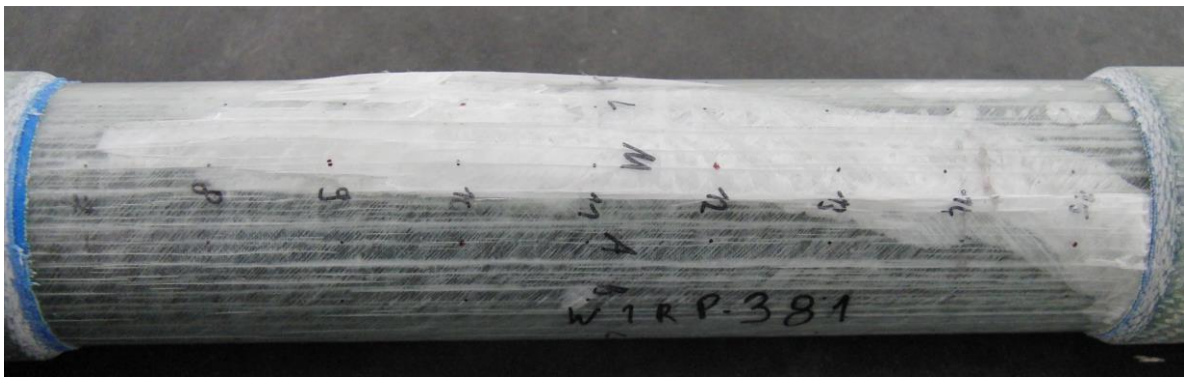

Figure 6.27 - Specimen W1RP-381 after failure

These results show that for a load ratio R=0,1 the joints of the mold, left from the RTM process are a production defect can influence the fatigue results, particularly if the tension part of the biaxial loads is more predominant. Unfortunately, with the data collected it's not possible to define a trend between this phenomenon and a shorter lifespan.

All the pictures taken during testing and after final failure are inside the CD handed in with this thesis.

6.7 Microscopy

The delaminations found in most of the specimens were taken to the microscope to see to in which layers these delaminations start to develop, and try to see a possible cause. The local cut made in specimen W1RP-406 (Figure 6.28) shows what seems to be some resin rich area near the 45º layer, which can be the cause for the early delaminations in this area.

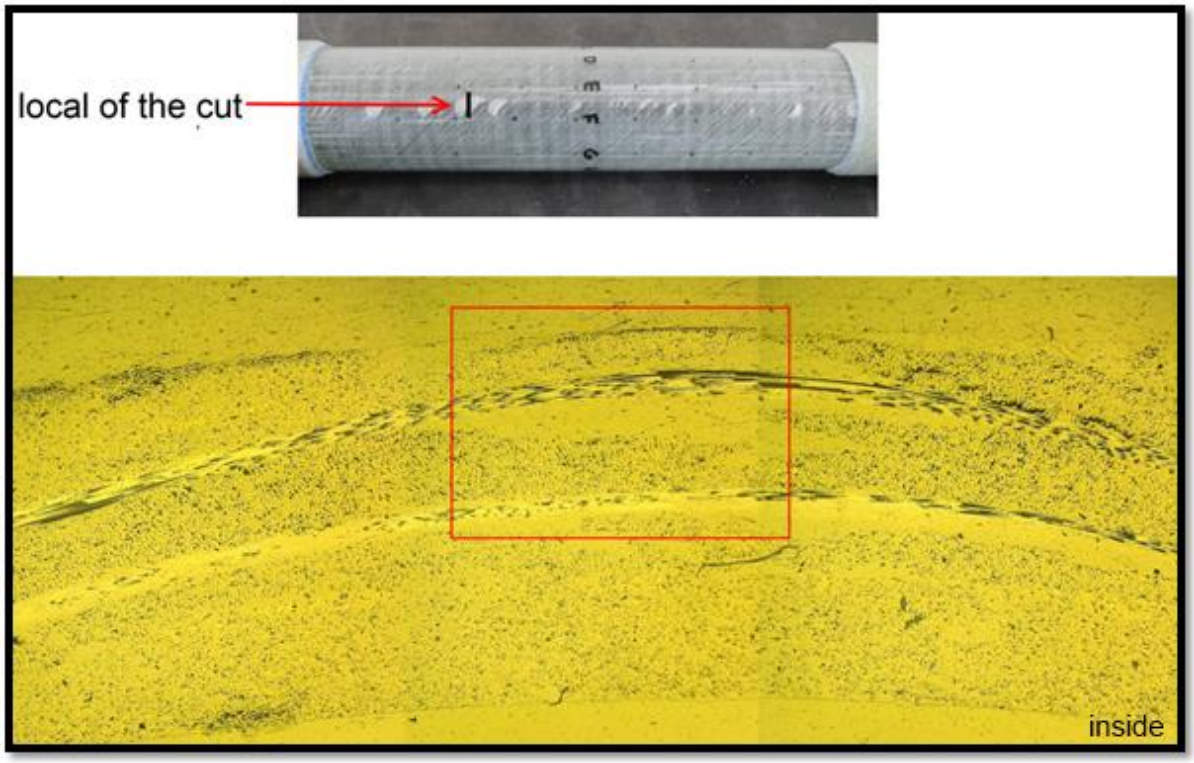

Figure 6.28 - Microscopy of the specimen W1RP-406

A cut in a different angle, aligned with the axis orientation of the specimen, on specimen W1RP-401, shows a similar resin rich area that is spread along the axis of the specimen. This reinforces the idea that this is related to the molding process, since this mold joint is also near this area. The pictures also show the crack that developed between layers, which seem to be between the -45º layer and 90º layer.

The microscope pictures of specimen W1RP-401 also showed the initiation of small cracks inside the 90º layer (Figure 6.30). This specimen was tested with a load angle of β=30º, for which the tension part is predominant, and therefore it is expected the cracks develop inside this layer.

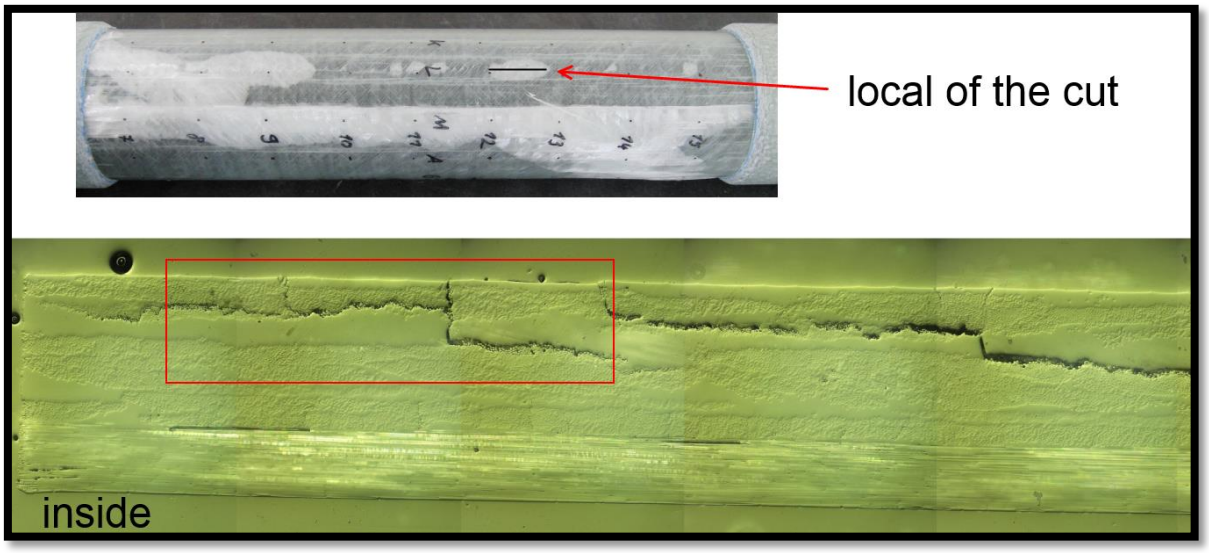

Figure 6.29 - Microscopy of the specimen W1RP-401

Figure 6.30 - Microscopy of the specimen W1RP-401

6.8 Calcination

Calcination results were sometimes slightly different for the same specimen, for the upper and lower ring. The specimens W1RP-407, W1RP-409 and W1RP-411 have the biggest difference, and the other results are fairly consistent. This is related to the manufacturing process, which cannot guarantee the thickness throughout the specimen.

The calcination results can be seen in Table 6.4:

Specimen	Ring position		ϕ
W1RP-367	above	21	0,4945
	below	2	0,4920
	average		0,4932
W1RP-368	above	20	0,5216
	below	2	0,5072
	average		0,5144
W1RP-370	above	19	0,5240
	below	1	0,5365
	average		0,5303
W1RP-371	above	20	0,5202
	below	2	0,5396
	average		0,5299
W1RP-381	above	20	0,5199
	below	2	0,5253
	average		0,5226
W1RP-389	above	20	0,5218
	below	2	0,5278
	average		0,5248
W1RP-400	above	19	0,4890
W1RP-402	above	19	0,5074
	below	3	0,5057
	average		0,5066

Specimen	Position		ϕ
W1RP-403	above	18	0,5142
	below	1	0,5198
	average		0,5170
W1RP-404	above	19	0,5118
	below	2	0,4997
	average		0,5057
W1RP-405	above	21	0,5205
	below	3	0,5134
	average		0,5169
W1RP-406	above	20	0,5041
	below	3	0,5041
	average		0,5041
W1RP-407	above	19	0,5272
	below	2	0,5038
	average		0,5155
W1RP-409	above	19	0,5200
	below	3	0,4895
	average		0,5048
W1RP-411	above	19	0,5168
	below	2	0,4904
	average		0,5036
W1RP-413	above	19	0,5034

Table 6.4 - Calcination results

The specimens W1RP-400 and W1RP-413 were tested for just one ring and the specimens W1RP-334 and specimen W1RP-401 were not tested. The W1RP-401 was not tested due to the bad failure during the fatigue test, which makes all the collected data for this specimen not valid to this work, and therefore the calcination test is not necessary.

The differences between the analytical and experimental fiber volume content can be found in Table 6.5.

Specimen	Analytically	Calcination	Difference
W1RP-334	0,530	not tested	-
W1RP-367	0,497	0,493	0,004
W1RP-368	0,530	0,514	0,016
W1RP-370	0,548	0,530	0,018
W1RP-371	0,540	0,530	0,010
W1RP-381	0,526	0,523	0,003
W1RP-389	0,522	0,525	0,003
W1RP-400	0,485	0,489	0,004
W1RP-401	0,493	not tested	-
W1RP-402	0,495	0,507	0,012
W1RP-403	0,511	0,517	0,006
W1RP-404	0,501	0,506	0,005
W1RP-405	0,495	0,517	0,022
W1RP-406	0,489	0,504	0,015
W1RP-407	0,505	0,516	0,011
W1RP-409	0,504	0,505	0,001
W1RP-411	0,490	0,504	0,014
W1RP-413	0,516	0,503	0,013

Table 6.5 - Difference between analytical and experimental fiber volume content

Most of the results for experimental and analytical fiber volume content differ for 1% or less, which demonstrates the suitability of the analytical prediction when initially calculating the loads for fatigue testing. The calcination results are also estimated to the whole specimen, made with the average of two rings cut at the ends. Although this should give a very close result to the specimen's real fiver content, better than the analytical prediction, is not an error-free result.

6.9 S-N Curves

All the s-N curves here presented are obtained with the following linearized s-N relationship:

$$\log(N) = A + B(S) \qquad \text{Equation 6.1}$$

The S refers to the stress parameter and N to the corresponding number of cycles to failure, while A and B are parameters that will be determined for the fatigue data. The stress parameter chosen is the normal stress for all the plots.

This method is in accordance with the standard ASTM E739-10.

6.9.1 Load angle β=60º

The S-N curve obtained for the specimens with a load angle β=60º is shown in Figure 6.31:

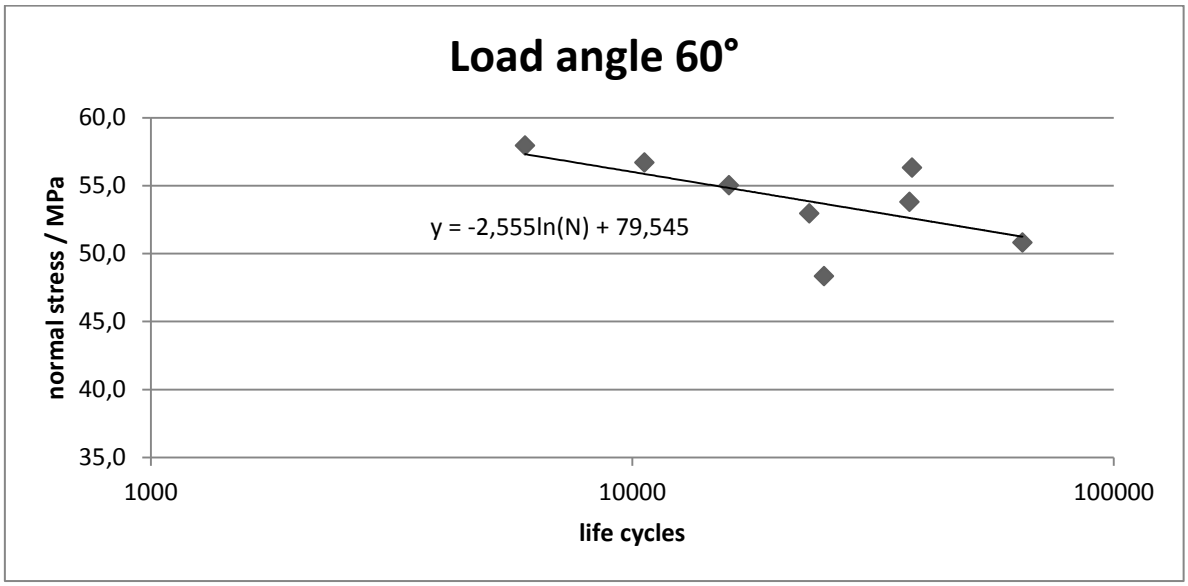

Figure 6.31 – S-N curve for the specimens with a load angle of β=60º

In this curve is visible that two specimens have a big gap to the S-N curve. These specimens are the number W1RP-334 and W1RP-405. The specimen W1RP-334 has a lifespan of 38100 cycles, but is one with the highest loads, which means that should have lasted around 10000 cycles. Therefore, this specimen is the one that falls above the S-N line. The specimen W1RP-405 has a lifespan of just 25048 cycles, but is the one with the lowest loads, meaning that should have lasted more than 65000 cycles. This specimen is the one that falls with a big gap below the s-N curve. There is not a clear reason for this two specimens fall out of the curve for a much bigger difference then the others, however composites are known for its variability for mechanical tests, and even the small difference between specimens, even if apparently unnoticeable can lead to random results. All the remaining results are consistent with each other and with the curve.

In Figure 6.32 is the comparison between the S-N curves for the lad ratio R=0.1 and Load ratio R=-1. For the load ratio R=-1 was omitted the data for the specimens which lasted more than 150000 cycles, so that the results are more comparable. The s-N curve for the load ratio R=-1 is below the same curve for load ratio R=0,1 which is what could be expected, since the stiffness degradation is bigger for this load ratio, and literature revision also indicated the load ratio R=-1 as more harmful. The slope of the both curves is very similar, which may indicate that a load ratio of R=-1 is always more harmful for fatigue life, even with higher number of cycles.

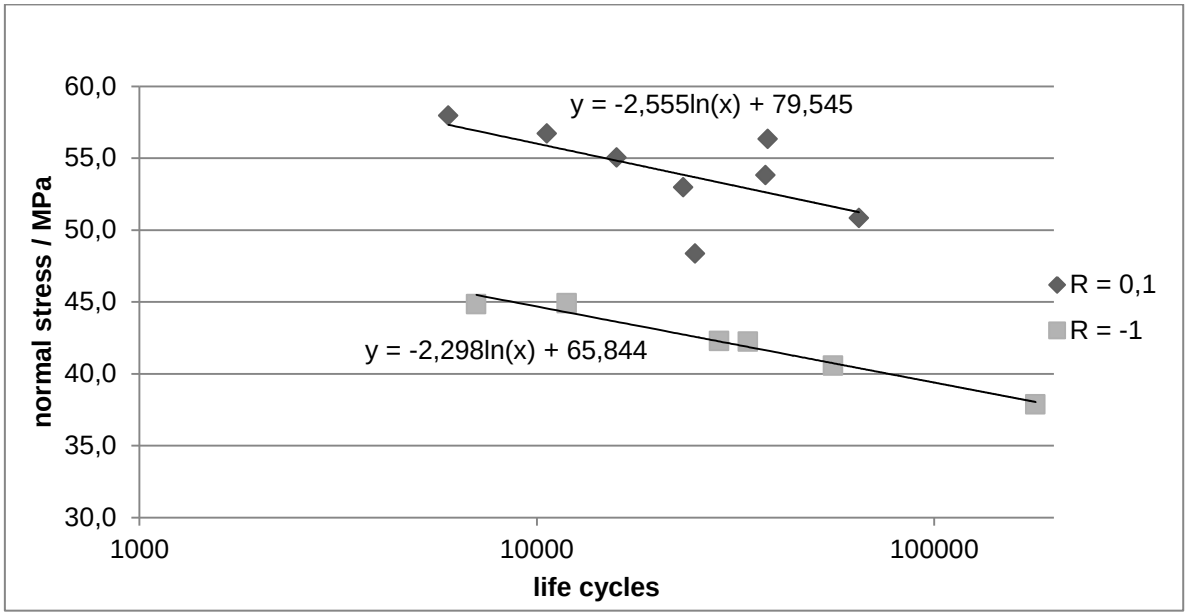

Figure 6.32 – Comparison of S-N curves between the load ratio R=0,1 and R=-1, for load angle of β=60º

6.9.2 Load angle β=30º

The S-N curve obtained for the specimens with a load angle β=60º is shown in Figure 6.33:

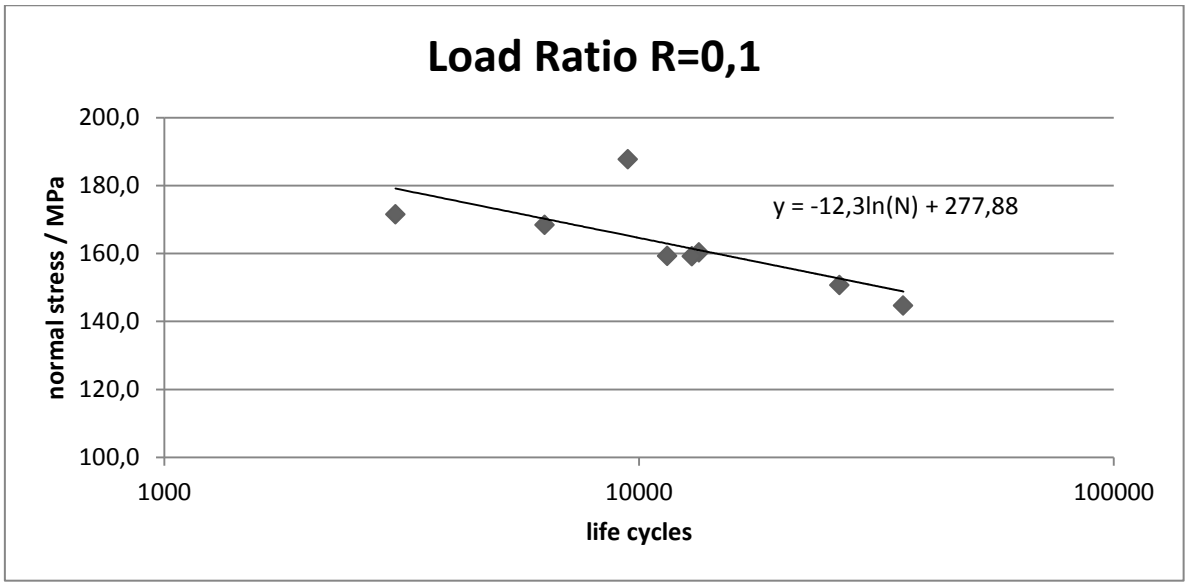

Figure 6.33 - S-N curve for the specimens with a load angle of β=60º

In this plot is also visible on point that falls out of the curve with a big gap. This specimen is the specimen number W1RP-370, which has a lifespan of 9478 cycles but is the one with the highest loads. With this high loads this specimen should have lasted less than 3000 cycles.

This specimen was the first to be tested, and as it was referred before, mislead the following tests, for which was used loads that turned out in to a small number of cycles. All the following tests are very consistent and fit very well the S-N curve.

Comparing the S-N curve for the load ratio R=0,1 with the one for the load ratio R=-1 is visible again that the load ratio R=-1 is below (Figure 6.34). For the load ratio R=-1 was again omitted the data for the specimens which lasted more than 100000 cycles, so that the results are more comparable. This result is what could be expected, since the stiffness degradation is bigger is bigger for the load ratio R=-1. However, unlike the load angle β=60º, for the load angle β=30º the slope between curves is slightly different. The S-N curve for the load ratio R=0,1 is slightly steeper, which may indicate that after a big amount of cycles, the load ratio R=0,1 could be more harmful.

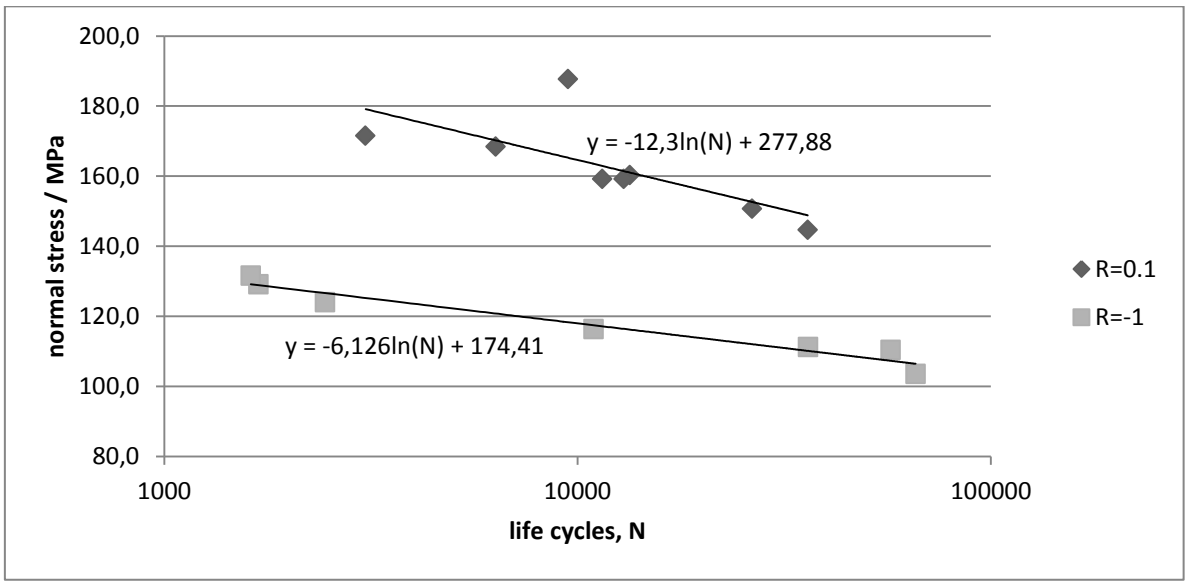

Figure 6.34 - Comparison of S-N curves between the load ratio R=0,1 and R=-1, for load angle of β=30º

6.10 Conclusion

After analyzing all the collected data, is evident that the load ratio R=0,1 is more harmful to the fatigue life of the specimens tested, than a load ratio R=-1. This was shown in all the data collected. Stiffness degradation is an indicator of the damage that the specimen suffered and it was higher for the load ratio R=-1, for both load angles β. However that the difference was bigger for the load angle β=60º, where for the load angle β=30º the difference was not as pronounced.

The crack densities results also showed that the load ratio R=-1 is more harmful, as for both load angles β it reached higher a saturation density when comparing the 45º and -45º directions. Plus, for the load ratio R=-1 there are also a big crack density for the 90º direction, as for the load ratio R=-1 almost all the cracks are oriented at +45º. The 0º orientation for the load ratio R=0,1 and load angle β=30º showed a slight increase in density. This is not an expected result, as for this load angle the tension part is stronger and the 0º layers are oriented in the traction direction, and therefore less likely to create cracks. One possible explanation is the combination of a higher tension stress with shear stress may lead to the appearance of some cracks in this direction. However, as it was said, the density is still very low, around 1,5 cracks per millimeter.

The results for the temperature monitoring showed a bigger average and maximum temperature for the load ratio R=-1 when compared to the load ratio R=0,1, which is also in agreement with the stiffness degradation results. The results for the load ratio R=0,1 and angle β=30º also show a bigger increase in average and maximum temperature when compared to the results for the load angle β=60º, but still lower than for the load ratio R=-1.

Overall the results are coherent, with the load ratio R=-1 having more stiffness degradation, higher crack densities and higher maximum and average temperatures during testing. These results can be explained mainly by two factors. The load ratio R=-1 has negative loads, which means that has compression loads, which has it was seen chapter 2 are more harmful to composites in general. The second factor is related to the amplitude of the loads, which is the difference between the maximum and minimum load. The load ratio R=0,1 means that the loads range is from 10% of the maximum load and 100%. The load ratio R=-1 has a much larger range, since the loads go from 100% to -100% of the maximum load. So despite the higher loads applied to the specimens for the load ratio R=0,1 , this amplitude is clearly bigger for the load ratio R=-1.

The tests realized with the load ratio R=0,1 also permitted to the discovery of two interesting effects. The first is the buckling effect, which happened in specimen W1RP-389. Since only this specimen showed such effects and it was tested, comparatively to the other specimens,

with higher loads (almost 60% over static failure), it's possible to say that it buckling can occur only if some conditions are combined: high loads, a very large delamination area and a load angle with predominant shear stress. The second effect is the relation between the mold joints and the final failure, mostly for the specimens with a load angle β=30º, since almost all of them showed similar failure, with the damaged zone spreading along this joint. When comparing this mold joints with the measured thickness of the specimens, some showed that the average thickness is lower in this area. Therefore the final failure may have occurred in this zone due to its geometric inhomogeneity.

The S-N curves obtained for the load ratio R=0,1 show a better lifespan for the same maximum load, when compared to the load ratio R=-1. This is true for both load angles, however for the load angle of β=30º, the S-N curve for load ratio R=0.1 is steeper, which may indicate that for a longer lifespan the load ratio R=0,1 may be more harmful. There are three results that don't fit in the s-N curve created, one for the load angle of β=30º and two for the load angle of β=60º. The reasons for this is however not clear.

7 Improvements to experimental setup and procedure

During the use of the machine was possible to identify some minor improvements:

- A polarizing filter to the high speed microscope would eliminate the light that is reflected on the specimen and allow a better visibility of the final failure. However, this would only be useful if this failure occurs at the front of the specimen, since this kind of filters does not work in metallic surfaces, like the ones used in the reflectors. Therefore, the improvement of using this filter is very limited.
- Replace the air conditioner pipes with plastic pipes instead of aluminum, which have lower thermal conductivity compared to the very high thermal conductivity of the aluminum, and therefore would not be affected as much with the outside temperature;
- Create a protocol that has a fixed number of cycles per set, since different intervals between fatigue tests can lead to different results.
- Increase the size of the reflectors, since there is space in the microscope video image and in thermo camera image for larger reflectors, and the current ones do not cover 100% of the specimen's surface.

During testing there were also found some sources of errors which can affect the final results:

- The optical laser sensor is not very stable when compared to the data obtained directly from the MTS machine. The calibration of the laser, and the distance of the laser to the axis of the specimen can introduce systematic error in the measures by the optical sensor, which lead to a final value
- The estimation of fiver volume content by calcination testing is also not 100% correct. The two rings used may not represent the whole specimen, and the real value may be slightly different. However it's impossible to do a full specimen calcination, even if done to the whole specimen after testing, some parts of the specimen are lost during failure and results would not be error-free.
- Strength of the specimen: every specimen is unique and therefore has different strengths.
- Crack counting software: every image is different and very difficult to count the cracks. Independently of the parameters chosen, there will be cracks not counted for some pictures and pictures with inexistent cracks counted. Overall the results are good, but there is a random error which is difficult to quantify.

8 Summary

In this work are tested tubular fiber reinforced specimens for them fatigue life. The specimens are biaxially loaded with tension and shear stresses, with a load angle β of 30° and 60° and a load ratio of R=0,1. The load angle β is the relation between the axial and shear stress, β=60º means that the shear stress is predominant, and β=30º means that the tension part is predominant. For every fatigue test is obtained data of stiffness degradation, temperature evolution during cyclic loading and crack densities for each layer orientation. The results are then compared to the results obtained in previous works with a load ratio R=-1 and the same load angles.

There were tested a total of 16 valid specimens, 8 for the load angle of β=60º and 8 for the load angle of β=30º. The lifespan obtained for the load β=60º is between 6000 cycles and 65000 cycles, ant the lifespan obtained for the β=30º is between 3000 cycles and 36000 cycles.

The results for stiffness degradation show a higher decrease in stiffness for the load ratio R=-1, either for the load angle of β=30º and for the load angle of β=60º. On average, for the load angle β=60º the young's modulus suffers a decrease of 6,2% with a standard deviation of just 0,4% and the shear modulus 12,9% with a standard deviation of 1,7%. These degradation percentages are therefore very consistent for all the specimens tested. For the load ratio of R=-1 with the same load angle β=60º, the degradation of the young's and shear modulus is more pronounced, 11,7% with a standard deviation (STD) of 2,2% for young's modulus and 26.7% with a standard deviation of 4.1%. For the load angle of β=30º, the load ratio R=0,1 has an average decrease of 7% with a standard deviation of 1,2%, and the shear modulus has a decrease of 10,8% with a standard deviation of 2,4%. The load ratio R=-1 has an average decrease of 9,9% for the young's modulus, with an standard deviation of 2%.

The results for crack densities showed that the load ratio R=0,1 has the most cracks oriented at the +45º direction. This happens for both load angles of β=30º and β=60º. Both load angles have for the +45º oriented cracks a rapidly increase in the first 10% of the life span and reach crack saturation around 3,5 cracks per millimeter. The cracks oriented at 0º, -45º and 90º do not show a clear trend for the load angle of β=60º, and usually don't exceed the 1 crack per mm density. For the load of β=30º there is a slight tendency to have more cracks oriented at 0º, which would not be expectable, since the load angle has higher loads in the direction of the cracks, but can be explained by the interaction of the two stress, shear and tension. Still, the density of cracks for this 0º orientation does not exceed 1,5 cracks per millimeter. Comparing the cracks densities obtained from the load ratio R=0,1 with the ones from the load ratio R=-1, the load ratio R=-1 has higher crack densities. Since the load ratio

R=0,1 has almost only cracks at +45º, the densities are only compared for the -45º and +45º directions, and the results show higher densities in both cases for the load ratio R=-1, which is in accordance to the stiffness loss obtained.

The data from the temperature monitoring also show higher temperature increase for the load ratio R=-1, either for the average and maximum temperature measured during the test. This happens for both load angles of β=60º and β=30º, although the difference is bigger for the load angle of β=60º.

The S-N curves obtained for the load ratio R=0,1 show a better lifespan for the same maximum load, when compared to the load ratio R=-1. This is true for both load angles, however for the load angle of β=30º, the S-N curve for load ratio R=0.1 is steeper, which may indicate that for a longer lifespan the load ratio R=0,1 may be more harmful. There are two results for the load angle of β=60º and one for the load angle of β=30º that does not fit very well the S-N curve. The reasons for this 3 bar results is however unknown.

There seems to be a relation between the mold joints and the final failure, mostly for the specimens with a load angle β=30º, since almost all of them showed similar failure, with the damaged zone spreading along this joint. When comparing this mold joints with the measured thickness of the specimens, some showed that the average thickness is lower in this area. Therefore the final failure may have occurred in this zone due to its geometric inhomogeneity.

Since it was not possible to understand if there is a relation between the number of cycles and the joints left from the manufacturing process this is something that can be studied in future works. The life span of both load angles is somehow limited, with the highest number of cycles being just 36000 for the load angle β=30º and 65000 for the load angle β=60º, and this is also something that can be improved in future works. The effects of voids and fibers waviness were neglected in this work, since all the specimens were chosen so that the defects were very low or none. However, the study of these defects for this load ratio is also a possible area for further exploratory study.

9 Literature

1. *Multiaxial fatigue behaviour of GFRP with evenly distributed or accumulated voids monitored by various NDT methodologies.* **F. Schmidt, M. Rheinfurth, P. Horst, G. Busse.** p207-216, Germany : ELSEVIER, 2012, Vol. 43.

2. **Vassilopoulos, Anastasios P. and Keller, Thomas.** *Fatigue of Fiber-reinforced Composites.* Lausanne, Switzerland : Springer, 2011. ISBN 978-1-84996-181-3.

3. **Moura, Marcelo F. S. de, Morais, Alfredo B. de e Magalhães, António G. de.** *Materiais Compósitos - Materiais, Fabrico e Comportamento Mecânico.* Porto, Portugal : Publindústria, Edições Técnicas, 2005. ISBN 978-972-8953-00-3.

4. *The Phenomena of Rupture and Flow in Solids.* **Griffith, A. A.** s.l. : Philosophical Transactions of The Royal Society, 1921.

5. **Aird, Forbes.** *Fiberglass and Composite Materials - An enthusiast's guide to high performance non-metallic materials for automative racing and marine use.* New York, USA : HPBooks, 1996. ISBN 1-55788-239-8.

6. **Karbhari, Vistasp M.** *Durability of composites for civil structural applications.* s.l. : CRC Press, 2007. ISBN 978-1-84569-356-5.

7. **Harris, Bryan.** *Fatigue in composites.* s.l. : CRC Press LLC, 2003. ISBN 1 85573 608 X.

8. **Nijssen, R.P.L.** *Fatigue Life Prediction and Strength Degradation of Wind Turbine Rotor Blade Composites.* 2007. ISBN-13: 978-90-9021221-0.

9. **Knops, Martin.** *Analysis of Failure in Fiber Polymer Laminates - The Theory of Alfred Puck.* Rendsburg, Germany : Springer, 2008. DOI 10.1007/978-3-540-75765-8.

10. *An engineering point of view about fatigue of polymer matrix composite materials.* **Bathias, Claude.** Pages 1094–1099, Paris, France : International Journal of Fatigue, 2006, Vol. 28. doi:10.1016/j.ijfatigue.2006.02.008.

11. **Hu, Ning.** *Composites and Their Properties.* Croatia : InTech, 2012. ISBN 978-953-51-0711-8.

12. *Evaluation of biaxial stress failure surfaces for a glass fabric reinforced polyester resin under static and fatigue loading.* **M.J. Owen, J. R. Griffiths.** Department of Mechanical Engineering, University of Nottingham, University Park, Nottingham, UK : JOURNAL OF MATERIALS SCIENCE, 1978, Vol. 13. DOI 10.1177/002199839402801503.

13. *Fatigue behaviour of composite bars subjected to bending and torsion.* **L. Ferry, D. Perreux,D. Varchona, N. Sicot b.** Pages 575–582, Besancon, France : Composites Science and Technology, 1998, Vol. 59. DOI 10.1016/S0266-3538(98)00103-1.

14. **Castro, Manuel Jorge Dores de.** *Couse material of the discipline "Técnicas de Diagnóstico de Avarias", ISEP.* Porto : s.n., 2012.

15. **Geier, Martin.** *Master Thesis: Experimentelle Untersuchung des Ermüdungsverhaltens von gewickelten Rohrproben unter biaxialer Belastung.* s.l. : Technische Universität Braunschweig - Institut für Flugzeug- und Leichtbau, 2010.

16. Owens Corning. [Online] [Cited: July 16, 2013.] http://www.owenscorning.com/.

17. Institute of Aircraft Design and Lightweight Structures. [Online] [Cited: 2 September 2013.] https://www.tu-braunschweig.de/ifl/versuchstechnik/versuchsanlagen/mts.

18. **ASTM International.** *Standard Practice for Statistical Analysis of Linear or Linearized Stress-Life (S-N) and Strain-Life (E-N) Fatigue Data.* ASTM E739-10, 2010.

19. **European Committee for Standardization.** *Bestimmung des Textilglas- und Mineralfüllstoffgehalts Kalzinierung.* EN ISO 1172, 1998.

10 List of figures

11 List of tables

12 Appendix

Crack densities results:

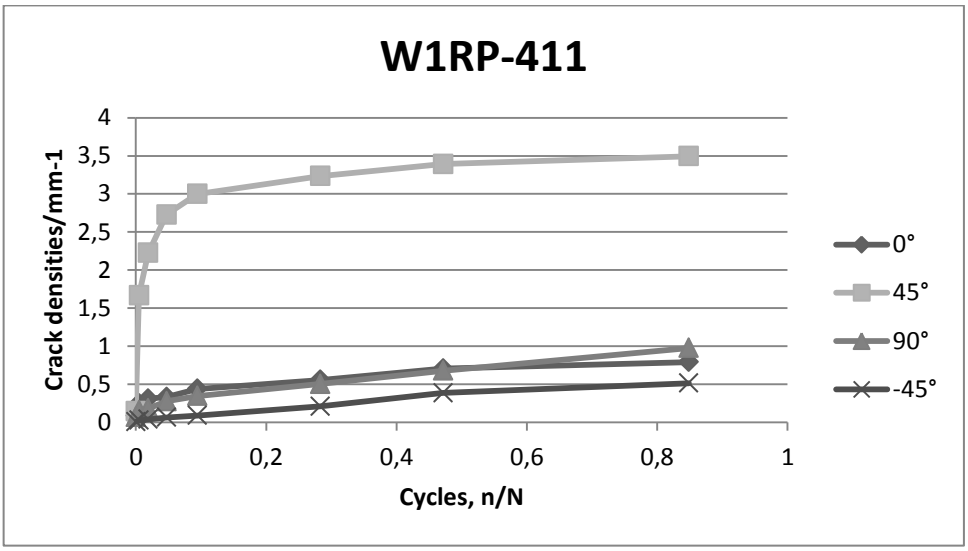

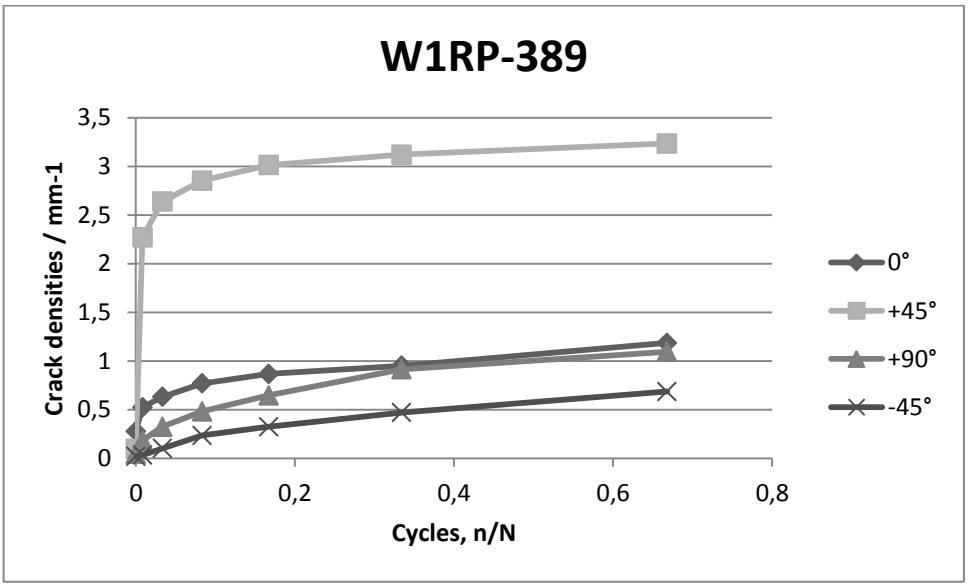

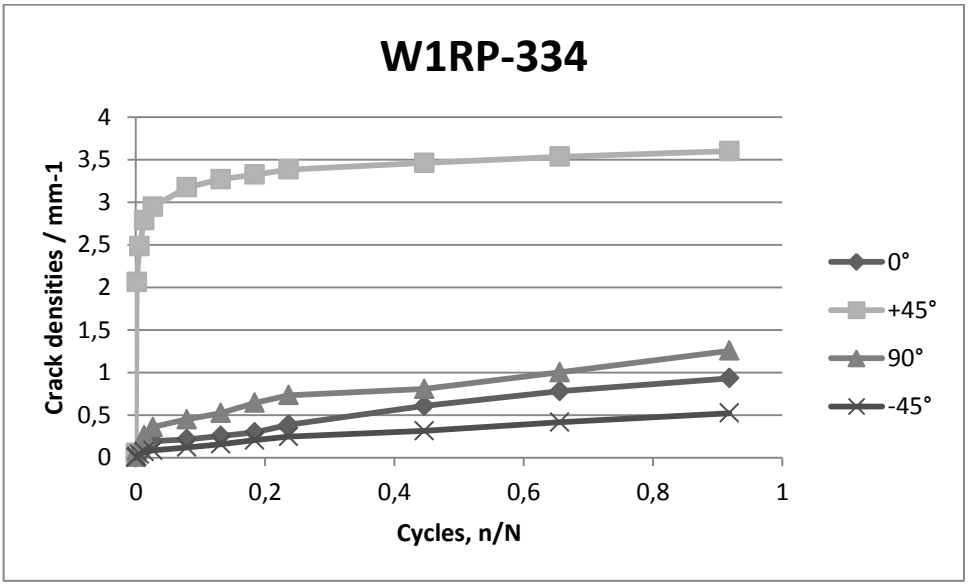

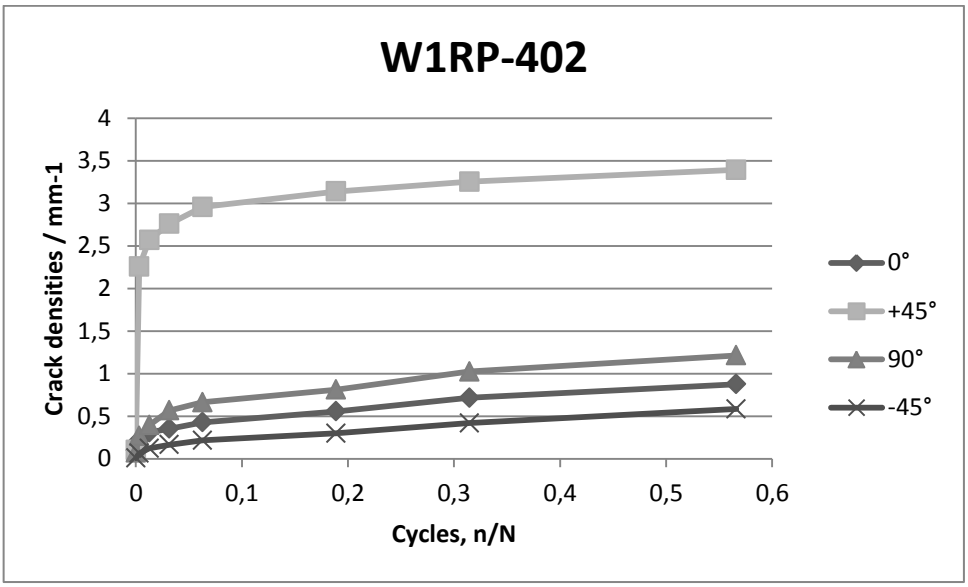
W1RP-402
Crack densities / mm-1
Cycles, n/N
0°
+45°
90°
-45°

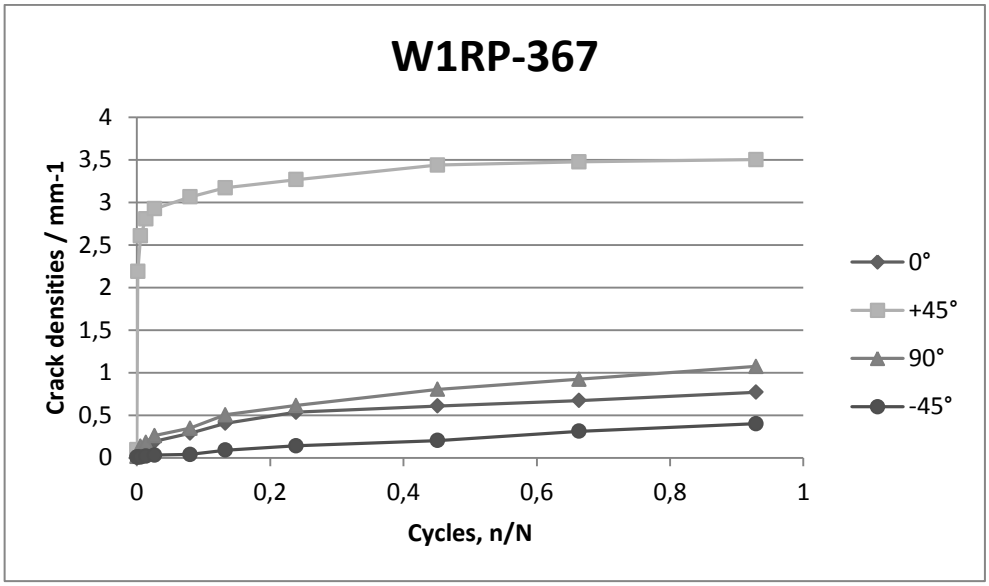
W1RP-367
Crack densities / mm-1
Cycles, n/N
0°
+45°
90°
-45°

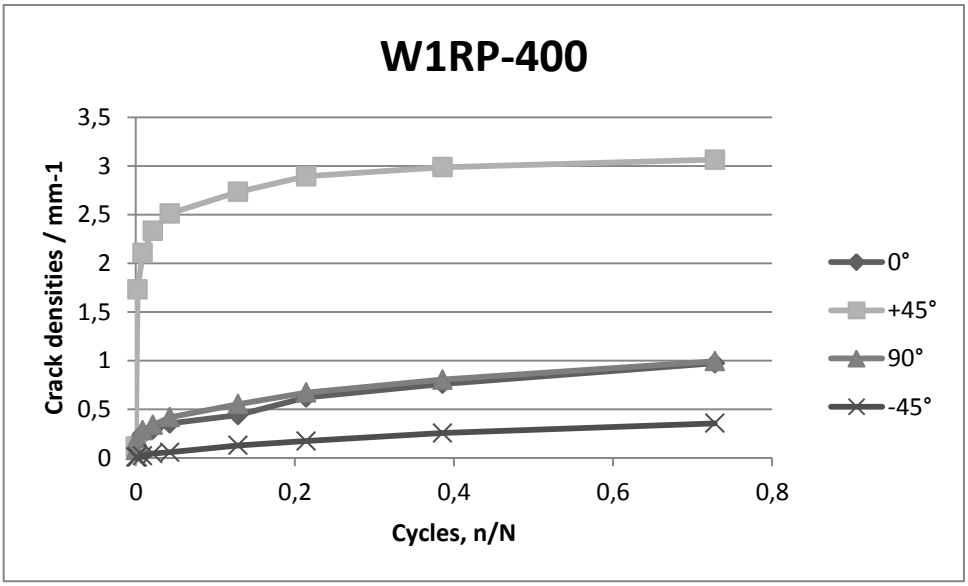
W1RP-400
Crack densities / mm-1
Cycles, n/N
0°
+45°
90°
-45°

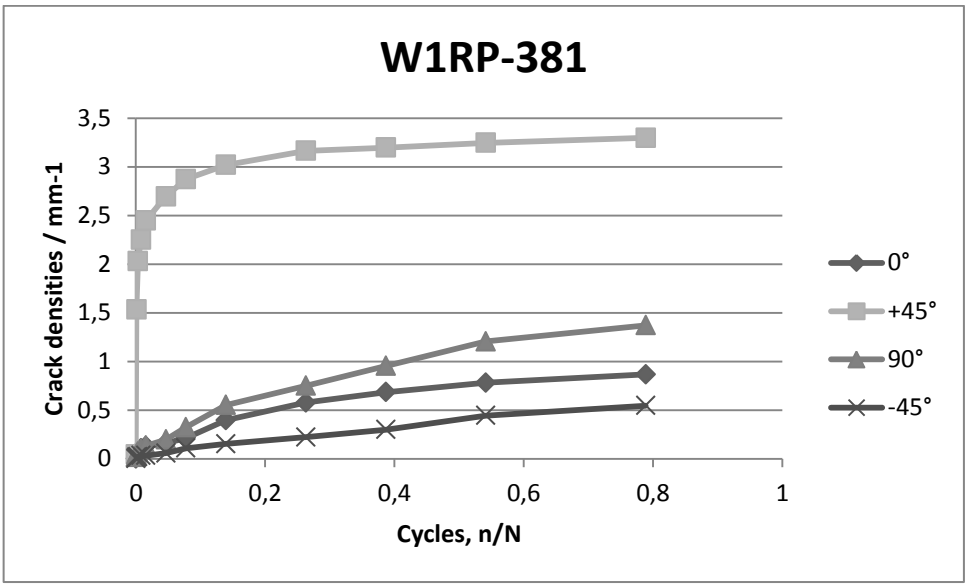
W1RP-381
Crack densities / mm-1
3,5
3
2,5
2
1,5
1
0,5
0
0
0,2
0,4
0,6
0,8
1
Cycles, n/N
0°
+45°
90°
-45°

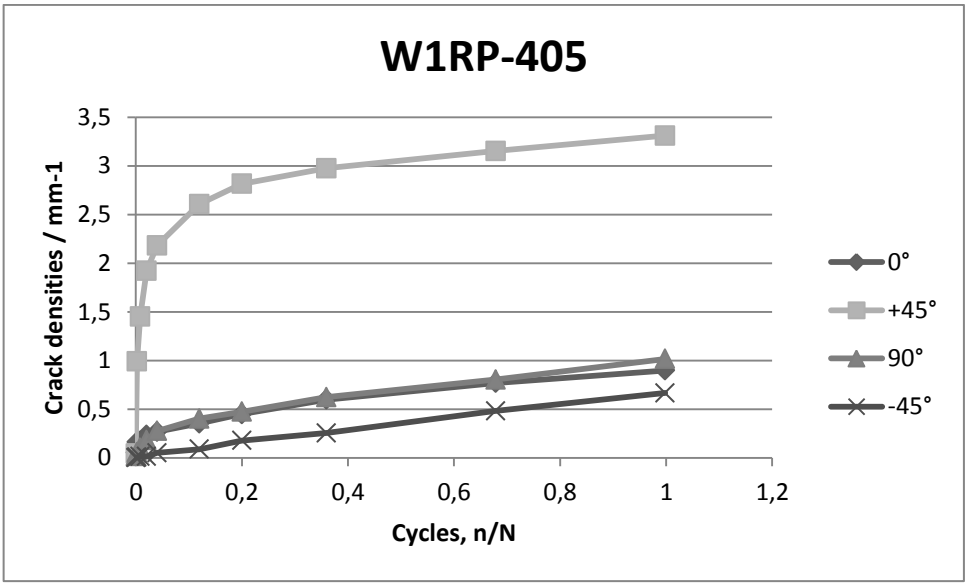
W1RP-405
Crack densities / mm-1
3,5
3
2,5
2
1,5
1
0,5
0
0
0,2
0,4
0,6
0,8
1
1,2
Cycles, n/N
0°
+45°
90°
-45°

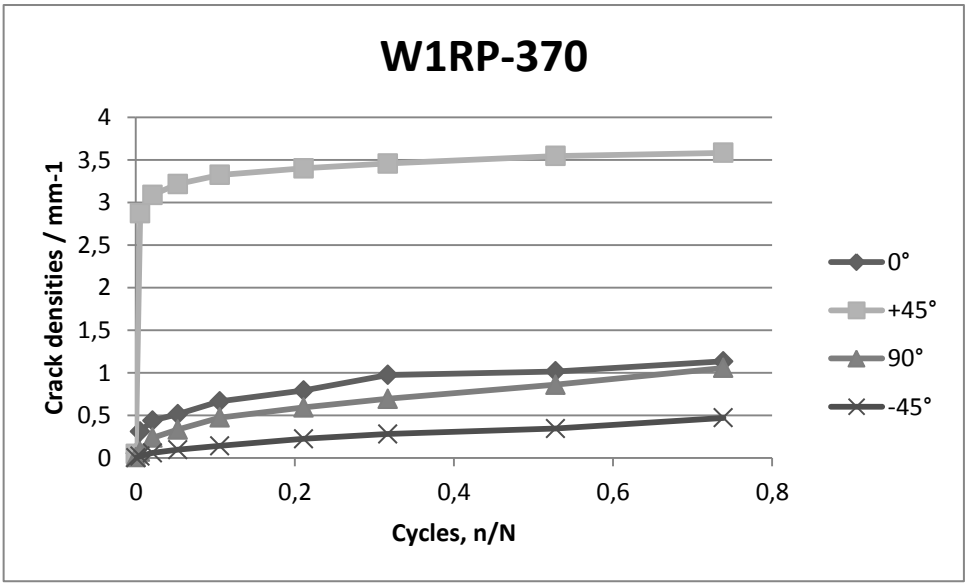
W1RP-370
Crack densities / mm-1
4
3,5
3
2,5
2
1,5
1
0,5
0
0
0,2
0,4
0,6
0,8
Cycles, n/N
0°
+45°
90°
-45°

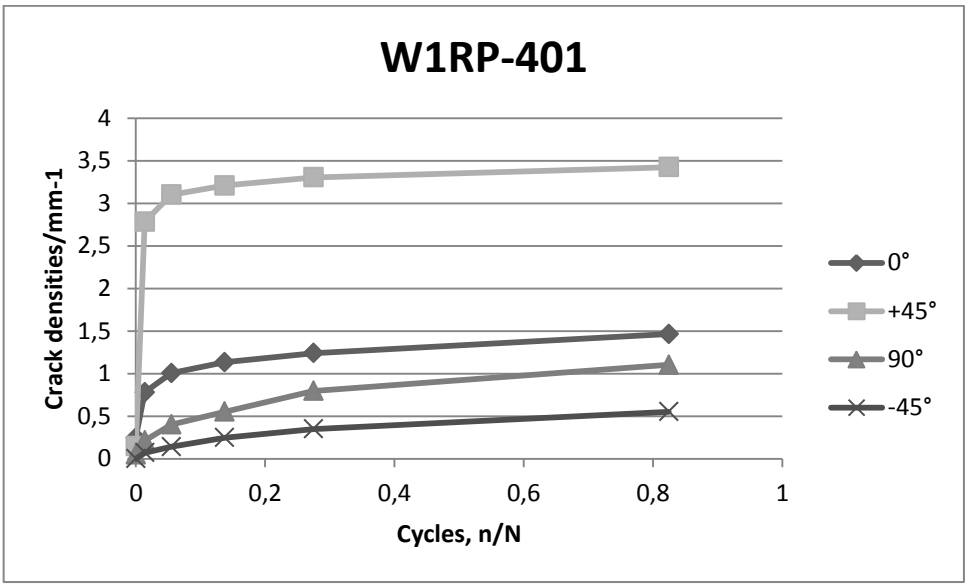
W1RP-401
Crack densities/mm-1
Cycles, n/N
0°
+45°
90°
-45°

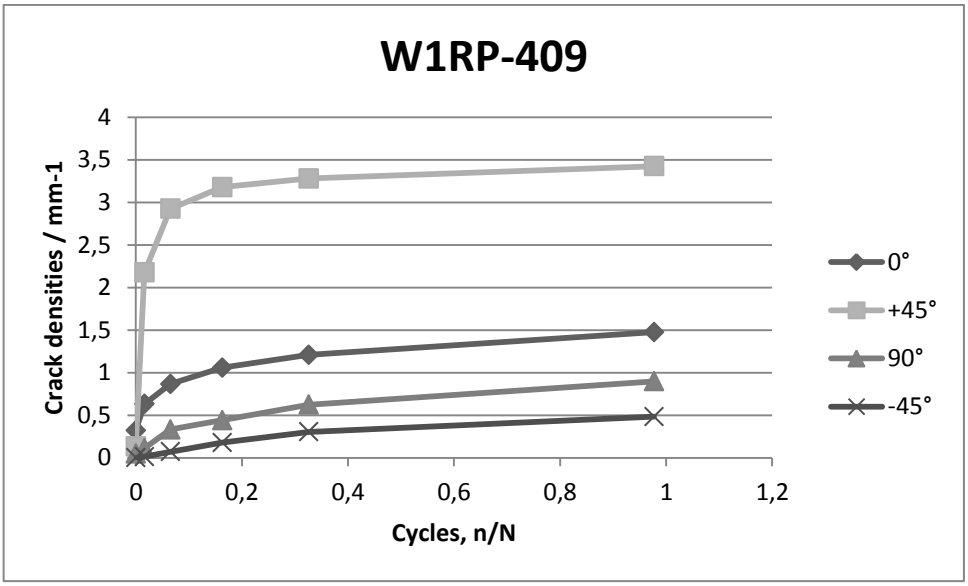
W1RP-409
Crack densities / mm-1
Cycles, n/N
0°
+45°
90°
-45°

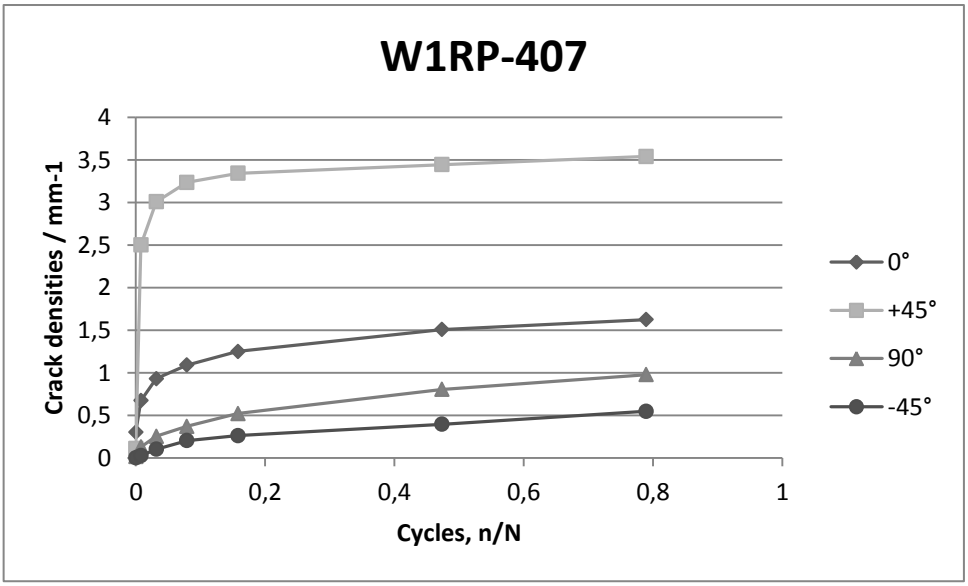
W1RP-407
Crack densities / mm-1
Cycles, n/N
0°
+45°
90°
-45°

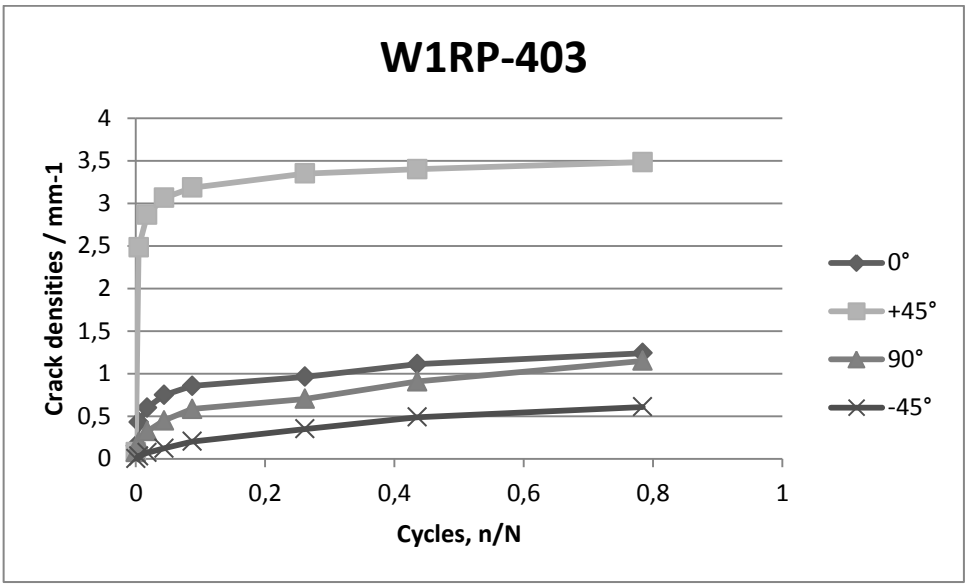
W1RP-403
Crack densities / mm-1
Cycles, n/N
0°
+45°
90°
-45°

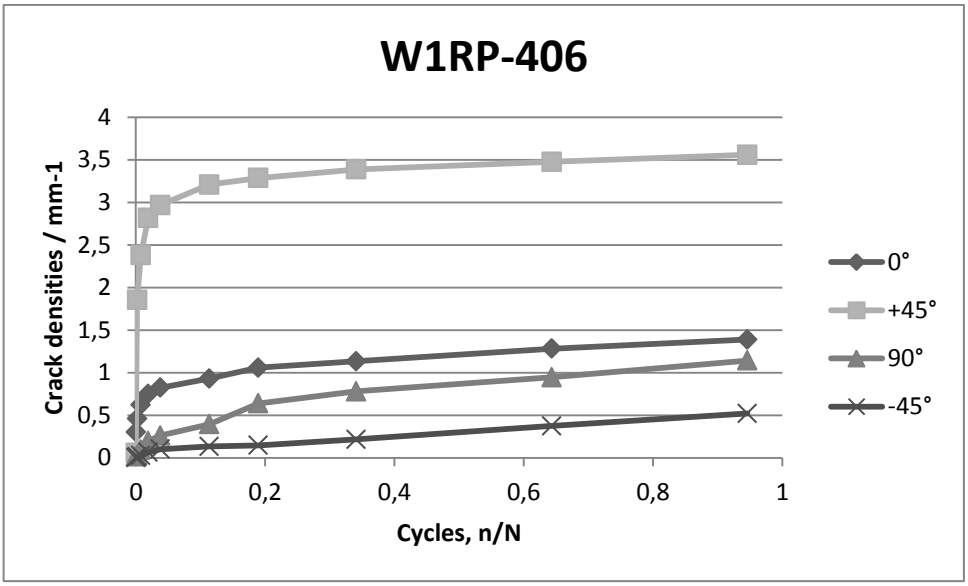
W1RP-406
Crack densities / mm-1
Cycles, n/N
0°
+45°
90°
-45°

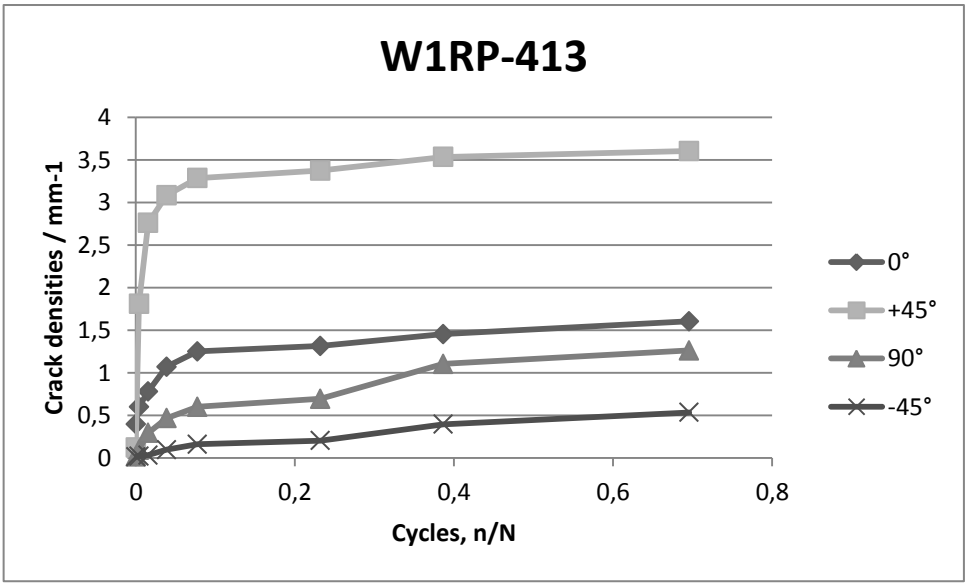
W1RP-413
Crack densities / mm-1
Cycles, n/N
0°
+45°
90°
-45°

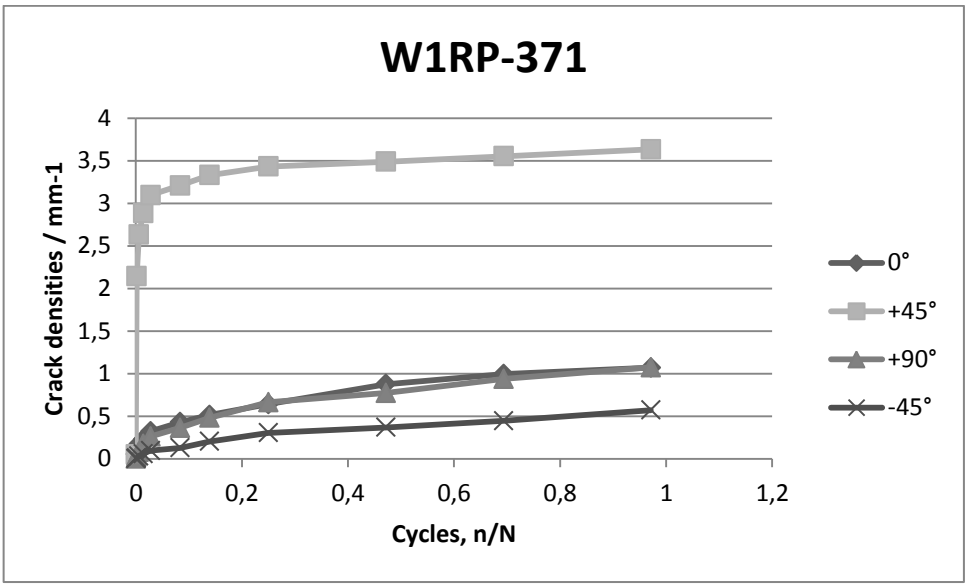
W1RP-371
Crack densities / mm-1
4
3,5
3
2,5
2
1,5
1
0,5
0
0
0,2
0,4
0,6
0,8
1
1,2
Cycles, n/N
0°
+45°
+90°
-45°

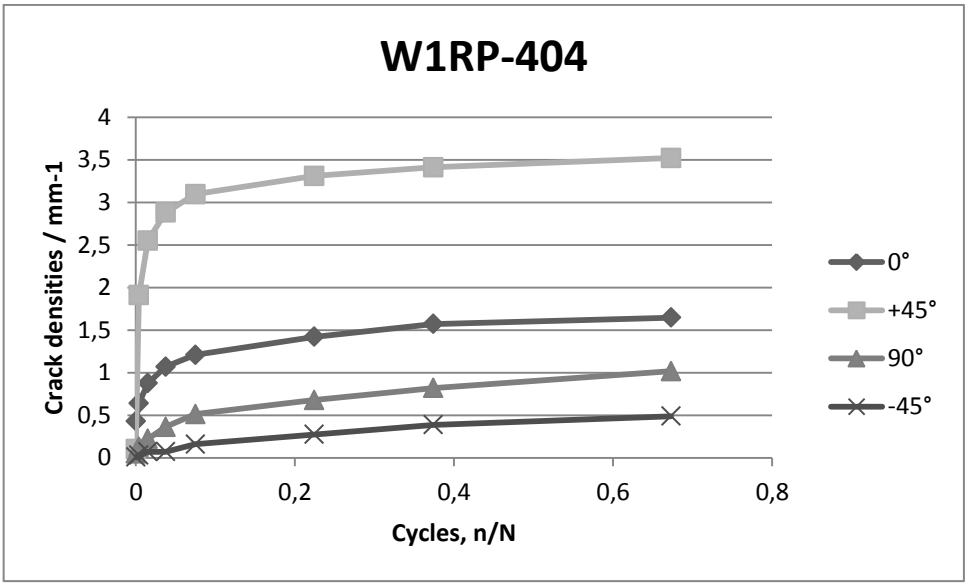
W1RP-404
Crack densities / mm-1
4
3,5
3
2,5
2
1,5
1
0,5
0
0
0,2
0,4
0,6
0,8
Cycles, n/N
0°
+45°
90°
-45°

Microscopy photos:

W1RP-370

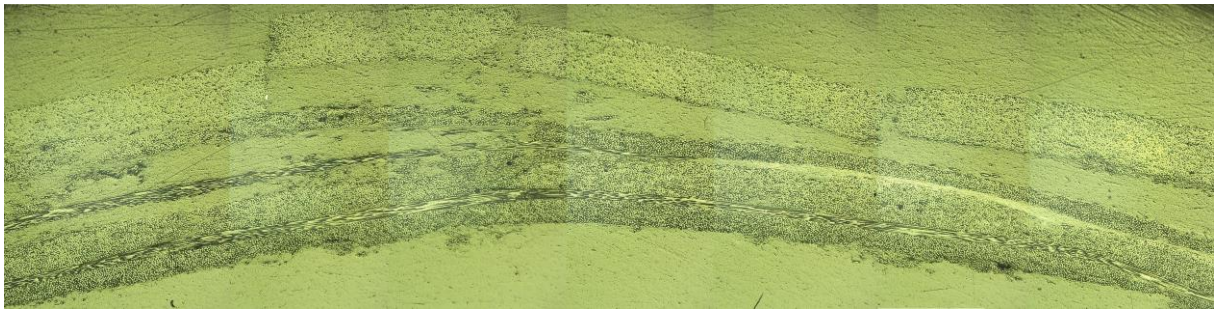

W1RP-381

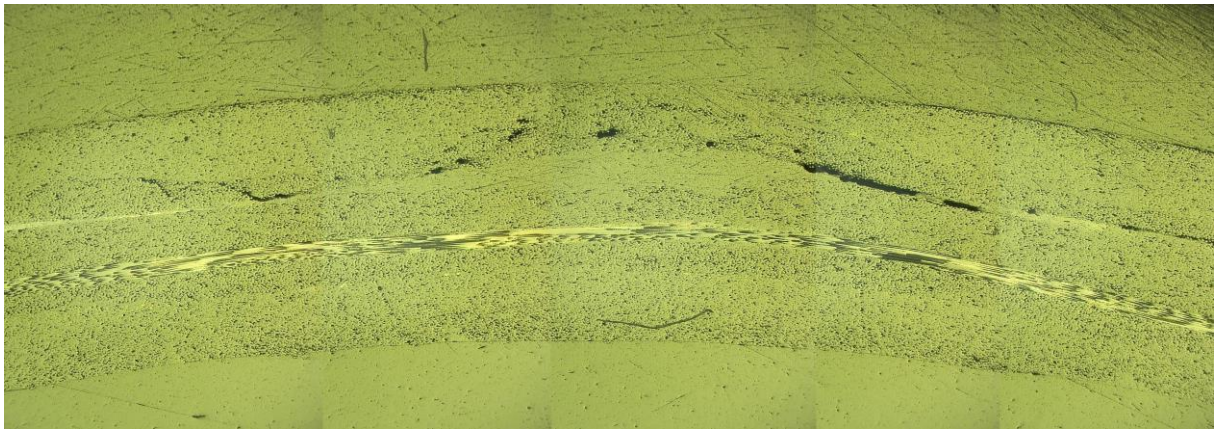

W1RP-401

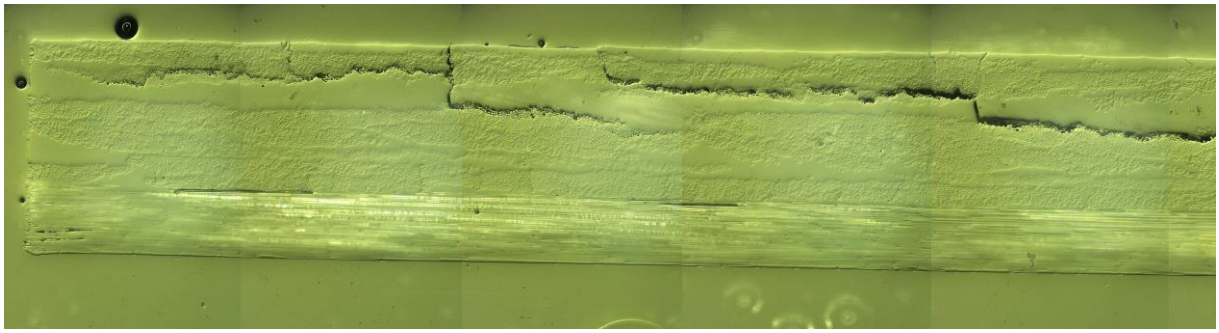

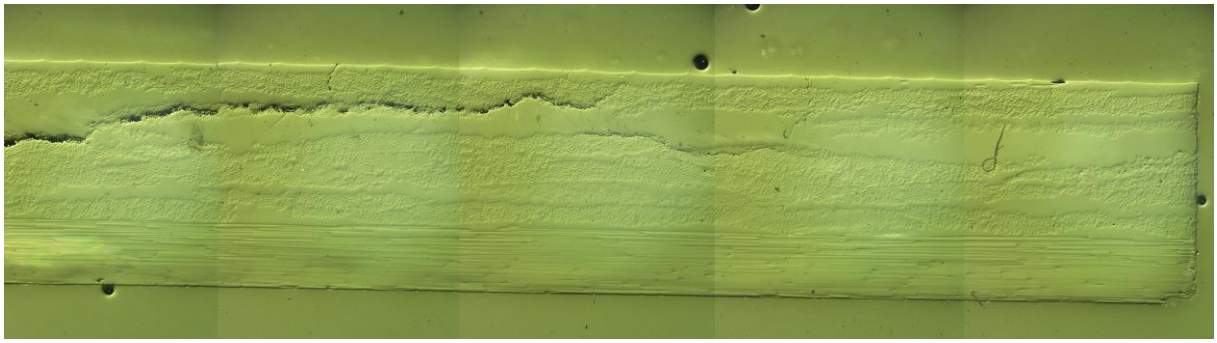

W1RP-406

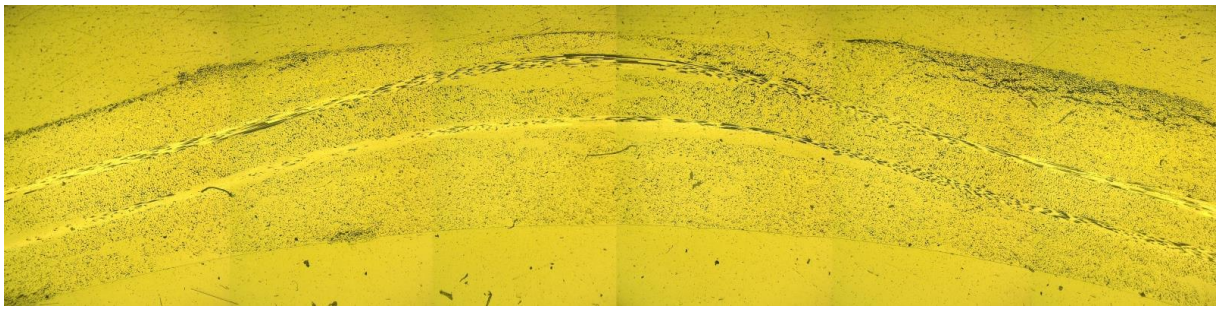

W1RP-407